MINISTÉRIO DA CIÊNCIA E TECNOLOGIA
INSTITUTO NACIONAL DE PESQUISAS ESPACIAIS

sid.inpe.br/mtc-m21b/2015/02.10.14.09-TDI

STUDY OF TRANSIENT MAGNETIC RECONNECTION AND ITS RELATION WITH THE VARIABILITY OF THE POLAR CAP POTENTIAL

Germán Fariñas Pérez

Master's Dissertation of the Graduate Course in Space Geophysics, guided by Drs. Walter Demetrio Gonzalez Alarcon, and Flávia Reis Cardoso, approved in March 05, 2015.

URL of the original document:
<http://urlib.net/8JMKD3MGP3W34P/3HTNDEL>

INPE
São José dos Campos
2015

PUBLISHED BY:

Instituto Nacional de Pesquisas Espaciais - INPE
Gabinete do Diretor (GB)
Serviço de Informação e Documentação (SID)
Caixa Postal 515 - CEP 12.245-970
São José dos Campos - SP - Brasil
Tel.:(012) 3208-6923/6921
Fax: (012) 3208-6919
E-mail: pubtc@sid.inpe.br

MINISTÉRIO DA CIÊNCIA E TECNOLOGIA
INSTITUTO NACIONAL DE PESQUISAS ESPACIAIS

sid.inpe.br/mtc-m21b/2015/02.10.14.09-TDI

STUDY OF TRANSIENT MAGNETIC RECONNECTION AND ITS RELATION WITH THE VARIABILITY OF THE POLAR CAP POTENTIAL

Germán Fariñas Pérez

Master's Dissertation of the Graduate Course in Space Geophysics, guided by Drs. Walter Demetrio Gonzalez Alarcon, and Flávia Reis Cardoso, approved in March 05, 2015.

URL of the original document:
<http://urlib.net/8JMKD3MGP3W34P/3HTNDEL>

INPE
São José dos Campos
2015

Cataloging in Publication Data

Fariñas Pérez, Germán.

F226s Study of transient magnetic reconnection and its relation with the variability of the polar cap potential / Germán Fariñas Pérez. – São José dos Campos : INPE, 2015.

xxviii + 79 p. ; (sid.inpe.br/mtc-m21b/2015/02.10.14.09-TDI)

Dissertation (Master in Space Geophysics) – Instituto Nacional de Pesquisas Espaciais, São José dos Campos, 2015.

Guiding : Drs. Walter Demetrio Gonzalez Alarcon, and Flávia Reis Cardoso.

1. FTE. 2. Transient magnetic reconnection. 3. Polar cap potential. 4. Solar wind-magnetosphere interaction. I.Title.

CDU 550.38:52-85

Aprovado (a) pela Banca Examinadora em cumprimento ao requisito exigido para obtenção do Título de ***Mestre*** em

Geofísica Espacial/Ciências do Ambiente Solar-Terrestre

Dra. Maria Virgínia Alves

Presidente / INPE / SJCampos - SP

Dr. Walter Demetrio Gonzalez Alarcon

Orientador(a) / INPE / SJCampos - SP

Dra. Flávia Reis Cardoso

Orientador(a) / EEL - USP / Lorena - SP

Dra. Cristiane Loesch de Souza Costa

Membro da Banca / INPE / São José dos Campos - SP

Dr. Arian Ojeda González

Convidado(a) / UNIVAP / São José dos Campos - SP

Este trabalho foi aprovado por:

( ) maioria simples

(x) unanimidade

Aluno (a): ***Germán Fariñas Pérez***

São José dos Campos, 05 de Março de 2015

"Mas a grandeza do homem consiste precisamente em querer melhorar a si mesmo, em impor-se Tarefas. No Reino dos Céus não há grandeza a conquistar, pois lá tudo é hierarquia já estabelecida, incógnita solucionada, viver sem fim, impossibilidade do sacrifico, repouso e deleite. Por isso, esmagado pelos sofrimentos e pelas Tarefas, belo na sua miséria, capaz de amar em meio às calamidades, o homem poderá encontrar sua grandeza, sua máxima medida, no Reino deste Mundo."

Alejo Carpentier
"O Reino deste Mundo"

To my parents **German** and **Olga**, to my sister **Evelyn** and to my wife **Madelin**

ACKNOWLEDGEMENTS

I express my sincere thanks to CNPq agency for the MSc Scholarship (grant 131355/2013-9). To INPE/DGE and to the Space Geophysics program for the knowledge gained about my field of study during the master course.

To my supervisors Dr. Walter D. Gonzalez and Dra. Flavia R. Cardoso for their valuable guidance, support and discussions during the past two years.

To the CCMC and Kameleon staff for the use of the tools to analyze the simulation data.

To Dr. Ramon E. Lopez for the original idea of the project and the helpful discussions.

To the reconnection group for their analysis during the weekly meetings. To my office mates (past and presents) and to my class mates for the long hours (day and night) that we spent working in the list of exercises.

To all my professors, since I was a child, that have been spent time to teach me the beauty of the human knowledge.

On the personal side, I am especially grateful to my parents. Only God knows how they fought to give us opportunities in a country that is not free. To my wife Madelin for being my partner in this long journey. To my little sister and family for all their support.

I would like to thanks the community of Cubans in São Jose dos Campos, especially those who arrived before me, for their help to come to Brazil and adapt myself during the first days.

I am grateful to all the people from many countries that I have met here in Brazil, for the possibility of looking the life from another point of view.

A special thanks to the Brazilian people for their hospitality, kindness and sympathy. Living in this country has been a wonderful experience. Thank you.

ABSTRACT

The polar cap potential is an important parameter available to describe the level of magnetospheric activity. It is a measure of the intensity of the magnetospheric convection. The convection process in the magnetosphere is not steady even under constant solar wind conditions. Bursty and unsteady processes in the magnetopause and in the magnetotail disturb the steady state of the magnetosphere and produce variability of the polar cap potential. In this work a three dimensional global magnetohydrodynamic simulation was analyzed in order to study transient magnetic reconnection at the dayside magnetopause and in the geomagnetic tail. The Block-Adaptive-Tree-Solarwind-Roe-Upwind-Scheme (BATS-R-US) code was used. Transient reconnection events associated with flux transfer events at the dayside magnetopause and instabilities at the magnetotail neutral sheet current were identified. Finally the influence of these events on the variations of the polar cap potential has been analyzed.

Keywords: FTE. Transient magnetic reconnection. Polar cap potential. Solar wind-magnetosphere interaction.

ESTUDO DA RECONEXÃO MAGNÉTICA TRANSIENTE E SUA RELAÇÃO COM A VARIABILIDADE DO POTENCIAL DA CALOTA POLAR

RESUMO

O potencial da calota polar é um parâmetro importante disponível para descrever o nível de atividade da magnetosfera. É uma medida da intensidade da convecção magnetosférica. O processo de convecção na magnetosfera não é estacionário, mesmo sob condições constantes do vento solar. Processos instáveis e transientes na magnetopausa e na cauda magnética perturbam o estado de equilíbrio da magnetosfera e produzem variabilidade do potencial da calota polar. Neste trabalho, foi analisada uma simulação magnetohidrodinâmica global tridimensional, a fim de estudar a reconexão magnética transiente na magnetopausa diurna e na cauda geomagnética. O código Block-Adaptive-Tree-Solarwind-Roe-Upwind-Scheme (BATS-R-US) foi usado. Os processos de reconexão transiente associados a eventos de transferência de fluxo na magnetopausa diurna e instabilidades na lâmina de corrente da magnetocauda foram identificados. Finalmente foi analisada a influência desses eventos sobre as variações do potencial da calota polar.

Palavras-chave: FTE. Reconexão magnética transiente. Potencial da calota polar. Interação vento solar-magnetosfera.

LIST OF FIGURES

Page

1.1 **(a)** Flux tube convection caused by magnetic reconnection and viscous interaction. **(b)** Magnetospheric flow in the equatorial plane. **(c)** Northern high-latitude ionospheric flow in magnetic local time (MLT). The hatched lines represent convection driven by viscous interaction and in the remaining regions the convection is caused by reconnection processes. The dashed line corresponds to the boundary of the polar cap. 2

1.2 Sketch of the flow velocity observed in the polar ionosphere. The dashed line represents the polar cap boundary. The solid lines with small arrows indicate the direction of the flow. The large arrows correspond to the electric field, where E_a and E_{PC} are the electric fields outside and inside, respectively, of the polar cap boundary. Magnetic Local Time is used. The points A and B show the centers of the convection cells. 3

1.3 Schematics of dawn to dusk ionospheric polar cap potential drop for IMF south. 4

2.1 Sketch of the response to an impulse of dayside reconnection in the polar cap ionosphere. The solid line represents the polar cap boundary and the arrows indicate the direction of the plasma flow. **(a)** Polar cap in zero flow equilibrium. The open magnetic flux inside the polar cap is constant (its value is F). **(b)** Displacement of the polar cap boundary. The dot-dash line indicates the new equilibrium boundary and the dashed line represents the part of the boundary where excited flow pass through. **(c)** Excitation of flows. **(d)** New equilibrium boundary with flux $F+dF$ (the open magnetic flux increases by an amount dF). 8

2.2 Sketch of the magnetosphere response to an impulse of dayside reconnection. **(a)** Equatorial cut. The solid line indicate the magnetopause after the impulse and the arrows shows the excited flow. The dot-dash line represents the new equilibrium magnetopause. **(b)** Cross-section of the tail viewed toward the sun. 9

2.3 Sketch of the response to an impulse of nightside reconnection in the polar cap ionosphere. The solid line represents the polar cap boundary and the arrows indicate the direction of the plasma flow. **(a)** Polar cap in zero flow equilibrium. The open magnetic flux inside the polar cap is constant (its value is F). **(b)** Displacement of the polar cap boundary. The dot-dash line indicates the new equilibrium boundary and the dashed line represents the part of the boundary where excited flow pass through. **(c)** Excitation of flows near to the midnight polar cap. **(d)** New equilibrium boundary with flux $F - dF$ (the open magnetic flux decreases by an amount dF). 10
2.4 Sketch of the breaking and reconnection of magnetic field lines on a X type configuration. The solid lines with arrows represent the magnetic field lines. The large arrows indicate the plasma flow. 11
2.5 A sketch illustrating northern and southern connected tubes created by a localized burst of reconnection. The polar cap boundaries are indicated. The tubes map to the equatorward edge of the open flux in the polar cap. In the ionosphere the foot of the connected tube corresponds to an equatorward bulge in the boundary between open and closed flux. 13
2.6 Classic Russell-Elphic 3-D model of a FTE in the northern hemisphere. Unsteady reconnection took place probably at the right lower edge of the figure. The flux tube created by the transient reconnection process travels in the direction of the large arrow. The flux tube bulges to the magnetosheath side and during its travel is wrapped by the not reconnected magnetosheath field lines (tilted solid lines with small arrows). The vertical solid lines with small arrows indicate magnetospheric magnetic field lines. 14
2.7 Illustration of the multiple X-line reconnection model. The dashed and solid lines with arrows represent the magnetic field lines at each side of the magnetopause. **(a)** At $t = t_1$ the magnetic field lines reconnect at the X-points in the three lines. **(b)** At $t = t_2$ two helical magnetic lines A_1A_2 and F_1F_2 are formed. **(c)** At $t = t_3$ two newly helical lines $A_1^{'}A_2^{'}$ and $F_1^{'}F_2^{'}$ are formed. As time goes on, the helical lines accumulate and a flux tube is developed. 15
2.8 Sequence of changes of magnetic and plasma configuration in the plasma sheet during a substorm for a noon-midnight plane ($X - Z$ plane). . . . 18

3.1 Illustration of the block based adaptive grid for a simulation of the global magnetosphere on a $Y = 0$ cut plane. 21

4.1 Global perspective of the interaction of the solar wind with the Earth's magnetosphere simulated by the BATS-R-US code. The pink lines represent the IMF and dipolar magnetic field. The white solid lines with arrows represent velocity streamlines. Two cuts are shown, one at $Y = 0$ and the other at $Z = 0$. The color code indicates the plasma density. The sun is on the left and the Earth is represnted as a black sphere in the center. 28

4.2 Observations of the simulated magnetic field in boundary normal coordinate system close to the magnetopause. The circles indicates samples taken every $15s$ by the virtual probe. **a)** The probe is located in the Northern Hemisphere at $x = 8.5R_E, y = -0.3R_E, z = 0.7R_E$. **b)** The probe is located in the Southern Hemisphere at $x = 8.5R_E, y = 0.8R_E, z = -1R_E$. 29

4.3 Illustration of the path chosen to plot the magnetic and plasma data using the Shue et al. (1997) model. In the case of vectorial data, as for example $\vec{B}$, a local magnetopause boundary coordinate system is used. The vector basis of this system is represented as: $\hat{N}$, blue arrow pointing normal to the magnetopause; $\hat{M}$, green arrow; and $\hat{N}$ color magenta arrow. The red surface represents an isosurface of $B_Z = 0$ **a)** Three-dimensional view, the Sun is to the right and the Earth to the left. **b)** Same as (**a**), but the view is from the negative Y axis. In this perspective it is shown that the path is very close to the magnetopause. 33

4.4 Plots of the normal component of the magnetic field **(bottom)** to the magnetopause and total magnetic field strength **(top)**. The x-axis corresponds to the length of the trajectory of the Shue et al. (1997) magnetopause model, taken as reference the subsolar point. Negative and positive values indicate that the measures were taken in the Southern and Northern Hemisphere respectively along the trajectory. Each color means a specific time run. The vertical dashed lines indicates the position of the negative and positive peaks of B_N. 35

4.5 Plots of the normal component of the magnetic field **(bottom)** and total magnetic field strength **(top)** for the time interval from 24:00 to 29:45. The x-axis corresponds to the length of the trajectory of the Shue et al. (1997) magnetopause model, taken as reference the subsolar point. Negative and positive values indicate that the measures were taken in the Southern and Northern Hemisphere respectively along the trajectory. Each color means a specific time run. The vertical dashed lines indicate the position of maximum peaks of the total magnetic field for the last three times. 37
4.6 Plots of the normal component of the magnetic field **(bottom)** and total magnetic field strength **(top)** for the time interval from 31:30 to 33:00. The x-axis corresponds to the length of the trajectory of the Shue et al. (1997) magnetopause model, taken as reference the subsolar point. Negative and positive values indicate that the measures were taken in the Southern and Northern Hemisphere respectively along the trajectory. Each color means a specific time run. The dashed vertical lines indicate the position of maximum peaks of the total magnetic field for the last three times. 39
4.7 Plots of the normal component of the magnetic field **(bottom)** and total magnetic field strength **(top)** for the time interval from 37:15 to 38:30. The x-axis corresponds to the length of the trajectory of the Shue et al. (1997) magnetopause model, taken as reference the subsolar point. Negative and positive values indicate that the measures were taken in the Southern and Northern Hemisphere respectively along the trajectory. Each color means a specific time run. The dashed vertical lines indicate the position of maximum peaks of the total magnetic field for the last three times. 40
4.8 The same as Figure 4.7 but for the time interval from $39:00$ to $41:30$. Each color means a specific time run. The vertical dashed lines indicates the position of positive peaks of B_N for the last three times. 41
4.9 The same as Figure 4.7 but for the time interval from 39:00 to 41:30. Each color means a specific time run. The vertical dashed lines indicates the position of the points between the two peaks of B_N that intersects the $B_N = 0$ line for the last three times. 42

4.10 Magnetic field topology over an isosurface of $B_Z = 0nT$. The surface is very close to the magnetopause, but in the magnetosheath side. The colors represent the magnetic topology as: red, closed; green, one end connected to the south and the other open; yellow, one end connected to the north and the other open; and blue, IMF lines. The black lines shows the intersection of the isosurface with the $Y = 0R_E$ and $Z = 0R_E$ planes. The view is from the north dawnward sun side. 44
4.11 Change of the magnetic topology for the noon-midnight plane ($Y = 0R_E$ plane) for different times. The colors represent the magnetic topology as: red, closed; green, one end connected to the south and the other open; yellow, one end connected to the north and the other open; and blue, IMF lines. The white cross markers show likely reconnection points. The dotted magenta line indicates the intersection of the isosurface of $B_Z = 0$ with the noon-midnight plane. 46
4.12 Formation of the FTE1 for the noon-midnight plane. The plasma thermal pressure is shown in color code. The green arrows indicate the projection of the magnetic field on the $X - Z$ plane. The white lines are projected magnetic field lines. **a)** Beginning of the formation of the pressure bulge at 24:15. **b)** The magnetic structure is well formed with a rotational magnetic field at 25:30. 47
4.13 Enhancement of the core magnetic field for the noon-midnight plane. The color code represents the GSM Y component of the magnetic field. The green arrows indicates the direction (not the magnitude) of the projected magnetic field in the noon-midnight plane. 50
4.14 3D perspective of the interlinked flux tubes. The view is from the north-duskward direction. The black sphere is the Earth. The color coded plane shows the intensity of the Y component of the magnetic field for the noon-midnight cut. 51
4.15 The six panels show cuts of the noon-midnight meridional plane at different times (for each FTE). In each panel the color coding indicates the thermal pressure. The green arrows indicates the direction (not the magnitude) of the projected bulk plasma velocity vector, in order to emphasize the flow vortices. The thin dotted blue line is the zero contour of the plasma velocity Z component, i.e, it separates regions of $V_Z > 0$ from regions of $V_Z < 0$. 53

4.16 Sequence of the subsolar magnetopause plots seen from the magnetosheath side for different times. The color coding represents the Z component of the plasma velocity over an isosurface of $B_Z = 0$ (magnetopause). The black line represents the stagnation ($V_Z = 0$) line. 56
4.17 Sequence of the subsolar magnetopause plots seen from the magnetosheath side for different times. The left column shows in color code the normal component of the magnetic field over an isosurface of $B_Z = 0$. The right column shows in color the tangential component of the magnetic field to the magnetopause. The black line represents the stagnation ($V_Z = 0$) line. 58
4.18 **(a)** North Polar Cap Potential derived from our simulation. **(b)** Zoom of the graphic showed in (**a**). Two large oscillations can be observed. The double arrows and the solid lines indicate the start and the end of each oscillation. 60
4.19 Illustration of the magnetic field lines in 3D due to suddenly reconnection in the plasma sheet current. The color are related to the topology as orange, closed; black, conected to the polar cap; and blue, IMF. The view is from the north, dawn, and tailward side of the magnetosphere, i.e., the earth is to the right. 62
4.20 Cuts of the magnetotail in the $X-Z$ plane at differents times, the Earth is to the right. In each panel the color coding represents the plasma density in particles per cm^3. The sequence of snapshots shows the formation, evolution and spreading of a plasmoid. 63
4.21 Magnetic topology at the plasma current sheet (represented as an isosurface of $B_X = 0$ (Harris, 1962)). The surfaces are located at $Z \approx 0$ with an inclination of $\approx 11^\circ$ respect to the ecliptic plane. The view is from above and the Earth is to the right. The colors represent areas of different magnetic field topology as red, closed; green south connected; yellow north connected; and blue open magnetic field lines. 64
4.22 Ionospheric potential pattern (color coded) in the polar cap. The black line and the arrows represent the open closed field line boundary and the ionospheric convection vectors respectively. **top)** Northern Hemisphere. **bottom)** Southern Hemisphere 67
4.23 North and South Polar Cap Potential during our simulation. 68
4.24 Ionospheric polar cap potential during our simulation. The blue line represents the south PCP and the black line the north PCP. The red boxes indicate the time onset of the FTEs. The green rectangles indicate the beginning and end of every substorm as labeled bellow the symbol. . 70

LIST OF TABLES

Page

3.1 Conditions of the 3D MHD simulation. 23

4.1 Summary of the characteristics of the FTEs observed in our simulation. 43

LIST OF ABBREVIATIONS

BATS-R-US	–	Block-Adaptive-Tree-Solarwind-Roe-Upwind-Scheme
CCMC	–	Community Coordinated Modeling Center
CDF	–	Common Data Format
DNL	–	distant neutral line
FTE	–	Flux Transfer Events
GM	–	Global Magnetosphere
GSM	–	Geocentric Solar Magnetospheric
IE	–	Ionospheric Electrodynamics
ISEE	–	International Sun-Earth Explorer
SWMF	–	Space Weather Modeling Framework
IMF	–	Interplanetary Magnetic Field
MHD	–	Magnetohydrodynamics
NENL	–	near Earth neutral line
PCP	–	polar cap potential

LIST OF SYMBOLS

$\vec{E}$	–	electric field vector
$\vec{V}$	–	plasma fluid velocity in the ionosphere
$\vec{u}$	–	plasma fluid velocity in the BATS-R-US equations
$\vec{B}$	–	magnetic field vector
$\vec{j}$	–	current density vector
ρ	–	plasma density
p	–	plasma pressure or thermal pressure
E	–	total energy of the plasma
e	–	thermal energy
μ_0	–	Permeability of vacuum
Φ	–	ionospheric electrostatic potential
Φ_{max}	–	maximum ionospheric electrostatic potential
Φ_{min}	–	minimum ionospheric electrostatic potential
Φ_{PC}	–	polar cap potential defined as $\Phi_{PC} = \Phi_{max} - \Phi_{min}$
B_X	–	GSM X component of the IMF
B_Y	–	GSM Y component of the IMF
B_Z	–	GSM Z component of the IMF
$\hat{N}$	–	base vector of the boundary normal coordinates, normal to the magnetopause
$\hat{L}$	–	base vector perpendicular to $\hat{N}$ along the projection of the GSM Z direction
$\hat{M}$	–	completes the orthogonal system ($\hat{M} = \hat{N} \times \hat{L}$).
B_L	–	L component of the magnetic field
B_N	–	N component of the magnetic field
B_M	–	M component of the magnetic field
F	–	open magnetic flux inside the polar cap
R_E	–	Earth radius (6371 km)
B_I	–	magnetic field at the E layer ionosphere(i.e., $120km$ altitude)
$B_{3.5}$	–	geomagnetic field at $3.5R_E$
$F_{10.7}$	–	solar flux intensity at $10.7cm$
R_I	–	Earth radius at the E layer altitude
$\sum$	–	integrated ionospheric conductance tensor
$J_{\|\|}$	–	field aligned current magnitude (parallel to the geomagnetic field)
V_A	–	Alfvén speed
V_{SW}	–	Solar wind speed
M_a	–	Alfvén Mach number ($M_a = V_{SW}/V_A$)
α_{X-line}	–	Tilt angle of the reconnection line with respect the horizontal Y axis

CONTENTS

Page

1 INTRODUCTION 1
1.1 Objectives 5

2 GENERAL CONCEPTS 7
2.1 Magnetic reconnection 11
2.2 Flux Transfer Events 12
2.3 Transient process in the magnetotail 16

3 METHODOLOGY 19
3.1 Ionospheric potential solver 22
3.2 Processing tools: the Kameleon software 24

4 RESULTS AND DISCUSSIONS 27
4.1 Transient Magnetic Reconnection at the subsolar magnetopause 28
4.1.1 FTEs detection and study 31
4.1.2 Generation and topology of the FTEs 43
4.1.3 Movement of the X-reconnection line 55
4.2 Transient magnetic reconnection in the magnetotail and variations of the polar cap potential 59
4.2.1 Magnetotail magnetic reconnection processes 59
4.2.2 Magnetic topology study of the first substorm-like event 63
4.3 Considerations about the FTE signature in the polar ionosphere 65

5 CONCLUSIONS 71

REFERENCES 75

APPENDIX A - MATLAB INTERFACE TO KAMELEON SOFTWARE 79

1 INTRODUCTION

The polar cap potential (PCP), also known as transpolar cap potential, is generated as a consequence of the solar wind-magnetosphere-ionosphere interaction. The solar wind transmits mechanical momentum and energy to the magnetosphere-ionosphere system. During this process geomagnetic field lines are convected antisunward driven by two principal mechanisms: magnetic reconnection and viscous interaction (Cowley, 1982).

Figure 1.1a illustrates the convection of the magnetic field lines. Open flux tubes produced by magnetic reconnection are transported over the poles from the dayside magnetosphere into the magnetotail where it reconnects again and flow back to the dayside, as proposed by Dungey (1961). All this process results in a large scale magnetospheric convection. The motion of the open magnetic field lines transmits stresses and forces to the polar cap ionosphere, producing a similar convection pattern in the ionosphere but of minor scale (two outer convection cells of Figure 1.1c).

In addition to magnetic reconnection, Axford and Hines (1961) proposed that viscous interaction produces convection of closed magnetic flux tubes around the flanks of the magnetopause and into the tail (Figure 1.1a). The closed flux tubes return to the dayside either forced by the tension of the convected magnetic field lines or with the help of the reconnection in the magnetotail (Cowley, 1982). A mirror of this magnetospheric convection is created in the polar ionosphere (two inner cells of Figure 1.1c), which is added to the ionospheric convection created by the magnetic reconnection mechanism.

These two processes can coexist on a continuous basis as illustrated in Figure 1.1b and c. The hatched regions correspond to convection due to viscous interaction. In Figure 1.1b a flow in an equatorial plane is shown. Near the magnetopause flanks, the magnetic field lines dragged by viscous-like forces transport plasma to the tail, flow is transported back to the dayside as these closed magnetic field lines relax. In the center of Figure 1.1b the flow is directed to the dayside and is driven by reconnection. The open flux tubes created by reconnection at the dayside (only the northern flux tube is shown in Figure 1.1a) travel to the tail. Reconnection in the tail between the northern and southern convected flux tubes produces a flow toward the Earth as shown in the central part of Figure 1.1b. The motion of the foot points of the convected flux tubes creates a flow pattern in the northern and southern polar ionosphere similar to the one shown in Figure 1.1c. As consequence of this process a line that separates open and closed flux tubes is created (circular dashed line of

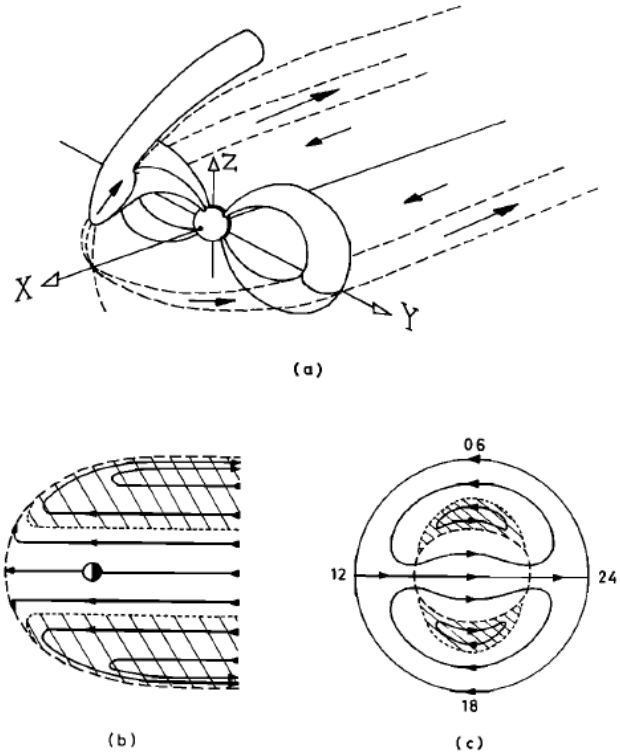

Figure 1.1 - **(a)** Flux tube convection caused by magnetic reconnection and viscous interaction. **(b)** Magnetospheric flow in the equatorial plane. **(c)** Northern high-latitude ionospheric flow in magnetic local time (MLT). The hatched lines represent convection driven by viscous interaction and in the remaining regions the convection is caused by reconnection processes. The dashed line corresponds to the boundary of the polar cap.

SOURCE: (Cowley, 1982).

Figure 1.1c). The region inside this line is defined as the polar cap, then the dashed line represents the boundary of the polar cap. The flow pattern on the ionosphere driven by reconnection is represented by the two larger convection cells, while the two inner cells completely outside of the polar cap are due to viscous interaction.

On the polar cap ionospheric F-region the plasma flow produces an electric field $\vec{E} = -\vec{V} \times \vec{B} = -\nabla\Phi$, where Φ is the electrostatic potential. This relation implies that the flow velocity $\vec{V}$ is parallel to the equipotential lines, i.e., equipotential electrostatic lines represent plasma flow lines. The diagram of Figure 1.2 shows the flow pattern over the polar cap, the lines represent both equipotential electrostatic field and flow lines.

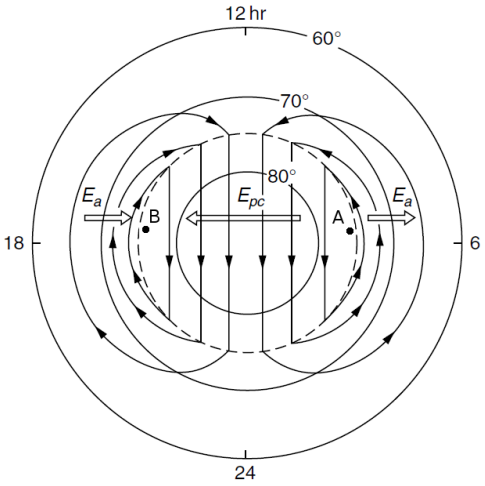

Figure 1.2 - Sketch of the flow velocity observed in the polar ionosphere. The dashed line represents the polar cap boundary. The solid lines with small arrows indicate the direction of the flow. The large arrows correspond to the electric field, where E_a and E_{PC} are the electric fields outside and inside, respectively, of the polar cap boundary. Magnetic Local Time is used. The points A and B show the centers of the convection cells.

SOURCE: Adapted from Kelly (2009).

The electrostatic potential drop measured by a polar-orbiting spacecraft on a pass over the high-latitute ionosphere is $\Phi(x) = \int_{low-latitute}^{x} \vec{E} \cdot \vec{ds}$, with the integral starting from a low-latitude point where the electric field is negligible and proceeding to a general point x along the path of the spacecraft. The difference between the maximum and the minimum values of $\Phi(x)$ is defined to be Φ_{PC}, the polar cap potential drop (Kivelson; Rusell, 1995). Figure 1.3 is a sketch of the typical potential drop through the dawn-dusk line starting from 6:00. The ionospheric potential first decreases because the angle between the path and the electric field is 180°. In the center of the first convection cell (point A Figure 1.2), the electric field changes direction. At this point the ionospheric potential reaches its minimum value and starts to increase until the center point of the second convection cell (point B Figure 1.2) where the electric field changes direction again. The ionospheric potential reaches its maximum value at this point. The polar cap potential Φ_{PC} is calculated as:

$$\Phi_{PC} = \Phi_{max} - \Phi_{min} \ , \tag{1.1}$$

where Φ_{max} and Φ_{min} are, respectively, the maximum and minimum ionospheric

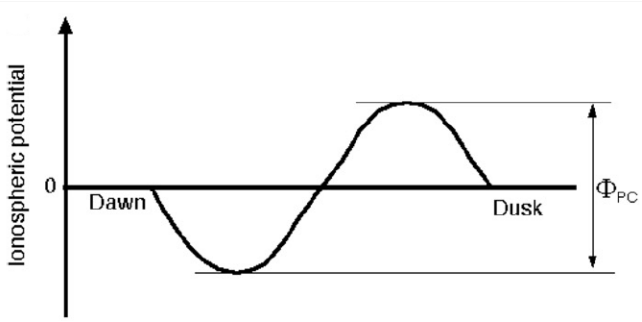

Figure 1.3 - Schematics of dawn to dusk ionospheric polar cap potential drop for IMF south.

SOURCE: Adapted from Lopez et al. (2012).

potentials measured at the center of the convection cells (points A and B).

The physical meaning of the polar cap potential as defined by Equation 1.1 is the following. If we visualize magnetic field lines as moving at velocity $\vec{v}$ across the dawn-dusk diameter of the polar cap (line joining the points A and B of Figure 1.2), then the dawn-dusk transpolar potential is equal to $\Phi_{PC} = vBl_{AB}$, where B is the magnitude of the polar magnetic field and l_{AB} is the longitude of the polar cap diameter. The quantity vBl_{AB} is the magnetic flux per unit time that cross the segment joining the points A and B. Therefore, the polar cap potential can be considered to represent the rate of transport of magnetic flux from the dayside magnetopause to the magnetotail. This means that the strength of the convection of magnetic field lines is characterized by the magnitude of the PCP.

A steady state convection pattern in the magnetosphere-ionosphere system is reached when the rate of reconnection at the dayside manetopause is equal to the rate of reconnection in the magnetotail. This condition is obtained at most 15% of the time because of the variability of the IMF. Even for large periods of constant IMF, transient reconnections at the dayside magnetopause and in the geomagnetic tail affect the balance of the convection pattern and produce variations of the polar cap potential. Hence departures from steady state must be considered the norm, rather than relatively infrequent events (Lockwood, 1991; Bristow et al., 2004).

In this work transient magnetic reconnection at the magnetopause and in the magnetotail is studied at a first stage. Reconnection often occurs in an impulsive way, both at the dayside magnetopause and in the tail. Under appropriate conditions (south-

ward IMFs), unsteady reconnection like Flux Transfer Events (FTE) are observed at the dayside magnetopause, each one lasting one or two minutes and separated typically by about 8 minutes. In the nightside tail also burst of reconnection occurs during periods of sustained southward IMF ($B_Z < 0$).

The coordinate system used is the Geocentric Solar Magnetospheric (GSM). The X-axis points to the Sun. The Y-axis is perpendicular to the geomagnetic (magnetic dipole) axis and is positive towards dusk. This axis lies in the geomagnetic equatorial plane and completes an orthogonal set $\vec{Y} = \vec{Z} \times \vec{X}$. The Z-axis is perpendicular to the X-axis and in the plane containing the X-axis and the magnetic dipole (geomagnetic) axis. It is positive towards north.

We analyze the signatures of transient magnetic reconnection at the magnetopause, as FTE, and in the magnetotail. We use computational simulation of the global magnetosphere under constant solar wind conditions. The characteristics of the reconnection process are studied, for example, the beginning and end of the burst of reconnection (time duration), the periodicity, spatial extension and the development of instabilities associated with the transient reconnection.

1.1 Objectives

The general objective is to use a simulation under constant south and duskward IMF ($B_Z < 0$ and $B_Y > 0$) to find a relation between reconnection and the variability of the PCP. As in Raeder (2006), constant solar wind conditions are chosen to test the hypothesis that transient magnetic reconnection do not need to be triggered by external sources (changes in solar wind conditions), rather than quasi-periodic impulses of reconnection in both the nightside and dayside magnetosphere occur spontaneously producing oscillations of the PCP.

We organize our work in three specific task or objectives, in order to reach our overall objective:

1- To find signatures of FTE as the principal source of transient magnetic reconnection at the magnetopause and study its principal characteristics: beginning and end of the reconnection process, periodicity, spatial extension, direction and speed of the convection created by the FTE and the possible generation mechanism.

2- To identify the occurrence of transient and unsteady magnetic reconnection at the magnetotail current sheet and study its different phases: start of the reconnection process, plasmoid formation and evolution, end of the reconnection process,

periodicity, and extension and location of the reconnection current sheets, among others.

3- To identify the presence of variations of the PCP and find a correlation with the occurrence of the transient reconnection events studied.

2 GENERAL CONCEPTS

In this chapter we start analyzing the response of the PCP to transient magnetic reconnection at the magnetopause and in the geomagnetic tail. Later, we study briefly the different models of bursty and unsteady magnetic reconnection in both the dayside and nightside magnetosphere.

As the PCP represents a measure of the strength of the flow through the polar cap boundary, its behavior depends of the flow variations in the polar cap region. Cowley and Lockwood (1992) proposed a two-component flow model where the variability of the flow depends of the sum of two intrinsically time-dependent components. One component is driven by dayside coupling and may to a first approximation be parametrized by the IMF vector. The second component is driven by tail processes and is related to the past history of the interplanetary medium and magnetosphere. The unbalance of this two components produces excitation and decay of flow as will be explained next.

The coupling processes at the magnetopause are often impulsive, FTEs are probably the most common source of this kind of impulsive reconnection. Cowley and Lockwood (1992) proposed that the perturbation of the polar cap boundary and the intensification of flows in localized places of the polar cap boundary are direct responses of the polar ionosphere to an impulsive reconnection event.

Figure 2.1a represents the polar cap boundary. Inside there are open magnetic flux (F) and outside closed magnetic flux, i.e., the solid line represents the closed-open field line boundary. First we consider the system in zero flow equilibrium. This is an unrealistic situation because it is expected that reconnection will occur in some part of the magnetopause for any orientation of the IMF, thus exciting flow in the interior of the polar cap boundary. Nevertheless, the concept of zero-flow equilibrium is important because represents a steady state that can be disturbed, then we can study the excitation and decay of flows taking as reference this state.

After the system is perturbed by an impulsive event at the dayside magnetopause, the open-closed field line is impulsively displaced equatorward in the noon sector as shown in Figure 2.1b. (The displacement is draw unrealistically large for reasons of clarity, actually the new amount of flow dF created by the FTE is very low compared with F (Lockwood et al., 1990)). The new equilibrium boundary is represented by a dot-dashed circle in Figure 2.1b. The perturbed part of the actual open-closed field line lies equatorward of the new equilibrium boundary and the other part lies

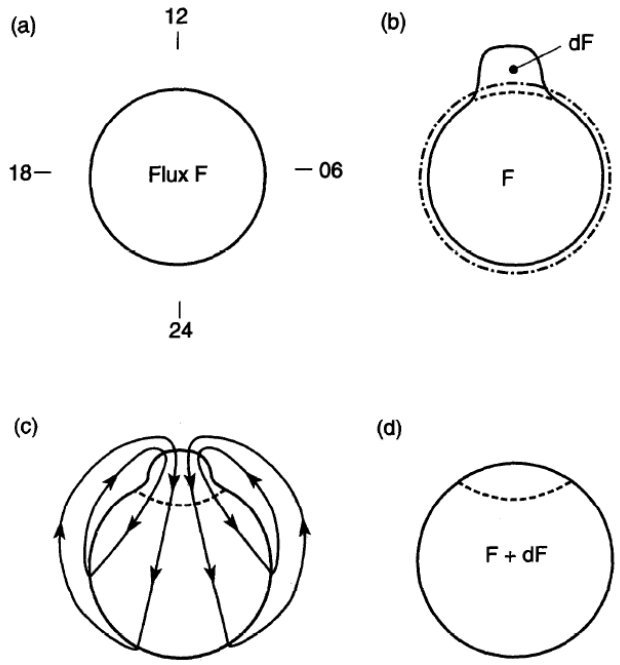

Figure 2.1 - Sketch of the response to an impulse of dayside reconnection in the polar cap ionosphere. The solid line represents the polar cap boundary and the arrows indicate the direction of the plasma flow. **(a)** Polar cap in zero flow equilibrium. The open magnetic flux inside the polar cap is constant (its value is F). **(b)** Displacement of the polar cap boundary. The dot-dash line indicates the new equilibrium boundary and the dashed line represents the part of the boundary where excited flow pass through. **(c)** Excitation of flows. **(d)** New equilibrium boundary with flux $F + dF$ (the open magnetic flux increases by an amount dF).

SOURCE: (Cowley; Lockwood, 1996).

poleward. In order for the system to reach a new equilibrium, the flow must be excited from the actual open-closed field line to the new equilibrium boundary, then the flow is excited poleward in the perturbed noon sector and equatorward elsewhere as shown in Figure 2.1c. When the equilibrium is achieved the flow will stop (Figure 2.1d).

The corresponding response in the magnetosphere to an impulse of magnetic reconnection is shown in Figure 2.2a for an equatorial cut and in Figure 2.2b for a magnetotail cross-section (Cowley; Lockwood, 1992; Cowley; Lockwood, 1996). The impulse of magnetic reconnection erodes the nose of the magnetopause as show in Figure 2.2a, newly opened flux tubes are created in the perturbed region and later are removed from the dayside to the tail, then the equilibrium of the dayside magne-

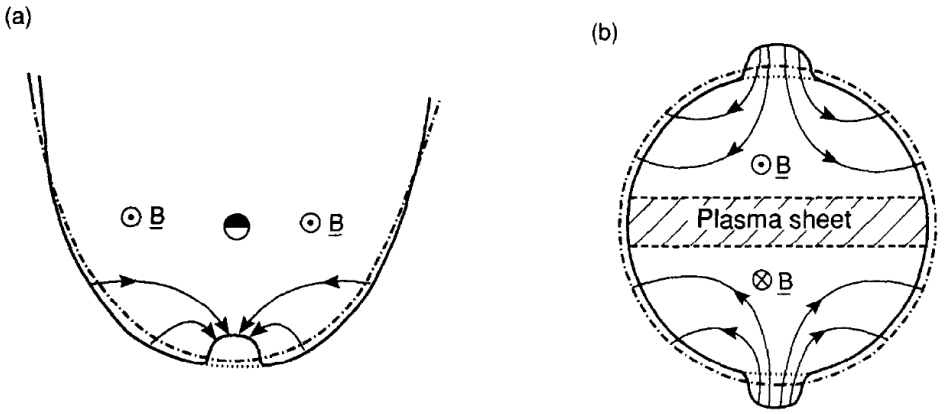

Figure 2.2 - Sketch of the magnetosphere response to an impulse of dayside reconnection. **(a)** Equatorial cut. The solid line indicate the magnetopause after the impulse and the arrows shows the excited flow. The dot-dash line represents the new equilibrium magnetopause. **(b)** Cross-section of the tail viewed toward the sun.

SOURCE: (Cowley; Lockwood, 1996).

topause is perturbed. Closed magnetic field lines move from the flanks of the dayside magnetopause to the perturbed region where the plasma pressure is lower. Flow is excited until the equilibrium is restored. The motion of the flow (and closed magnetic fields) represented in Figure 2.2a corresponds to the ionospheric flow on closed flux tubes of Figure 2.1c. Similarly, the addition of open magnetic flux to the tail excites flow outward of the perturbed region toward the inner of the magnetotail boundary until the equilibrium is achieved (Figure 2.2b), this flow corresponds to the ionospheric flow on open flux tubes of Figure 2.1c at the nightside part.

Tail processes are the second component that can affect the flows (and the PCP) in the polar cap region. An impulsive reconnection event like substorm destroys open flux in the magnetotail, then a perturbation at the midnight is created. The excitation and decay of flows due to this perturbation is shown in Figure 2.3, which is similar to Figure 2.1. However there are some differences, in this case the flow is more concentrated in the midnight (Figure 2.3c), the amount of open flux in the polar cap decreases and consequently the polar cap area corresponding to the new equilibrium boundary (Figure 2.3d) also decreases.

The corresponding behavior of the PCP during the processes of excitation and decay of flow for both dayside and nightside reconnection is as follow. First the flow is

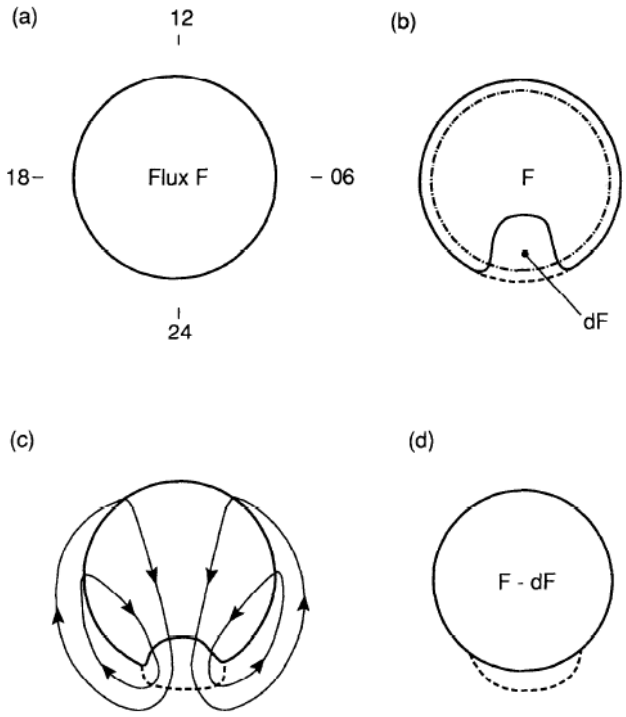

Figure 2.3 - Sketch of the response to an impulse of nightside reconnection in the polar cap ionosphere. The solid line represents the polar cap boundary and the arrows indicate the direction of the plasma flow. **(a)** Polar cap in zero flow equilibrium. The open magnetic flux inside the polar cap is constant (its value is F). **(b)** Displacement of the polar cap boundary. The dot-dash line indicates the new equilibrium boundary and the dashed line represents the part of the boundary where excited flow pass through. **(c)** Excitation of flows near to the midnight polar cap. **(d)** New equilibrium boundary with flux $F - dF$ (the open magnetic flux decreases by an amount dF).

SOURCE: (Cowley; Lockwood, 1996).

excited, then the strength of the flow increases. The PCP as a measure of the strength of the convection flow also increases. When the perturbed system starts to achieve the condition of equilibrium the flows begin to decay, which produces a decrease in the PCP. Therefore, an impulse of magnetic reconnection produces an increase and subsequent decrease of the PCP. The characteristic time for the excitation and decay of flow due to a single burst of reconnection is of order $10 - 15$ minutes (Cowley; Lockwood, 1992).

In the previous analysis it was considered only the case of B_Z southward and that the processes of magnetic reconnection are impulsive in character. The inclusion of a B_Y component produces asymmetry with respect to the noon-midnight line.

Nevertheless the general principle remains, both impulsive magnetic reconnection at the dayside magnetopause and in the magnetotail produce excitation and decay of flow in the polar cap region and, consequently, an increase followed by a period of decrease of the PCP.

2.1 Magnetic reconnection

Magnetic reconnection is the process where magnetic energy is converted into kinetic energy and heat (thermal energy) in physical plasmas. This process is very complex from a theoretical and experimental point of view. The simplest model of magnetic reconnection is illustrated in Figure 2.4. Consider at $t < 0$ a magnetic topology of antiparallel magnetic field frozen into the plasma. The Ampere's law implies that a current sheet must be present between the antiparallel magnetic fields. The direction of the electric current is perpendicular to the plane of the figure. Whenever the resistivity, at an arbitrary point within the field reversal region becomes nonzero, the magnetic field may diffuse around this point (called X-point). Exactly at the center of the thin current sheet, the two inward magnetic lines have opposite direction and cancel each other at the X-point. This produces the X-type configuration shown in the middle panel of Figure 2.4, with the magnetic field being zero at the center of the X, called the magnetic *neutral point*. The field lines forming the X and passing through the neutral point are called separatrices (Baumjohann; Treumann, 1997).

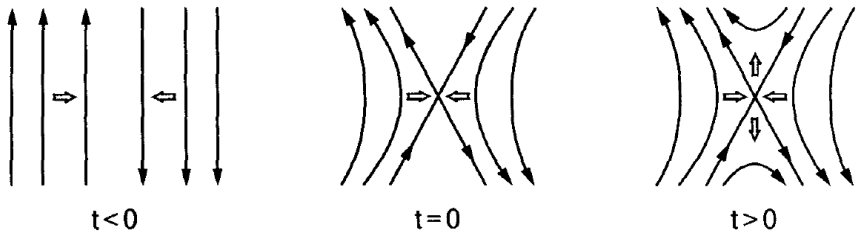

Figure 2.4 - Sketch of the breaking and reconnection of magnetic field lines on a X type configuration. The solid lines with arrows represent the magnetic field lines. The large arrows indicate the plasma flow.

SOURCE: (Baumjohann; Treumann, 1997).

The final result is a change of the global topology and connectivity as shown in the third panel of Figure 2.4. Two new magnetic field lines are formed at $t > 0$. This process is called breaking and reconnection of magnetic field lines. The region in the vicinity of the neutral point where the magnetic lines break and reconnect is

called diffusion region. The initially antiparallel field lines carry only plasma from its corresponding side. However, after they reconnect, the new merged lines transport a mixture of plasma from both sides. The merged field lines are expelled up and down from the diffusion region due to magnetic tension forces. Then, the outgoing plasma (up and down) is accelerated and magnetic energy is converted into kinetic energy. Also, part of the incoming magnetic energy is dissipated into ohmic heating in the diffusion region due to the finite resistivity.

This process can be steady as long as oppositely directed magnetic field lines are being pushed into the diffusion region and as long as the resistivity allows the magnetic field vanishes in this small space. However, instabilities in the current sheet, as for example the tearing instability, produce reconnection in an inherently time-dependent way with impulsive and bursty releases of energy.

2.2 Flux Transfer Events

Although some characteristics of Flux Transfer Event (FTE) were first reported by Haerendel et al. (1978), the description and terminology that we use today was given by Russell and Elphic (1978) as a result of data analysis of the ISEE (International Sun-Earth Explorer) spacecraft mission.

The FTEs are illustrated in Figure 2.5 for the IMF conditions of $B_Z < 0$ and $B_Y > 0$. The flux tubes formation process starts with the unsteady and localized reconnection at the dayside magnetopause, which leads to a creation of flux tubes connecting interplanetary and magnetospheric fields. In this model reconnection occurs over a narrow longitude segment, creating two pairs of elbow-like flux tubes, one in the northern hemisphere and a mirror image in the southern hemisphere. Instead of convecting along the other field lines in the magnetosheath, the new reconnected flux tubes attempt to shorten itself due to tension forces. This process is illustrated in Figure 2.5. The shortening process pulls the magnetosheath field lines out of the magnetopause boundary and twist it out of the vertical direction into the magnetosheath field direction. Figure 2.6 shows the classical 3-D form of a FTE due to Russell and Elphic (1978). Reconnection between the magnetosheath and magnetospheric magnetic fields took place outside the figure, probably near the lower right edge of Figure 2.6.

This classical description explains two important characteristic of FTE reported by observations. First, the component of the magnetic field normal to the magne-

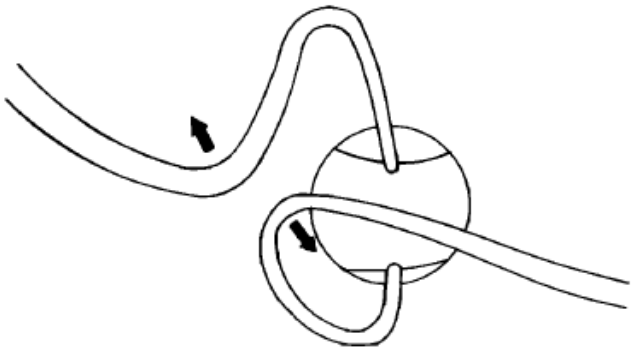

Figure 2.5 - A sketch illustrating northern and southern connected tubes created by a localized burst of reconnection. The polar cap boundaries are indicated. The tubes map to the equatorward edge of the open flux in the polar cap. In the ionosphere the foot of the connected tube corresponds to an equatorward bulge in the boundary between open and closed flux.

SOURCE: (Southwood, 1987).

topause[1] (B_N) increases when the spacecraft encounters the flux tube, also during the pass of the satellite, B_N experiments a change of polarity that is caused by the overlay of magnetospheric and magnetosheath field lines around the flux tube. The second important characteristic is the enhancement of the core magnetic field (B_M), which is because of the tension on the flux tube field lines is larger as compared with the surrounding magnetospheric and magnetosheath field lines.

Multiple observations of FTEs suggest a frequency of repetition of these events of approximately 8 minutes. The duration of each FTE seems typically to be 1-2 minutes, and with a bulk speed transverse to the magnetic field of $100 - 200\, kms^{-1}$. For large FTEs the area of the flux tube cross section is typically $1R_E$, where R_E is the mean radius of the Earth (approximately 6371 km).

Lee and Fu (1985) showed that if magnetic reconnection with multiple X-reconnection lines occur, instead of single line reconnection as proposed by Dungey (1961), then FTEs are naturally formed. For clarity the multiple X-line reconnection model is illustrated in Figure 2.7 for the case of three reconnection lines and not

[1]The magnetic perturbation of FTEs are best observed in magnetopause boundary coordinate system. In this system the N component points outward, normal to the magnetopause, L is perpendicular to N along the projection of the GSM Z direction, while M completes the right-handed coordinate system and point westward toward morning. The relation between the GSM to the magnetopause boundary coordinate system is explained in Section 4.1.

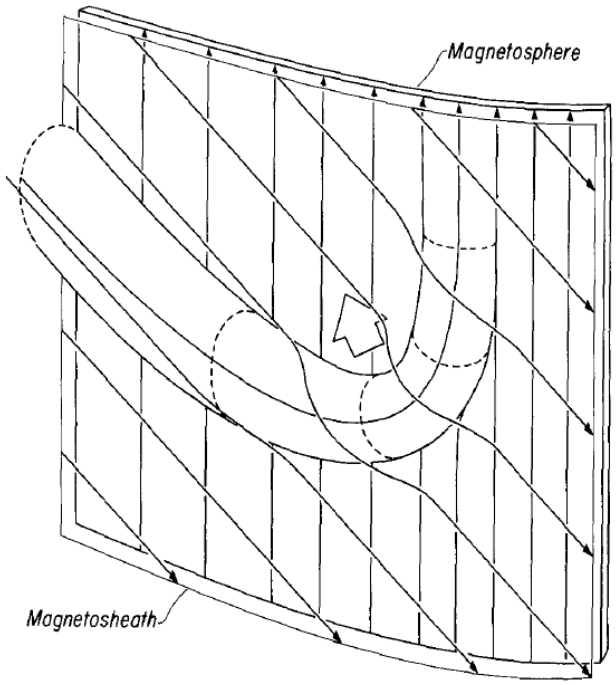

Figure 2.6 - Classic Russell-Elphic 3-D model of a FTE in the northern hemisphere. Unsteady reconnection took place probably at the right lower edge of the figure. The flux tube created by the transient reconnection process travels in the direction of the large arrow. The flux tube bulges to the magnetosheath side and during its travel is wrapped by the not reconnected magnetosheath field lines (tilted solid lines with small arrows). The vertical solid lines with small arrows indicate magnetospheric magnetic field lines.

SOURCE: (Russell; Elphic, 1978).

exactly antiparallel magnetic lines, i.e., $B_Y \neq 0$. The central line is the reconnection line that corresponds to the Gonzalez and Mozer (1974) model and it extends around the dayside magnetopause. The others reconnection lines have a limited extension. If reconnection takes place at the three X-lines as shown by the X points in Figure 2.7a, the reconnected field lines will contract due to magnetic tension forces. The result is a formation of two helical magnetic lines $A1A2$ and $F1F2$ (see Figure 2.7b). The rest of the magnetic fields lines $B1B2$, $C1C2$,...,$J2J1$, are similar to the reconnected field lines in the single reconnection case. As times goes on more pairs of helical lines $A1A2$ and $F1F2$ are added, indicated by Figure 2.7c, and this leads to the formation of two helical flux tubes, ones in each hemisphere, that resembles the elbow-like description of the FTE.

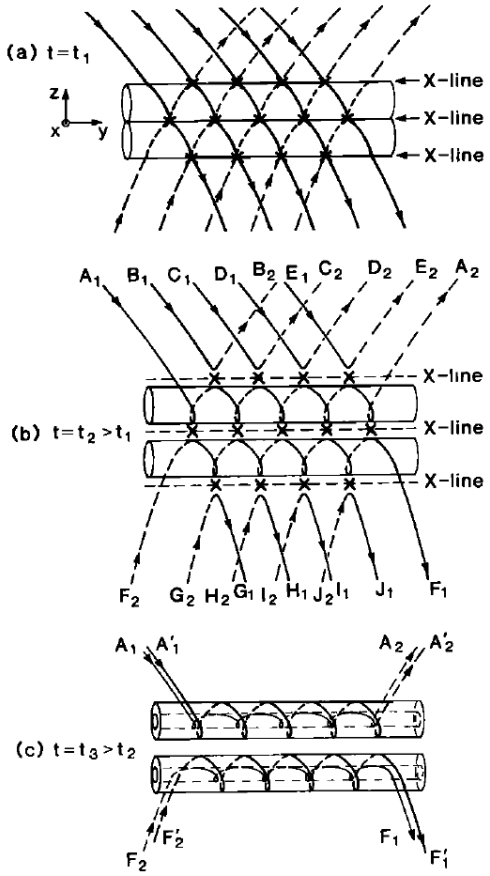

Figure 2.7 - Illustration of the multiple X-line reconnection model. The dashed and solid lines with arrows represent the magnetic field lines at each side of the magnetopause. **(a)** At $t = t_1$ the magnetic field lines reconnect at the X-points in the three lines. **(b)** At $t = t_2$ two helical magnetic lines A_1A_2 and F_1F_2 are formed. **(c)** At $t = t_3$ two newly helical lines $A_1^{'}A_2^{'}$ and $F_1^{'}F_2^{'}$ are formed. As time goes on, the helical lines accumulate and a flux tube is developed.

SOURCE: (Lee; Fu, 1985).

The multiple X lines are created due to the development of plasmoids or magnetic islands at the subsolar magnetopause. Lee and Fu (1985) showed by two dimensional MHD simulations that when the characteristic length of the system (L) is much greater than the current layer separating the two plasma regions, the current sheet becomes unsteady and the tearing instability grows at substantial rates, generating islands of large size. This is a typical scenario at the dayside magnetopause, where $L \simeq 10R_E$ and the thickness of the current layer (l) is $l \simeq 500km$ and hence $L \gg l$. The new reconnection lines appear at the X points between the magnetic islands. In the presence of B_Y this magnetic islands become flux embedded in the magnetopause

with a helical field inside. As this tubes grow to a large value, the reconnection of magnetic field lines will slow down and stop. Reconnection will begin again when the saturated magnetic flux tubes are convected out of the reconnection region. The presence of B_Y is essential for the formation of the flux tube with helical fields. If $B_Y = 0$, this model leads to the formation of isolated magnetic loops instead of helical flux tubes as in Figure 2.7c.

Another model for the formation of FTE has been proposed by Liu and Hu (1988). This model is a combination of the Kelvin-Helmholtz instability and the tearing mode when a strong shear flow exits across a current sheet. Near the stagnation point the flow perpendicular to the magnetopause is almost zero, then below and above of that point the flow is parallel to the magnetopause current layer. In these regions the magnetopause should be susceptible to the Kelvin-Helmholtz instability. The characteristic vortices of this instability twist the magnetic field lines. As the result some of the magnetic field lines in the vortices will be antiparallel to the field lines at the magnetopause boundary. Magnetic reconnection occurs leading to the formation of magnetic islands like in the multiple X-line reconnection model. The presence of a B_Y component in these islands represents flux tubes extending in the dawn-dusk direction above and below the subsolar point.

A further model for FTEs was proposed by Scholer (1988) and Southwood et al. (1988) in terms of time-dependent reconnection at a single X-line. The proponents of this model argue that periods of increased reconnection or a sudden onset of reconnection lead to a pair of bulges in the magnetopause of limited extension in the dawn-dusk direction. These bulges are then transported northward and southward to the cusp regions with the Alfvén speed. This model considers a small extent of the X-line so the reconnection produces two flux tubes, one in each hemisphere.

2.3 Transient process in the magnetotail

The steady convection pattern proposed by Dungey (1961) may not be reached due to transient and not steady processes at the dayside magnetopause and in the magnetotail. The formation and ejection of plasmoids in the magnetotail and its relation with the polar cap potential are explained briefly in this section.

All the flux that is transported to the tail has to be reconnected and move back to the dayside magnetopause. However, the instantaneous rate of magnetic merging between the IMF and the terrestrial field at the dayside magnetopause is not necessarily the same as in the magnetic tail, only the average rates are equal. As a

consequence, not all the flux transported to the tail is instantaneously reconnected back to the frontside, therefore a portion of the flux is accumulated in the tail increasing the magnetic flux density. When the amount of magnetic flux stored in the tail is enough to become unsteady, it reconnects suddenly and the magnetic energy is released in an explosive way. This process occurs more frequently during periods of IMF south, because in that case the merging rate at the dayside magnetopause is higher and the reconnection rate in the tail is not so fast for managing the amount of convected flux.

The source of the transient phenomena in the magnetotail is the development of the tearing instability. At the beginning of the process the magnetic field lines are stored in the tail lobes, the increase of magnetic flux of opposite polarity at both sides of the neutral current sheet produces an stretching and intensification of the current sheet. After a period of time, the plasma sheet become sufficiently thin and the stability of the current sheet decreases (Schindler, 1974). Then the tearing instability abruptly set in and lead to changes in the magnetic field topology.

An sketch of the development of the tearing instability in the tail is showed in Figure 2.8 using the terminology of substorms (Baumjohann; Treumann, 1997). In the first phase, named the growth phase, the plasma sheet becomes more tail-like due to a thinning of the current sheet. A distant neutral line (DNL) is formed around $100 - 200 R_E$. The second phase, denominated onset and expansion, is characterized by the formation of a new near Earth neutral line (NENL) at around $15 R_E$. The excess of magnetic flux deposited in the tail is reconnected in this new X-line, which defines the time of reconnection onset. The magnetic topology changes, reconnected magnetic field lines move back to their normal dipolar shape at the Earth side. Tailward between the two neutral lines a plasmoid is formed. The plasmoid is defined as an O-shaped magnetic field structure which contains high beta and high density plasma (Otto et al., 1990). In the third phase, named recovery phase, the NENL begins to move tailward and pushes the plasmoid in the same direction until it is finally ejected from the magnetotail. Plasma is lost to the downtail solar wind and the former NENL becomes a DNL.

It is important to clarify that although we use the terminology and the sequence of events of a substorm, the process explained above is not restricted to substorm events. A magnetospheric substorm occurs after a southward turning of the IMF, the time duration is typically 1-3 hours and involve a great amount of energy capable of producing auroras, magnetic disturbances and large variations of the polar

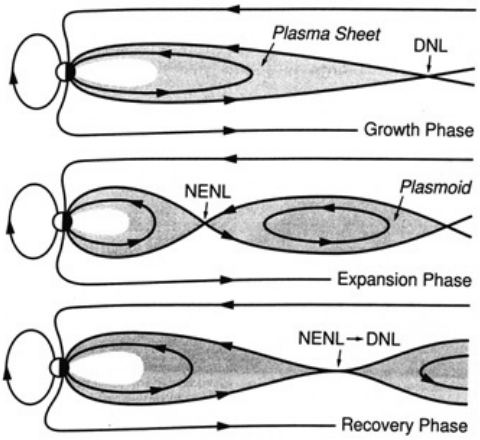

Figure 2.8 - Sequence of changes of magnetic and plasma configuration in the plasma sheet during a substorm for a noon-midnight plane ($X - Z$ plane).

SOURCE: (Baumjohann; Treumann, 1997).

cap potential. However, burst of reconnection on the tail with duration of about 5 minutes and separated typically by a few tens of minutes can take place in the plasma sheet. This kind of events is generated also during periods of southward B_Z and follows the same sequence of events of Figure 2.8. The growth rate of the tearing instability associated with these rapid events are considerably greater than for substorm events, but the amount of energy involved is less than a magnetospheric substorm.

We believe that this kind of events (we will call it substorm-like events) could generate decay and excitation of flows at the midnight polar cap ionosphere as explained at the beginning of this chapter. Therefore variations of the average steady state polar cap potential could be produced.

3 METHODOLOGY

The PCP is generated by the convection pattern formed during the interaction of the solar wind with the Earth magnetic field. This problem is of great complexity. The resulting hydromagnetic flow is a complicated balance of thermal, kinetics and magnetic effects.

Experimental and simulation methods have been used to study the magnetospheric processes. The experimental method consists of measurements by satellites instruments obtained during passes through the magnetosphere. However due to the increased computer capabilities have become possible to simulate the dynamics of the terrestrial magnetosphere. The resolution in space and time obtained by satellite usually is not enough to study a variety of phenomena in the magnetosphere. Satellite takes an observation in one specific point of space and after an orbit is completed a new measure is taken at this point, then many details of the dynamic process under study can be lost. To overcome this difficulty the magnetosphere is modeled by solving the equations of magnetohydrodynamics (MHD) on a supercomputer, then the results of the computer simulation can be compared with satellite data in order to validate the model.

In this work we use computational simulation to study the transient magnetic reconnection and its relation to the PCP. The code used is the Block-Adaptive-Tree-Solarwind-Roe-Upwind-Scheme (BATS-R-US) and was developed by the Computational Magnetohydrodynamics Group at the University of Michigan, now Center for Space Environment Modeling. The BATS-R-US code solves the following 3D ideal MHD equations in volume finite form using numerical methods related to the Riemman solver (Powell et al., 1999; Tóth et al., 2012):

conservation of mass (one scalar equation),

$$\frac{\partial \rho}{\partial t} + \nabla \cdot (\rho \vec{u}) = 0 \; ; \tag{3.1}$$

conservation of momentum (three equations: one for each vectorial component),

$$\frac{\partial \rho \vec{u}}{\partial t} + \nabla \cdot (\rho \vec{u}\vec{u} + p\bar{\bar{I}}) = \vec{j} \times \vec{B} \; ; \tag{3.2}$$

Faraday's Law (three equations: one for each vectorial component),

$$\frac{\partial \vec{B}}{\partial t} + \nabla \cdot (\vec{u}\vec{B} - \vec{B}\vec{u}) = -\vec{u}\nabla \cdot \vec{B} \; ; \tag{3.3}$$

conservation of energy (one scalar equation),

$$\frac{\partial E}{\partial t} + \nabla \cdot [(E + p + \frac{\vec{B} \cdot \vec{B}}{2\mu_0})\vec{u} - \frac{1}{\mu_0}(\vec{u} \cdot \vec{B})\vec{B}] = -\frac{1}{\mu_0}(\vec{u} \cdot \vec{B})\nabla \cdot \vec{B} \; ; \tag{3.4}$$

where ρ is the mass density of the plasma, p the plasma pressure, $\vec{u}$ is the mean velocity of the plasma, $E = \rho e + \rho\frac{\vec{u}\cdot\vec{u}}{2} + \frac{\vec{B}\cdot\vec{B}}{2\mu_0}$ is the total energy and e is the thermal energy.

In addition, the ideal gas equation of state $e = \frac{p}{(\gamma-1)\rho}$ is used to relate the thermal and total energy with the pressure p, γ is the ratio of the specific heat at constant pressure to the specific heat at constant volume. The Ampère's law is used to relate the magnetic field with the current density.

These equations are expressed in terms of eight dependent variables: the density (ρ), the three Cartesian components of the momentum ($\rho\vec{u}$), the three components of the magnetic field (B_X, B_Y and B_Z) and the total plasma energy (E).

BATS-R-US uses a block based adaptive Cartesian grid that allows to specify where the user wants more resolution or let the code determine where more resolution is needed based in criteria defined by the user. The grid is organized in blocks of arbitrary size and the blocks are composed by cells. Each block has the same number of cells. The MHD equations (3.1), (3.2), (3.3), (3.4), written in a more compact form, are integrated over a cell in the grid.

The advantage of the block adaptive scheme is that the blocks can be refined in a region where more resolution is needed. This method avoids under resolving the solution in regions of great interest (high gradient regions) and over resolving the solution in less interesting regions (low gradient regions). The refinement criteria used in the BATS-R-US code to build the adaptive grid are based in the local values of:

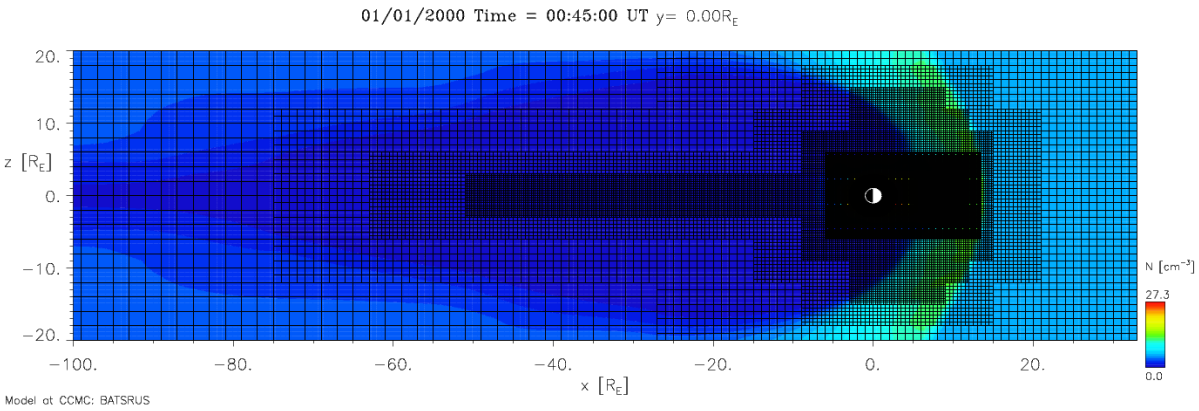

Figure 3.1 - Illustration of the block based adaptive grid for a simulation of the global magnetosphere on a $Y = 0$ cut plane.

SOURCE: Created at Community Coordinated Modeling Center (2014).

$$\left.\begin{aligned} \epsilon_c &= |\nabla \cdot \vec{u}|\sqrt{V}, \\ \epsilon_r &= |\nabla \times \vec{u}|\sqrt{V}, \\ \epsilon_t &= |\nabla \times \vec{B}|\sqrt{V}, \end{aligned}\right\} \tag{3.5}$$

These values $\epsilon_c, \epsilon_r, \epsilon_t$ characterize respectively the compressibility, rotationality and current density of a region of volume V. Then, in regions where at least one of this three quantities is greater than a threshold value, a refinement of the blocks must be applied (Powell et al., 1999). In Figure 3.1 it is illustrated the concept of the adaptive grid used in simulations of the global magnetosphere. The blocks are showed as rectangles because the image represents a 2D cut at $Y = 0$ (plane $X - Z$). In the distant magnetotail ($X < -80R_E$) the size of the blocks are $2R_E$, then the block size is reduced successively by two in regions close to the plasma sheet and to the magnetopause because those are zones of higher density current and rotationality.

BATS-R-US is the source code for a variety of models used by the Space Weather Modeling Framework (SWMF) for simulating and forecasting of space weather. We use in our work the Global Magnetosphere (GM) component of the SWMF. Its domain surrounds the Earth and it extends about $30R_E$ towards the sun, about $250R_E$ towards the magnetotail and about $40R_E$ in the Y and Z GSM directions. The GM component is adapted for simulating the interaction of the solar wind with the Earth's magnetosphere (Tóth et al., 2012).

In this work, we look for signatures of unsteady magnetic reconnection in the magnetopause (specifically FTEs) and instabilities in the plasma current sheet associated with substorm-like events. The magnetopause boundary layer has an approximately thickness of $500km$, then the block size must be at least $\frac{R_E}{16} \sim 335km$. The high resolution in the magnetopause is required to detect disturbances near the magnetopause current layer that cause FTE. In the plasma sheet region ($-60R_E < X < -5R_E$) a block size of $\frac{R_E}{8}$ would be recommended, because the thickness of the current sheet during the growth phase of a substorm event is estimated to be as thin as $0.2R_E$ (Sergeev et al., 1990). As we will show in the next section, signatures of instabilities and ejections of plasmoids in the plasma sheet are observed using a resolution of $\frac{R_E}{4}$ in that region.

The BATS-R-US code runs more efficiently in parallel computer system (cluster). Because of the block based structure, most of the blocks of the grid can easily be performed in separate processors. The 3D global MHD simulations we need for our study are performed at the Community Coordinated Modeling Center (CCMC). The CCMC provides to the space scientific community a framework to run, visualize and analyze modern space research models (Community Coordinated Modeling Center, 2014).

The magnetic reconnection process occurs due to the numerical dissipation (numerical resistivity). Raeder (2006) finds out that the successful simulation of FTEs depends on the numerical resolution of the model. It was shown in that paper that for a resolution of $0.08R_E$, the numerical dissipation is supressed sufficiently in order for FTEs form and survive. We use in our work the same run of Cardoso et al. (2013), which have a finer resolution of $\frac{R_E}{32} \approx 0.03R_E$ at the magnetopause[1]. Therefore, the numerical resistivity in our simulation is significantly smaller than in Raeder (2006).

The conditions of the run are shown in Table 3.1. The resolution in the magnetotail region near the plasma sheet is $\frac{R_E}{4}$.

3.1 Ionospheric potential solver

The Ionospheric Electrodynamics (IE) is a SWMF component which is coupled to the GM component. The IE model is a two dimensional height-integrated spherical surface at a nominal ionosphere altitude (at around 110 km for the Earth). It uses

[1] After analyzing carefully the grid resolution of Cardoso et al. (2013) simulation, we found that at the magnetopause the grid resolution is $\frac{R_E}{32}$ instead of $\frac{R_E}{16}$, as it was indicated, which is even smaller.

Table 3.1 - Conditions of the 3D MHD simulation.

Model	BATS-R-US
Simulation Time	45 min
Dipole Tilt	no
Solar Wind Density	5 n/cc
Solar Wind Temperature	232000 K
X component of SW velocity	-600 km/s
Y component of SW velocity	0 km/s
Z componet of SW velocity	0 km/s
IMF B_X	0 nT
IMF B_Y	14 nT
IMF B_Z	-14nT

the field aligned currents to calculate conductances based on empirical relations, and then it solves for the electrical potential on a 2D spherical grid (Tóth et al., 2012). The methodology used by this model and how it is coupled to the GM component can be summarized in the following steps from Ridley et al. (2004):

1- The field aligned currents (parallels to the geomagnetic field) are calculated at $3.5R_E$. The formula used by the IE model is $J_{||} = (\nabla \times \vec{B}) \cdot \vec{b}$, where $J_{||}$ is the field aligned current, $\vec{B}$ is the geomagnetic field at $3.5R_E$, and $\vec{b}$ is the unitary vector (direction) of the geomagnetic field at $3.5R_E$;

2- The calculated field aligned currents are mapped down to the E layer ionosphere along the geomagnetic field, and multiplied by the factor $B_I/B_{3.5}$, where $B_{3.5}$ is the geomagnetic field at $3.5R_E$ and B_I the magnetic field at the E layer ionosphere (i.e., $120km$ altitude) ;

3- A conductance pattern is generated. Two methods are commonly used:

3-1 A uniform ionospheric conductance is assumed (as in our simulation),

3-2 The ionospheric conductance caused by solar radiation and particle precipitation are calculated by some of the existing models (e.g Torr et al. (1979); Frahm et al. (1997)). The solar radiation parameter used is the $F_{10.7}$ (solar flux intensity at $10.7cm$). The particle precipitation pattern is calculated from empirical models which use the field aligned currents as an input parameter;

4- The ionospheric electric potential is solved using the expression:
$J_{||}(R_I) = [\nabla_\perp \cdot (\sum \cdot \nabla\Phi)_\perp]_{R=R_I}$, where $\sum$ is the integrated ionospheric con-

ductance tensor, Φ is the potential and R_I is the Earth radius at the E layer altitude;

5- The ionospheric potential is mapped back to the inner magnetosphere ($2.5R_E$) along the geomagnetic field;

6- The electric field and velocities are calculated at the inner boundary from the ionospheric using the equations $\vec{E} = -\nabla\Phi$ and $\vec{V} = \frac{\vec{E}\times\vec{B}}{B^2}$, where $\vec{E}$ is the electric field and $\vec{V}$ the velocity. Finally, the velocity vector is used as inner boundary condition to the GM component.

In our simulation we use a uniform conductance pattern with Hall and Pedersen conductances of zero and 5 mhos respectively. The uniform zero Hall and non zero Pedersen conductance pattern is a simple way to estimate a quasi-realistic magnetospheric configuration.

3.2 Processing tools: the Kameleon software

Kameleon is a set of subroutines developed at the CCMC to improve the analysis and dissemination of the different output formats of space weather model data (Community Coordinated Modeling Center, 2014). The Kameleon software is divided in two packages: the Kameleon Converter Package and the Kameleon Access and Interpolation Library, both can be downloaded at CCMC Kameleon (2014).

The Kameleon Converter Package is used to convert the output format of a specific Space Weather model to a Common Data Format (CDF). Therefore the Kameleon Converter allows to standardize the format of the output files generated by the different space weather simulation models.

The Kameleon Access and Interpolation Library is used to get access to the data stored in a CDF file previously converted by the Kameleon Converter. There are two versions of the Kameleon software, the first one (the original) is written in C code and the second one (called generation 2) is an extension of the original version to other programing languages as JAVA, C++, and Phyton and has support for more models.

We analyzed our simulation using the visualization tools available at the CCMC website and the Kameleon software. The Kameleon set allows us to directly access the simulation data and to build up more specialized output plots.

We use the original version of the Kameleon software, which has support for the following models:

1) 3D Magnetosphere: BATS-R-US, OpenGGCM/UCLA-GGCM;

2) Ionosphere: CTIP;

3) Heliosphere: ENLIL;

4) Solar: MAS.

The first step is to convert the original output files of the BATS-R-US simulation to CDF files. This is done by the CCMC site through the CDF request service, the time steps or the interval of interest of the run can be specified. After we have stored in local disk the CDF files of the run, we used the Kameleon Access Interpolation Library to interpolate the value of a variable at one specific point.

The Kameleon Access and Interpolation Library has 17 main C routines that are currently available. The main library of routines are written in C, but most of the functionality provided by these C routines can be acquired by using the FORTRAN interface that is also included within this library. We use only three routines to get the value of a variable at a space point, these are ***open_cdf*** to open a CDF file, ***interpolate_batsrus_cdf*** to interpolate a variables stored in a CDF file, and ***close_cdf*** to close a previously open CDF file. For spatial interpolation, an example of how only three calls are required to get a value for any specified variable and position is shown below:

...

```
open_cdf(cdf_name, 0);
interp_value = interpolate_batsrus_cdf(variable_name, x, y, z, 0, 0);
close_cdf();
```

...

The variable *cdf_name* is the path/filename of the CDF file that contains data to be interpolated, *variable_name* is one of the principals output variables of the BATS-R-US code (*rho, b1x, b1y, b1z, bx, by, bz, ux, uy, uz, jx, jy, jz, p, e*) and x, y , z are the position at which variables will be interpolated. The return variable *interp_value* contains the interpolated value. More information about how to use these functions in a custom application can be found at CCMC Kameleon (2014).

We developed a set of MATLAB functions in order to call Kameleon subroutines inside a MATLAB environment. This has been done with the objective of taking advantage of the higher level functions available in MATLAB. Therefore working inside this environment allow us to create more specialized plots to process our data. The MATLAB functions we developed are listed in Appendix A.

4 RESULTS AND DISCUSSIONS

In this chapter we analyze the results from a single simulation run with the initial conditions described in Table 3.1. We are interested on studying the polar cap potential affected by bursty and unsteady processes in the magnetopause and in the magnetotail. The GSM coordinate system is used.

A global view of the interaction of the solar wind with the Earth's magnetosphere in our MHD simulation can be seen in Figure 4.1. The orientation of the IMF (pink lines) and the formation of the magnetosheath (green region of density ≈ 10 particles per cm^3) can be observed. The plasma flow is represented by the white solid lines with arrows.

From a global point of view of our simulation, the bow shock lies around $14R_E$ and the magnetopause is about $8.5R_E$, therefore the magnetosheath have a thickness along the Sun-Earth line of approximately $5.5R_E$. The plasma density in the magnetosheath is about $10cm^{-3}$ which is low compared to the typical conditions of the solar wind. The low density and the higher thickness of the magnetosheath are due to the strong IMF. For intense IMF the solar wind Alfvén speed ($V_A = \frac{B}{\sqrt{\mu_0 \rho}}$) increases, so the Alfvén Mach number ($M_a = V_{SW}/V_A$) is lower than the small IMF case. A low Mach number means that the bow shock is not close to the compression limit of 4, therefore the magnetosheath is less compressed for large IMF (Lopez et al., 2010).

The solar wind and IMF parameters were kept constant during the whole simulation run, confirming that FTEs can develop spontaneously without changes of the solar wind conditions (Raeder, 2006).

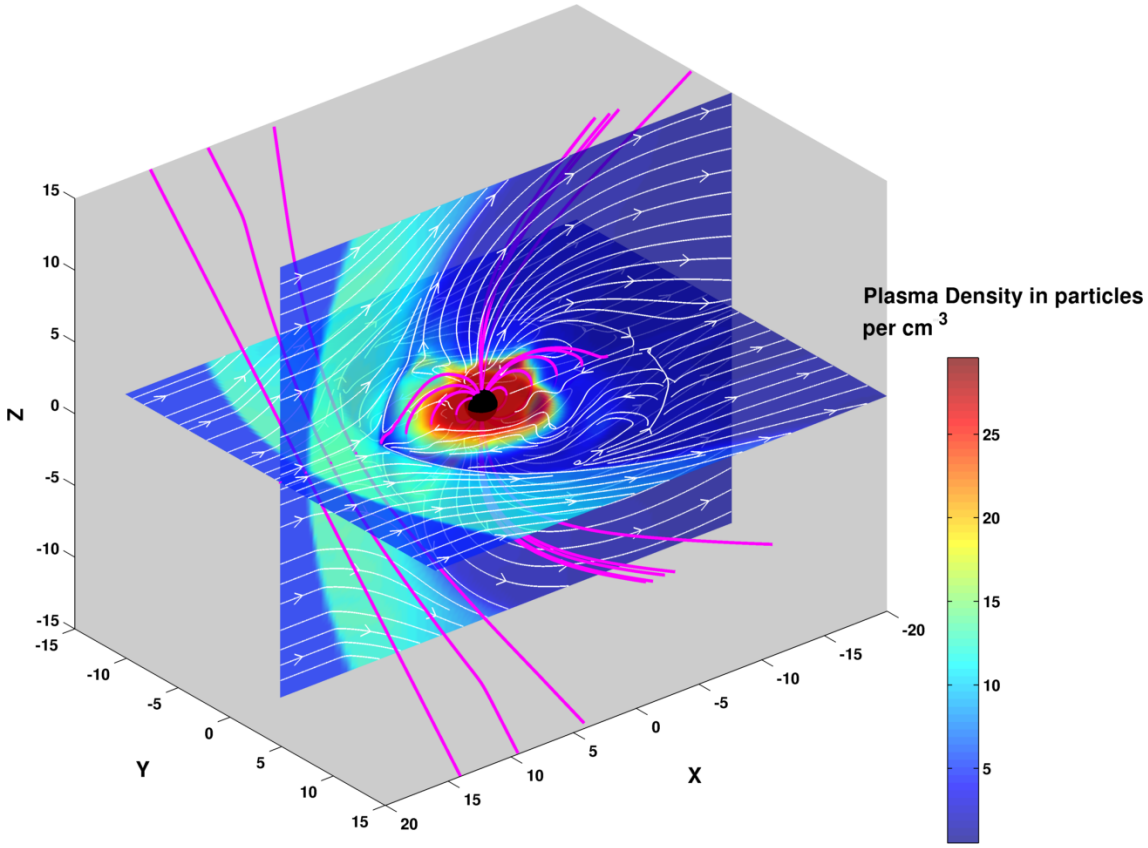

Figure 4.1 - Global perspective of the interaction of the solar wind with the Earth's magnetosphere simulated by the BATS-R-US code. The pink lines represent the IMF and dipolar magnetic field. The white solid lines with arrows represent velocity streamlines. Two cuts are shown, one at $Y = 0$ and the other at $Z = 0$. The color code indicates the plasma density. The sun is on the left and the Earth is represnted as a black sphere in the center.

4.1 Transient Magnetic Reconnection at the subsolar magnetopause

We have detected signatures of FTE events at the subsolar magnetopause. Figure 4.2 shows the magnetic field at two specific space points near the subsolar magnetopause. The magnetic probes were placed in the Northern Hemisphere at $x = 8.5R_E, y = -0.3R_E, z = 0.7R_E$ (Figure 4.2(a)) and in the Southern Hemisphere at $x = 8.5R_E, y = 0.8R_E, z = -1R_E$ (Figure 4.2(b)). The first probe was located in the northern dawn quadrant ($Z > 0, Y < 0$) and the second in the southern dusk quadrant ($Z < 0, Y > 0$). We put many probe points around the subsolar magnetopause, but the two points of Figure 4.2 have been chosen because the magnetic signatures of the FTEs were more clear observed in these particular locations.

For every step of the run, the magnetic field components are measured in the GSM

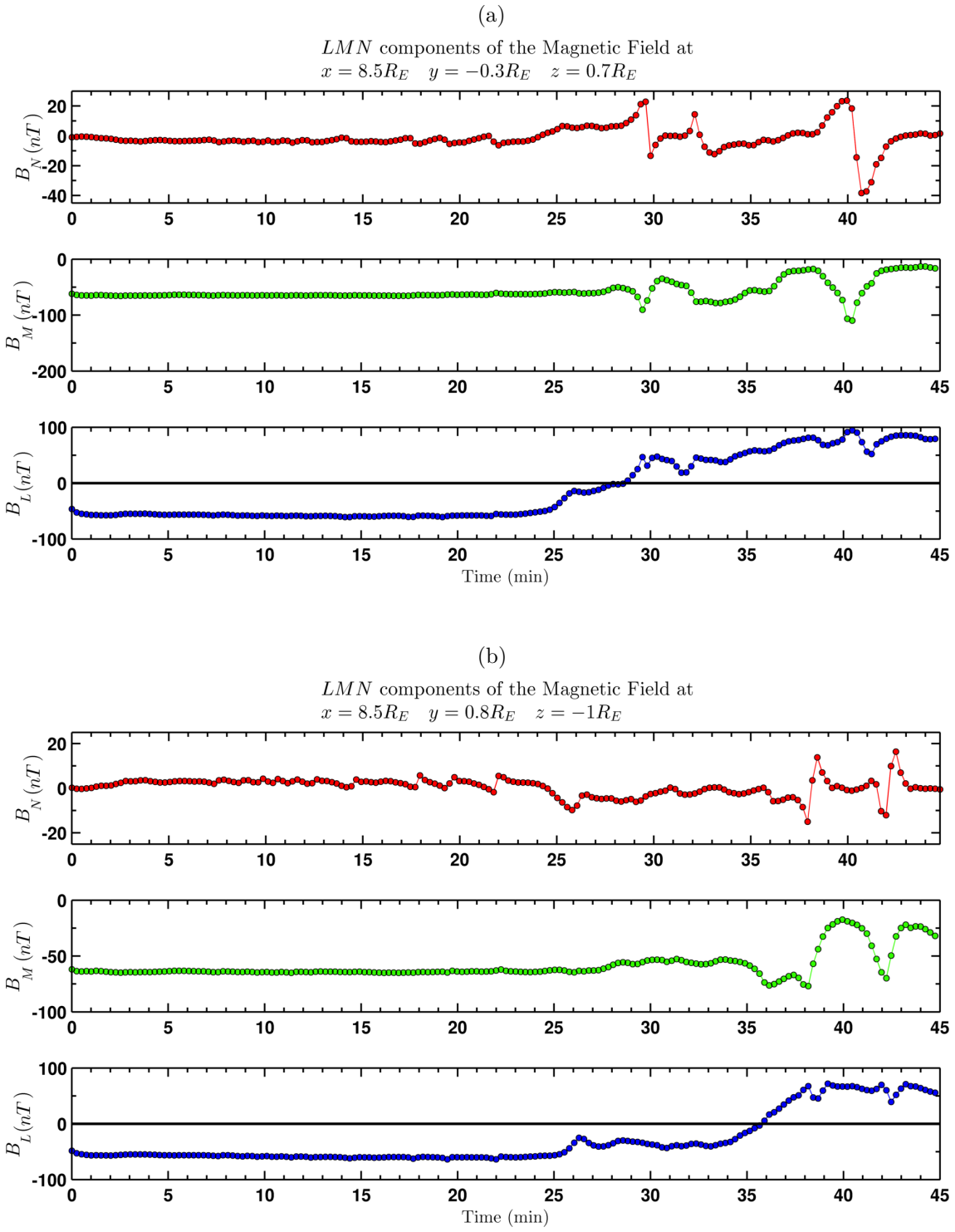

Figure 4.2 - Observations of the simulated magnetic field in boundary normal coordinate system close to the magnetopause. The circles indicates samples taken every $15s$ by the virtual probe. **a)** The probe is located in the Northern Hemisphere at $x = 8.5R_E, y = -0.3R_E, z = 0.7R_E$. **b)** The probe is located in the Southern Hemisphere at $x = 8.5R_E, y = 0.8R_E, z = -1R_E$.

coordinate system. Afterward, we convert the components of the magnetic field from GSM coordinate to magnetopause boundary coordinate system using the following steps:

1- The subsolar magnetopause is calculated as an isosurface of $B_Z = 0$;

2- The two nearest points of the isosurface to the probe location are found. With these three points we can define two tangential vectors to the magnetopause. The unitary vector normal to the magnetopause ($\hat{N}$) is calculated as the vectorial product of the tangential vectors and divided by the norm of the result;

3- The other two base vectors of the LMN coordinate system are defined as: $\hat{M} = \hat{N} \times \hat{z}$ and $\hat{L} = \hat{M} \times \hat{N}$;

4- The components of $\vec{B}$ are transformed from the GSM system to the boundary normal system using the following transformation matrix:

$$\begin{pmatrix} B_L \\ B_M \\ B_N \end{pmatrix} = \begin{pmatrix} \hat{L}_X & \hat{L}_Y & \hat{L}_Z \\ \hat{M}_X & \hat{M}_Y & \hat{M}_Z \\ \hat{N}_X & \hat{N}_Y & \hat{N}_Z \end{pmatrix} \begin{pmatrix} B_X \\ B_Y \\ B_Z \end{pmatrix}, \tag{4.1}$$

where $\hat{L}_i, \hat{M}_i, \hat{N}_i$ with $i = X, Y, Z$, are respectively the GSM components of the $\hat{L}, \hat{M}, \hat{N}$ vectors.

Figure 4.2(a) shows the magnetic data at the point located in the Northern Hemisphere. The typical bipolar signature of the FTE (bipolar B_N) can be observed in the first panel of Figure 4.2(a). Three events have been detected by the probe at the Northern Hemisphere. The first one takes place at about 29:00 (minutes:seconds) of simulation, the second one at about 32:00 and the third one about 40:00. In all the cases the normal magnetic field B_N goes first outward to the magnetopause (+ positive) followed by an inward (- negative) perturbation of B_N. Therefore, the polarity of the bipolar signature is of the "direct" (+/−) kind (Cowley, 1982). In all the events, except the second one, the bipolar signature is almost symmetric. In the second event (at 32:00), the leading outward magnetic field B_N is larger than the inward B_N behind it. We believe that the center of the structure of the second FTE in the Northern Hemisphere does not pass near the magnetic probe.

Figure 4.2(b) shows the magnetic field data at a point located near the subsolar point, but southward of the equator (South Hemisphere). Two bipolar signatures

were detected by the probe at 38:00 and 42:00 of simulation (first panel Figure 4.2(b)). In this case the normal magnetic field B_N in both events first point inward (- negative) as the structure approaches the probe and then outward (+ positive) as it departs. This polarity is called "reverse" and was first reported by Rijnbeek et al. (1982). The reverse polarity $(-/+)$ is associated with FTEs located south of the equator. Therefore our observation of the simulated bipolar signatures is in agreement with previous observations: "direct" in the northern hemisphere and "reverse" in the southern hemisphere. Actually, if we are going to be more rigorously, the bipolar signature of FTEs are "direct" or "reverse" depending if the probe (or spacecraft) is located north or south respectively to the X reconnection line.

In the second panel of Figures 4.2 a and b, is shown the $\hat{M}$ component of the magnetic field B_M. This component points dawnward.We can observe an intensification of the B_M component during these FTE events. This behavior is named in the literature as enhancement of the core magnetic field and is another typical signature of the FTEs. The second panel of Figure 4.2(a) (Northern Hemisphere) shows a clear enhancement of the B_M component (core magnetic field) related to the bipolar signatures observed at the time 29:00 and 40:00. There is also an increase of the B_M component associated with the second FTE at 32:00, but we can not determinate exactly if it is related to this event due to the spread of the enhancement. In the same way, associated with the second bipolar signature of Figure 4.2(b) (Southern Hemisphere) there is a very clear increase of the B_M component at $\sim$ 42:00. It is not the case for the FTE at about 38:00, where the intensification of the core magnetic field is not very obvious. This result is not contradictory because the defining signature of FTEs is the bipolar signature of B_N. The intensification of the core magnetic field is not reported in every FTE, therefore is not a necessary condition.

The third panel of Figure 4.2 a and b shows when the magnetopause crosses the virtual probe. This time is defined as the intersection of the $B_L = 0$ line with the curve of the B_L data. In this case all the FTEs magnetic field data were collected at the magnetosphere side.

4.1.1 FTEs detection and study

Starting from approximately the minute 25 of simulation (Figure 4.2), we detected five FTEs. Three of them were observed only in the Northern Hemisphere and from now on they will be called FTE1, FTE2 and FTE4. The other two FTEs were detected only in the Southern Hemisphere and from now on they will be called FTE3 and FTE5. The designation of the numbers are due to the occurrence in time.

We observe in both hemispheres a series of bipolar signatures of minor strength in the B_N component during the time interval between the minutes 16 and 23 (see Figure 4.2 a and b first panel). These events occur quasi-periodically with a period of $\sim$ 2 min. Hereafter, this sequence of events between 16-23 minutes will be named FTEs0.

The virtual probe method used in Figure 4.2 has the disadvantage that we don't know the exact time of the formation of the FTE, because it give us only the time of crossing of the structure through the virtual probe. Another disadvantage is that the resolution is limited to the 15s time step of the simulation. Thus, to study the principal characteristic of the FTEs, we create a more specialized method that take advantage of the high spatial resolution at the subsolar magnetopause. This method is illustrated in Figure 4.3.

First we find out the position of the magnetopause at the subsolar point at about 20 : 00 after the simulation starts. The subsolar magnetopause is calculated as an isosurface of $B_Z = 0$, which is represented in Figure 4.3 (red surface). The calculated distance of the magnetopause at the subsolar point is $8.44R_E$ at about 20 : 00. A distance slightly greater than this is substituted in the following formula of the Shue et al. (1997) model of the magnetopause:

$$r = r_0 \left(\frac{2}{1 + cos\theta} \right)^{\alpha} , \tag{4.2}$$

where r is the radial distance and θ is the solar zenith angle. This model has two parameters, r_0 and α, representing the standoff distance of the subsolar magnetopause and the level of tail aperture respectively. We used the stand off distance of $r_0 = 8.62R_E$ and a value of $\alpha = 0.05$. Using these values we calculated a line that fit very well with the magnetopause. Finally the quasi-parabolic line is rotated 30^o counterclokwise (black line Figure 4.3 a and b) to cover better the northern dawn quadrant ($Z > 0, Y < 0$) and the southern dusk quadrant ($Z < 0, Y > 0$).

For every specific time of the run we measure the magnetic and plasma data in 300 points of the line path, always starting from the Southern Hemisphere. The normal vector to the magnetopause $\hat{N}$ is calculated deriving the normal in spherical coordinates of the curve in Figure 4.3 (Equation 4.2). The vector $\hat{M}$ and $\hat{L}$ are calculated respectively as $\hat{M} = \hat{N} \times \hat{z}$ and $\hat{L} = \hat{M} \times \hat{N}$. Finally we transform the B_X, B_Y, B_Z components into B_N, B_M, B_L using as basis the $\hat{L}, \hat{M}, \hat{N}$ vectors. Figure 4.3(a) shows for a few points the normal boundary system at that points.

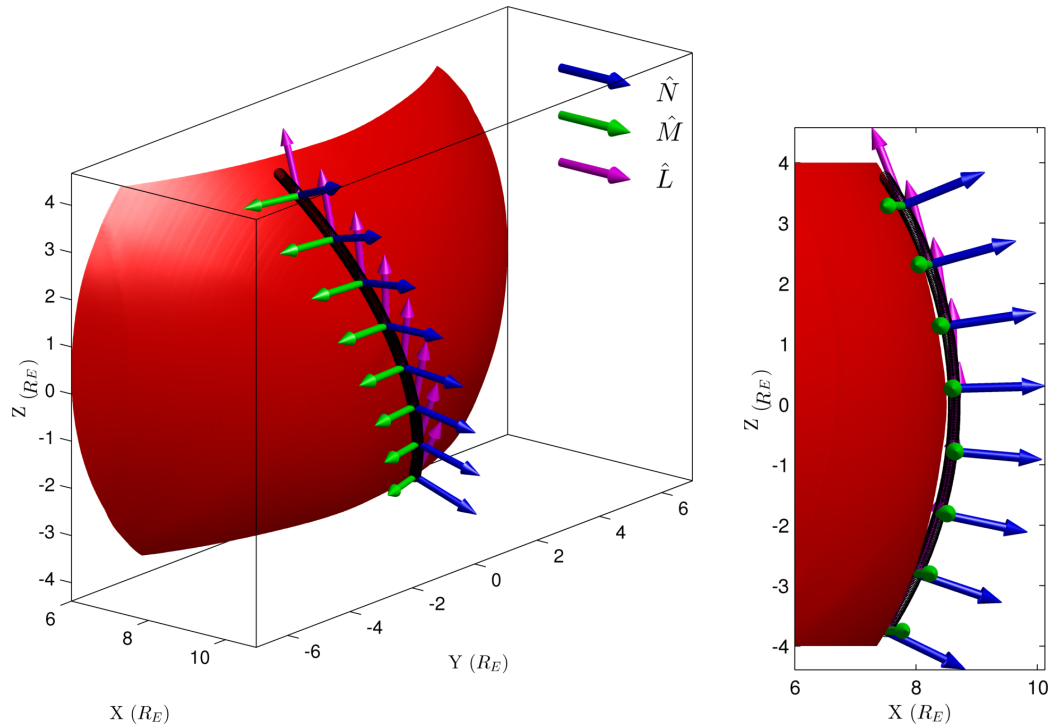

(a) (b)

Figure 4.3 - Illustration of the path chosen to plot the magnetic and plasma data using the Shue et al. (1997) model. In the case of vectorial data, as for example $\vec{B}$, a local magnetopause boundary coordinate system is used. The vector basis of this system is represented as: $\hat{N}$, blue arrow pointing normal to the magnetopause; $\hat{M}$, green arrow; and $\hat{N}$ color magenta arrow. The red surface represents an isosurface of $B_Z = 0$ **a)** Three-dimensional view, the Sun is to the right and the Earth to the left. **b)** Same as (**a**), but the view is from the negative Y axis. In this perspective it is shown that the path is very close to the magnetopause.

Figure 4.3(b) is the same as the previous one but with the view from the negative Y axis.

FTEs0

The results of the probing method described above is shown in the sequence of Figures 4.4, 4.5, 4.6, 4.7 and 4.8 for every FTE. This method is essentially a spatial plot through a trajectory very close to the magnetopause, starting from the point $X = 7.5R_E$, $Y = 2.17R_E$, $Z = -3.75R_E$ and ending at $X = 7.5R_E$, $Y = -2.17R_E$, $Z = 3.75R_E$, i.e., from southern-dusk quadrant to northern-dawn quadrant.

We start detecting signatures of instabilities at the subsolar magnetopause at about 07:00. Small bipolar signatures of about 4nT peak to peak of B_N were detected in both hemispheres. Between 07:00 and 15:00 we observe at least 7 events with these characteristics, each one lasting ∼1 minute. The variation in B_N is too low to affirm that these events are FTEs, however this is a sign that the magnetopause is becoming unsteady as will be shown in the next subsections.

From 17:45 to 22:30 sequences of three bipolar signatures of B_N were observed in both hemispheres (see Figure 4.2 a and b during this interval). These series of FTEs have a periodicity of ∼2 minutes and as a whole we named it FTEs0 because they share the same properties. In particular, Figure 4.4 shows the evolution of the first FTE of the sequence of events observed from 17:45 to 22:30, in terms of B_N component (bottom plot) and the total magnetic field $|\vec{B}|$ (top plot). Each color represents a different time instant for the same event. The negative/positive portion of the abscissa in the plot of Figure 4.4 corresponds to the southern/northern half of the magnetopause model curve. The plot begins in the Southern Hemisphere and ends in the Northern Hemisphere (see Figure 4.3). The x-axis represents the distance from the subsolar point along the path.

The bipolar signature of this FTE is first observed about 17:45 (yellow line). It is not observed at the subsolar point, but only after it travels $1R_E$ in both directions. It reaches the highest B_N bipolarity at 18:30 (red line), which value is $\Delta B_N \approx 15nT$ peak to peak. It is important to notice that because the plot always begins in the southern end of the model curve, the bipolar signature is always a negative pulse followed by a positive pulse. This aspect can be explained as follow: the trajectory path first reach the FTE at its southern side, where the magnetic field enters to the magnetopause (negative sense), and at the northern side of the FTE the magnetic

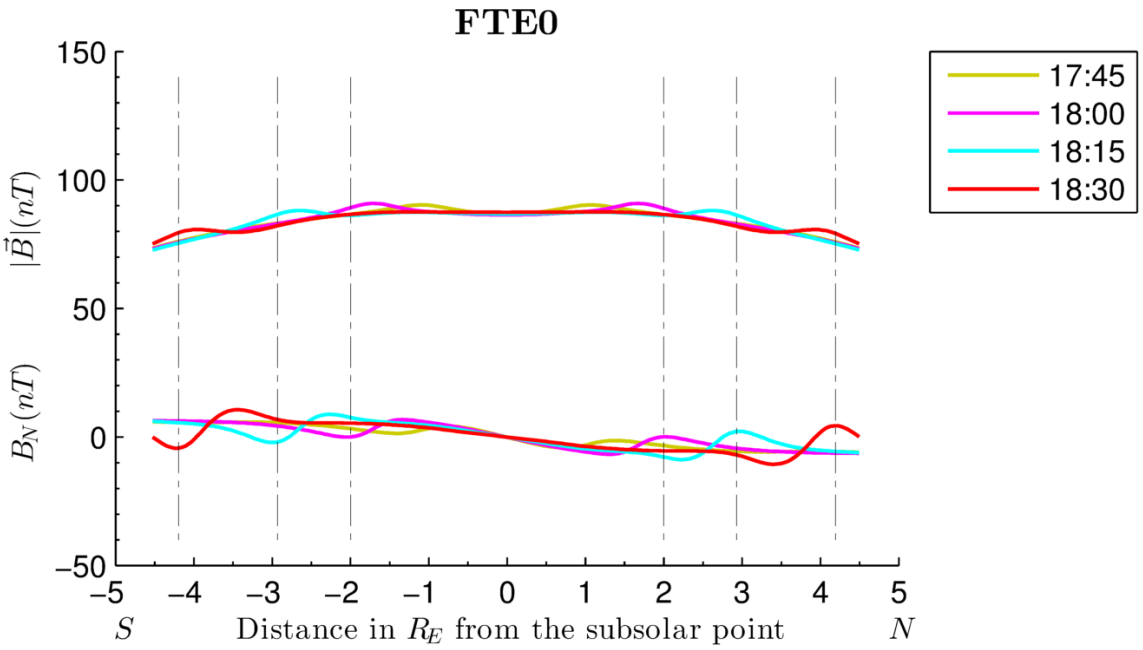

Figure 4.4 - Plots of the normal component of the magnetic field **(bottom)** to the magnetopause and total magnetic field strength **(top)**. The x-axis corresponds to the length of the trajectory of the Shue et al. (1997) magnetopause model, taken as reference the subsolar point. Negative and positive values indicate that the measures were taken in the Southern and Northern Hemisphere respectively along the trajectory. Each color means a specific time run. The vertical dashed lines indicates the position of the negative and positive peaks of B_N.

field points outward of the magnetopause (positive sense).

Analyzing Figure 4.4 we can notice that the FTE develops at the subsolar point, probably product of transient reconnection, and two magnetic field signatures are produced in each hemisphere due to this single FTE. This case is in agreement with the "bursty X line" reconnection model for FTE generation (Scholer, 1988), for which a single FTE produces two pressure bulges with bipolar signatures in each hemisphere.

The advantage of this kind of plot is that we can measure directly the propagation speed of the FTE, using either the maximum of the $|\vec{B}|$ or the maximum positive/negative excursion of the B_N component. In the case of the three events called FTEs0, we use the maximum of the B_N for the Northern Hemisphere (see the vertical dashed lines at the positive part of Figure 4.4) and the minimum of the B_N for the Southern Hemisphere. Only the positive or negative peak of the B_N component

can be chosen to calculate the propagation velocity of the events called FTEs0. The total magnetic field can not be used to that end, since there are not signatures of intensification of the core magnetic field that we can track. Then, we compute two velocities and the mean velocity of the FTE is the average of the two velocities. For example:

$$V_1 = \left(\frac{D^+_{B_N}(18:15) - D^+_{B_N}(18:00)}{15\,s} \right) \tag{4.3}$$

where $D^+_{B_N}(18:15)$ is the distance at which the B_N is maximum for the time 18:15 (see Figure 4.4 second vertical dashed line at the north side), $D^+_{B_N}(18:00)$ is that same distance 15s earlier (see Figure 4.4 first vertical dashed line at the north side). Substituting these values from Figure 4.4 and the value of $R_E = 6371km$ we obtain $V_1 = 395km/s$. The same procedure is performed for the time instants at 18:30 and 18:15 (third an second vertical dashed lines of Figure 4.4):

$$V_2 = \left(\frac{D^+_{B_N}(18:30) - D^+_{B_N}(18:15)}{15\,s} \right) \tag{4.4}$$

the result is $V_2 = 536km/s$. Therefore the mean velocity is : $V_m = \left(\frac{V_1 + V_2}{2} \right) = 465km/s$. The same value is obtained for the southern bipolar signature, in this case the minimum peak of B_N is used.

Two velocities are calculated because we noticed that the FTEs are accelerated since its formation, therefore we calculated one velocity at the beginning and another one at the end in order to estimate an average value. The calculation of the acceleration of FTEs will be left for future works.

FTE1

Figure 4.5 shows the evolution of the FTE1, where the bipolar signature of B_N was first detected at 24 : 00 (yellow line at the bottom plot). It starts to grow at the magnetopause subsolar point up to a value of $B_N = \pm 35nT$ or $70nT$ peak to peak, which is considered a high value (see red line of B_N). From 24:00 to 27:45 the FTE does not move from the subsolar point. Also it can be noticed from Figure 4.5 (red and green lines at the top plot) an strong intensification of the total magnetic field (B_T) from $\sim 60nT$ up to $\sim 120nT$ at the center. This increase of B_T is directly related with an intensification of the core magnetic field relative to the ambient

magnetic field by the ratio: $\delta B = \left(\frac{B_{Tcenter}}{B_{Tambient}}\right) \approx 2$.

At about 27:45 the bipolar signature and the peak of the magnetic field magnitude start to move to the north (positive x-axis). Also the strength of both the bipolar signature and the total magnetic field at the center begins to decrease as the structure move away from the subsolar point.

The mean velocity is calculated using the same procedure for the early FTEs (FTEs0), but in this case the peaks of total magnetic field magnitude are taken as reference points of the center of the structure. The mean velocity of the structure is $V_m = 120km/s$, which is very close to the average value of $125km/s$ found in observations (Dailey et al., 1985).

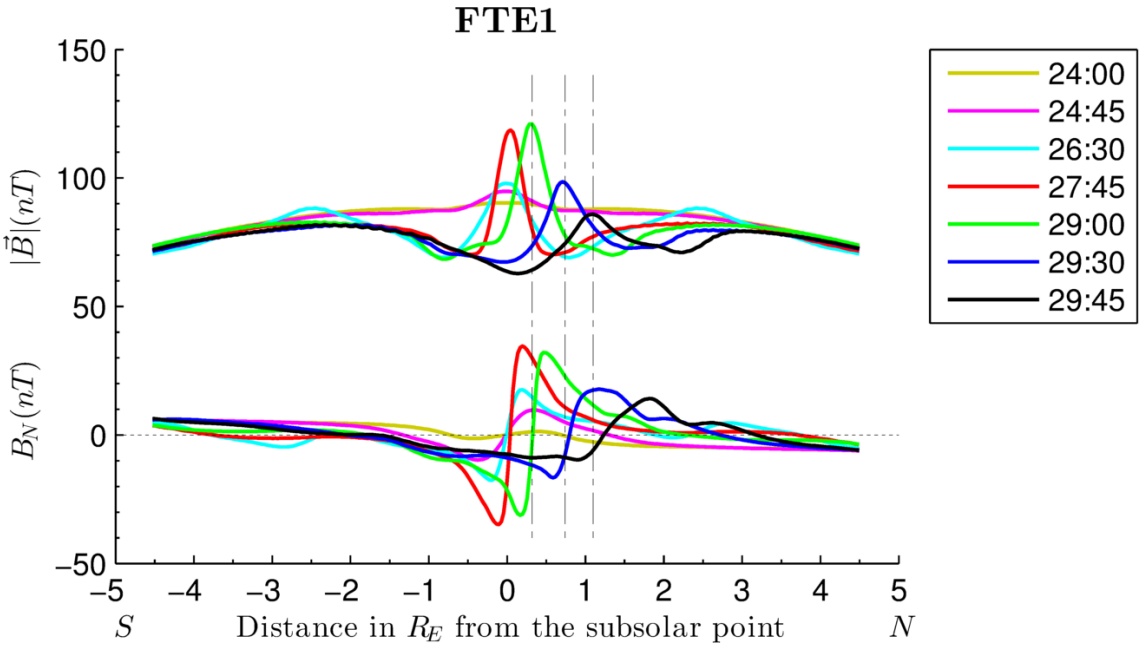

Figure 4.5 - Plots of the normal component of the magnetic field **(bottom)** and total magnetic field strength **(top)** for the time interval from 24:00 to 29:45. The x-axis corresponds to the length of the trajectory of the Shue et al. (1997) magnetopause model, taken as reference the subsolar point. Negative and positive values indicate that the measures were taken in the Southern and Northern Hemisphere respectively along the trajectory. Each color means a specific time run. The vertical dashed lines indicate the position of maximum peaks of the total magnetic field for the last three times.

This FTE is the first in our simulation that breaks the hemispheric symmetry in the magnetopause in the sense that this and the next events will produce a magnetic

perturbation in only one hemisphere, i.e., the single FTEs will propagate only to the Northern Hemisphere or the Southern Hemisphere. In the case of the FTEs observed before this one, two bipolar signatures were reported in each hemisphere (see Figure 4.4).

FTE2

The evolution of the magnetic signature of the event FTE2 is shown in Figure 4.6. The bipolar signature was first detected about 31 : 30 (yellow line at the bottom plot), which can be considered the start of the formation of the FTE. The region of formation of the bipolar signature is displaced from the subsolar point towards the south by $0.4R_E$, i.e., the point of formation is around $-0.4R_E$. This is an indication that the X-reconnection line have moved to the south. The bipolar signature grows as the time goes on and simultaneously it moves to the north. The maximum value peak to peak of B_N is reached at about 33:00 (green line at the bottom plot) and the value is $27nT$ ($B_N^+ \approx -15nT$ and $B_N^- \approx 12nT$).

The total magnetic field also shows an intensification at the center of the FTE compared with the magnetic field at the edges of the structure (top plot of Figure 4.6). The ambient magnetic field at the edges and at the center (time 33:00) is about $66nT$ and $90nT$ respectively, which represent a relative increase of ~ 1.4. This increase occurs during the movement of the FTE. After about 34:30 (not shown in Figure 4.6) the two signatures disappear.

The points where the normal magnetic field is zero (between the negative and positive peaks), coincide with the maximum values of the total magnetic field (vertical dashed lines of Figure 4.6). These points can be considered the center of the FTE and they are used to measure the mean velocity, which is $V_M = 102km/s$.

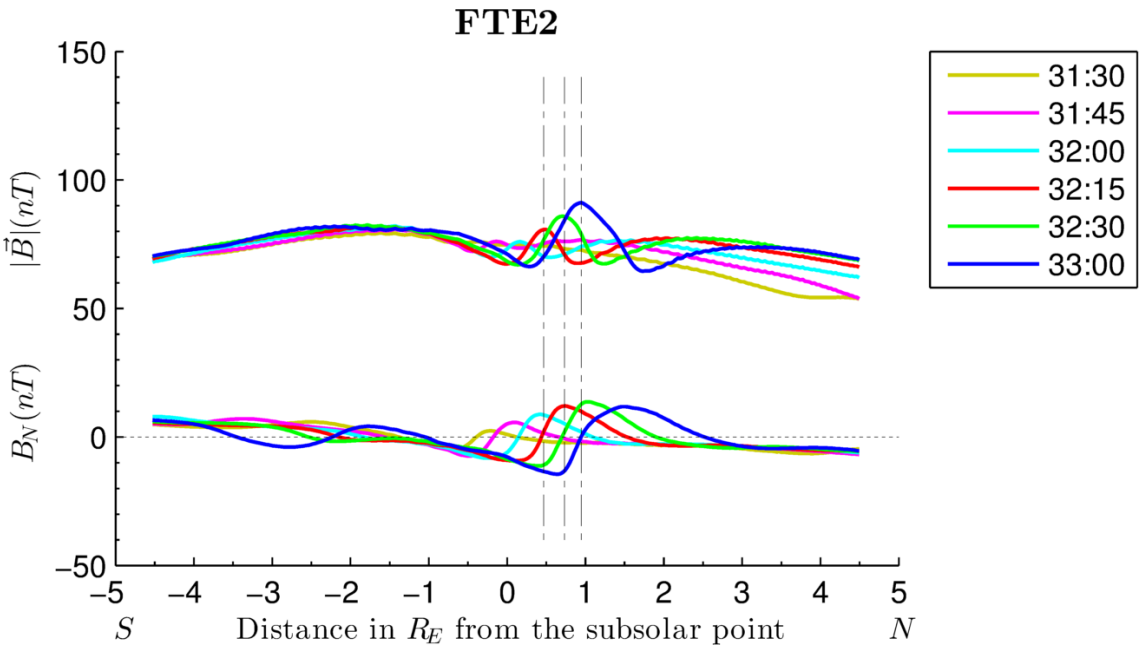

Figure 4.6 - Plots of the normal component of the magnetic field **(bottom)** and total magnetic field strength **(top)** for the time interval from 31:30 to 33:00. The x-axis corresponds to the length of the trajectory of the Shue et al. (1997) magnetopause model, taken as reference the subsolar point. Negative and positive values indicate that the measures were taken in the Southern and Northern Hemisphere respectively along the trajectory. Each color means a specific time run. The dashed vertical lines indicate the position of maximum peaks of the total magnetic field for the last three times.

FTE3

This FTE originate at about 37 : 15 (yellow line in Figure 4.7 bellow) and ends at $\sim 38:45$ (not shown). The magnitude of the bipolar signature is $\sim 29nT$ peak to peak ($B_N^- = -10nT$, $B_N^+ = 19nT$)). The relative increase of the magnetic field intensity compared with the ambient magnetic field is $\delta B = 1.85$ (from $\sim 55nT$ on the sides to $\sim 100nT$ at the center).

The principal difference of this event with the previous ones is that it propagates to the south as time advances (see sequence of colored lines in Figure 4.7). The measured propagation speed for this FTE is $V_M = 229km/s$.

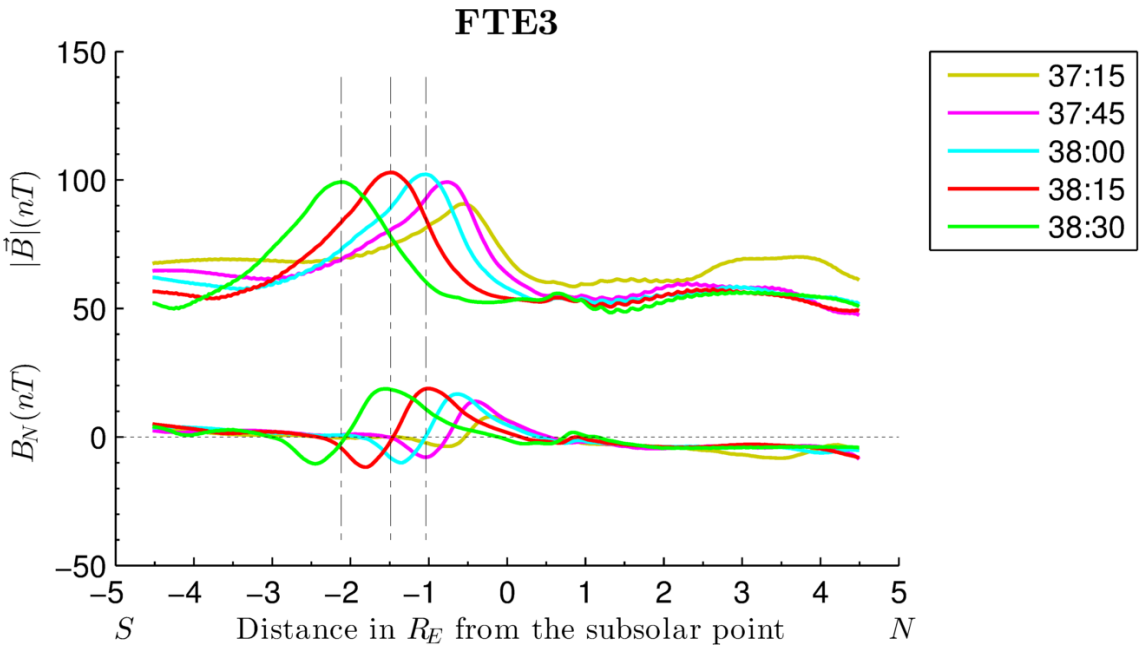

Figure 4.7 - Plots of the normal component of the magnetic field **(bottom)** and total magnetic field strength **(top)** for the time interval from 37:15 to 38:30. The x-axis corresponds to the length of the trajectory of the Shue et al. (1997) magnetopause model, taken as reference the subsolar point. Negative and positive values indicate that the measures were taken in the Southern and Northern Hemisphere respectively along the trajectory. Each color means a specific time run. The dashed vertical lines indicate the position of maximum peaks of the total magnetic field for the last three times.

FTE4

This event produces the largest magnetic perturbation of all the FTEs. It originates around 39 : 00 at a location of $0.5R_E$ northward to the subsolar point (see Figure 4.8). During the first minute of formation (from 39 : 00 to 40 : 00) both the bipolar signature and the total magnetic field increase, however the structure remains at the same place. At some point between 40 : 00 and 40 : 45 the FTE began to move towards north, with a mean speed of $V_M = 127km/s$, which is very close to the average speed of FTE1.

In this case we use the positive peak of B_N (B_N^+) as reference point to measure the mean speed of the FTE (see the three vertical dashed lines at the bottom plots of Figure 4.8). This choice is because of the maximum of the total magnetic field and the negative peak of B_N (B_N^-) do not move at the same speed of B_N+. The leading part seems to move faster than the trailing part of the FTE between 40:45 and 41:30

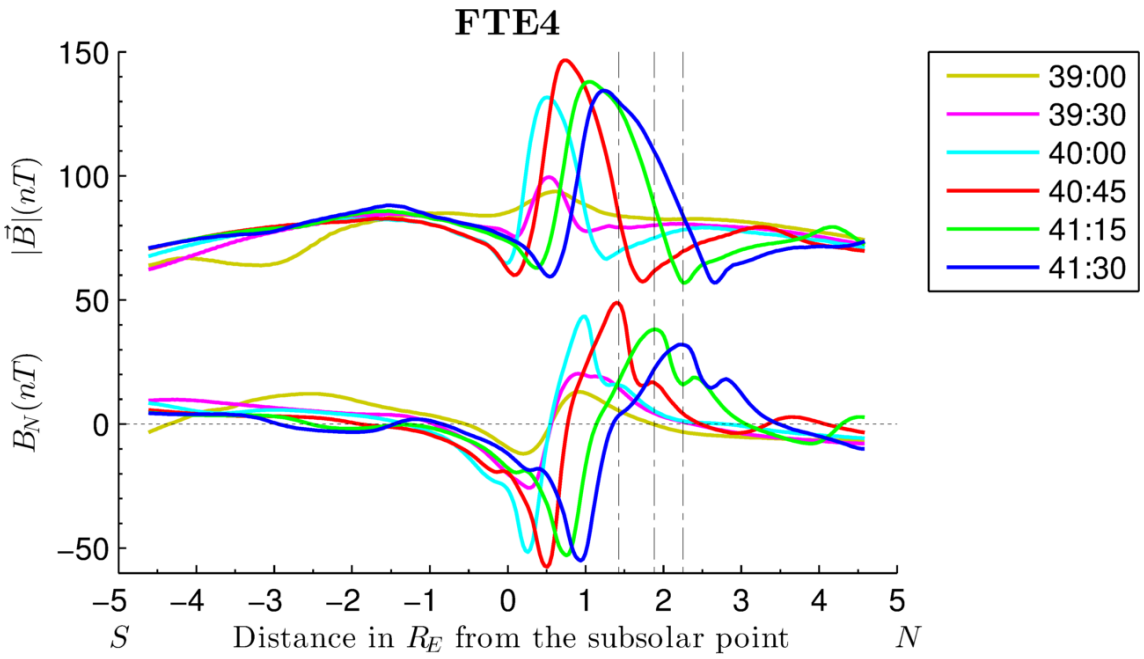

Figure 4.8 - The same as Figure 4.7 but for the time interval from 39 : 00 to 41 : 30. Each color means a specific time run. The vertical dashed lines indicates the position of positive peaks of B_N for the last three times.

but later the B_N^+ peak disappear and just the B_T intensification signature and the B_N^- peak are present (see right part Figure 4.9). During 41:45 to 42:45 the speed of the trailing edge of the structure increases, i.e, it is higher than at the beginning (40:45 to 41:30). If we calculate the mean velocity of the trailing edge using the maximum B_T peak or B_N^- for the whole movement time (40:45 to 42:45), we get a mean speed of $\approx 143 km/s$.

The maximum value of the bipolar signature is $\sim 100nT$ peak to peak ($B_N^+ = 48nT$, $B_N^- = -56nT$) which is very high compared with the observations. The core magnetic field (as measured by the total magnetic field) increase from $\sim 60nT$ to $\sim 146nT$, or a relative increase of $\delta B = \frac{146nT}{60nT} = 2.4$.

FTE5

Finally the last FTE observed in our simulation, FTE5, is shown in the left half of Figure 4.9 (negative x-axis part). The magnetic perturbations on the positive part (Northern Hemisphere) are due to the last stage of FTE4.

The bipolar B_N signature of this FTE starts at about 41 : 45 and arise around $-1R_E$ from the subsolar point (Southern Hemisphere). The value of the maximum bipolar

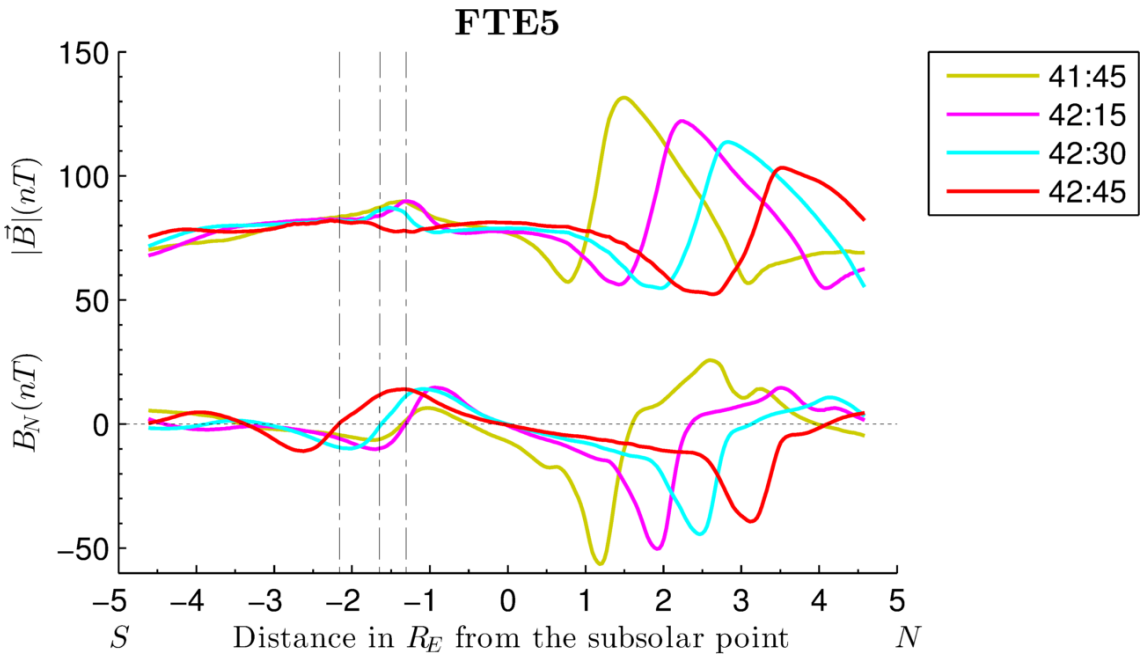

Figure 4.9 - The same as Figure 4.7 but for the time interval from 39:00 to 41:30. Each color means a specific time run. The vertical dashed lines indicates the position of the points between the two peaks of B_N that intersects the $B_N = 0$ line for the last three times.

B_N is $\sim 20nT$ peak to peak ($B_N^+ = 15nT$, $B_N^- = -10nT$). A very weak intensification of the total magnetic field from $\sim 82nT$ to $90nT$ is observed ($\delta B = 1.1$). The bipolar signature grows from $41:45$ to $42:15$ and after this time it starts to move towards south with a mean velocity of $V_M \approx 182km/s$. The points between the two peaks of B_N that intersects the $B_N = 0$ line are chosen as reference points.

The characteristics of the events analyzed in this section are summarized for more clarity in Table 4.1.

Table 4.1 - Summary of the characteristics of the FTEs observed in our simulation.

	FTEs0	**FTE1**	**FTE2**	**FTE3**	**FTE4**	**FTE5**
Bipolar B_N start time (minutes:seconds)		24:00	31:30	37:15	39:00	41:45
Bipolar B_N end time (minutes:seconds)		30:00	34:30	38:45	43:00	43:00
Lasting time of the bipolar signature[1]	1 min	6 min	3min	1min30s	4min	1min15s
Magnitude of the bipolar signature peak to peak	15 nT	70 nT	27 nT	29 nT	100 nT	20 nT
Relative total magnetic field intensification $\delta B = \left(\frac{B_{Tcenter}}{B_{Tambient}}\right)$	-	2.0	1.4	1.85	2.4	1.1
Direction of propagation, North (N) or South (S)	N and S	N	N	S	N	S
Time of movement start	-	28:00	31:30	37:15	40:30	42:15
Speed of propagation (km/s)	465	120	102	229	135	182

[1] In the table *min* stands for minute and *s* for seconds.

4.1.2 Generation and topology of the FTEs

In the last section was shown that despite we observed small magnetic perturbations before the time 24:00, it is after this time that the subsolar magnetopause becomes very unsteady with the occurrence of five well formed FTEs with significant magnetic signatures. The time t = 24:00 can be considered as a breakpoint of the stability and symmetry of the subsolar magnetopause. Throughout this section we analyze the mechanism of generation of the first well formed FTE (FTE1) and the evolution of the magnetic reconnection processes in the dayside magnetopause.

Figure 4.10 a and b show the magnetic topology on a surface very close to the magnetopause, but in the magnetosheath side. The surface is calculated as an isosurface of $B_Z = 0$, which is a very good approximation of the subsolar magnetopause for the conditions of the IMF that we are dealing with, i.e, B_Z southward.

For every point of the isosurface we trace the magnetic field line that belong to this point. If the two ends of the magnetic field lines are inside of the inner magnetosphere ($< 3R_E$), this is a closed or geomagnetic field line. If the magnetic line have only one end inside the inner magnetosphere, then this kind of lines can be classified in two types: connected to the Northern Polar Cap or connected to the Southern Polar Cap in dependence if the coordinate Z of the end point inside a sphere of radius $3R_E$ is positive or negative respectively. If neither of the two extreme points of the magnetic field are inside of the inner magnetosphere, then this is an open magnetic line (IMF) which have the two ends in the interplanetary space. We give the following color classification to the points in Figure 4.10 (and Figure 4.11):

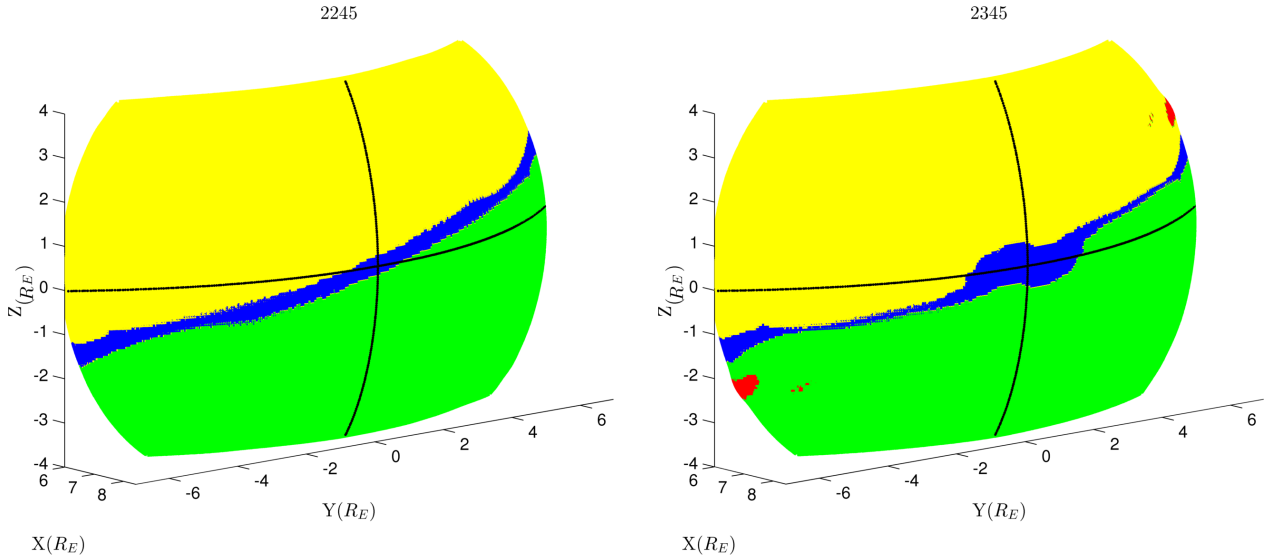

(a) (b)

Figure 4.10 - Magnetic field topology over an isosurface of $B_Z = 0nT$. The surface is very close to the magnetopause, but in the magnetosheath side. The colors represent the magnetic topology as: red, closed; green, one end connected to the south and the other open; yellow, one end connected to the north and the other open; and blue, IMF lines. The black lines shows the intersection of the isosurface with the $Y = 0R_E$ and $Z = 0R_E$ planes. The view is from the north dawnward sun side.

1) red color, if the point belong to a closed (dipolar) magnetic field line;

2) yellow color, if the point belong to magnetic lines with one end on the Northern Polar Cap and the other in the interplanetary space;

3) green color, if the point belong to a magnetic field line with one end connected to the Southern Hemisphere and the other in the interplanetary space;

4) blue color, if the point belong to an IMF field line.

The idea of this technique is to study the magnetic topology of the system, i.e., the structure of the magnetic flux tubes.

An important aspect need to be clarified here. Open and semi-open magnetic field lines do not exist in nature. This is an essential consequence of the Maxwell equations, which postulate no existence of magnetic monopoles. Therefore, the open and semi-open magnetic field lines actually are closed at some point very distant from the source. This terminology is used in the literature to emphasize that the “open”

magnetic line closes at a far point of the interplanetary or interstellar space, i.e., is not tied to the Earth system.

We observe in Figure 4.10(a) that the magnetopause at the magnetosheath side is separated in two principal topological regions: one in the top half with magnetic lines connected to the Northern Polar Cap (yellow region) and the other one in the bottom half with magnetic lines connected to the Southern Hemisphere (green region). The two regions are separated by a thick blue line which represents a region of IMF lines. If we plot a surface very close to the magnetopause at the magnetospheric side (not shown), the whole surface would be of color red (closed geomagnetic line). Figure 4.11 shows the magnetic topology in the noon-midnight plane ($Y = 0$ cut) for the different times, the classification of the regions are the same. The dotted line of the first and second panel indicates the interception of the isosurface of $B_Z = 0$ at 22:45 and 23:45 respectively. A comparison between Figure 4.10(a) and Figure 4.11 (first panel) reveals that the thick blue line is very close to the interception point of the four topological regions where magnetic reconnection occurs. Therefore, the blue band in Figure 4.10(a) is a very good approximation of the reconnection X-line through the magnetopause.

To validate this idea we have calculated the inclination of the reconnection X-line identified by the topology method and compared to the inclination of the X-line as calculated by the well known Gonzalez and Mozer (1974) model. To estimate the inclination of the reconnection X-line from the topology, two points at the blue band of Figure 4.10(a) are chosen (for example the point $x = 7.8R_E$, $y = 3.45R_E$, $z = 0.8R_E$ and the subsolar point). The angle between the projection of the X-line over a plane YZ and the equatorial plane is: $\alpha_{X-line} = \arctan \frac{Z}{Y} \approx 13°$.

In order to calculate the tilt angle of the X-line we use Equation 4.5 (Gonzalez and Mozer (1974) model):

$$\sin\beta = \frac{B_G - B_M \cos\alpha}{\left({B_G}^2 + {B_M}^2 - 2B_G B_M \cos\alpha\right)^{\frac{1}{2}}} , \tag{4.5}$$

where B_G and B_M are respectively the magnitude of the magnetic field extracted $1R_E$ inside and outside the subsolar magnetopause. The magnetic field inside and outside are the geomagnetic and magnetosheath field respectively. The parameter α is the magnetic shear angle between the two magnetic field vectors at the subsolar point, which in our case the value corresponds to 126°. The angle that the field

B_G (geomagnetic field) make with the reconnection line is β, and it is calculated by Equation 4.5. Thus the 90° complement of β is the tilt angle with respect the horizontal Y axis. The result was $\alpha_{X-line} = 14.1°$ which is very close to the value of 13° found using the topology method. Then, until about t=22:45 reconnection is happening along an extended X-line with an inclination of $\approx 13°$ with respect to the equatorial plane.

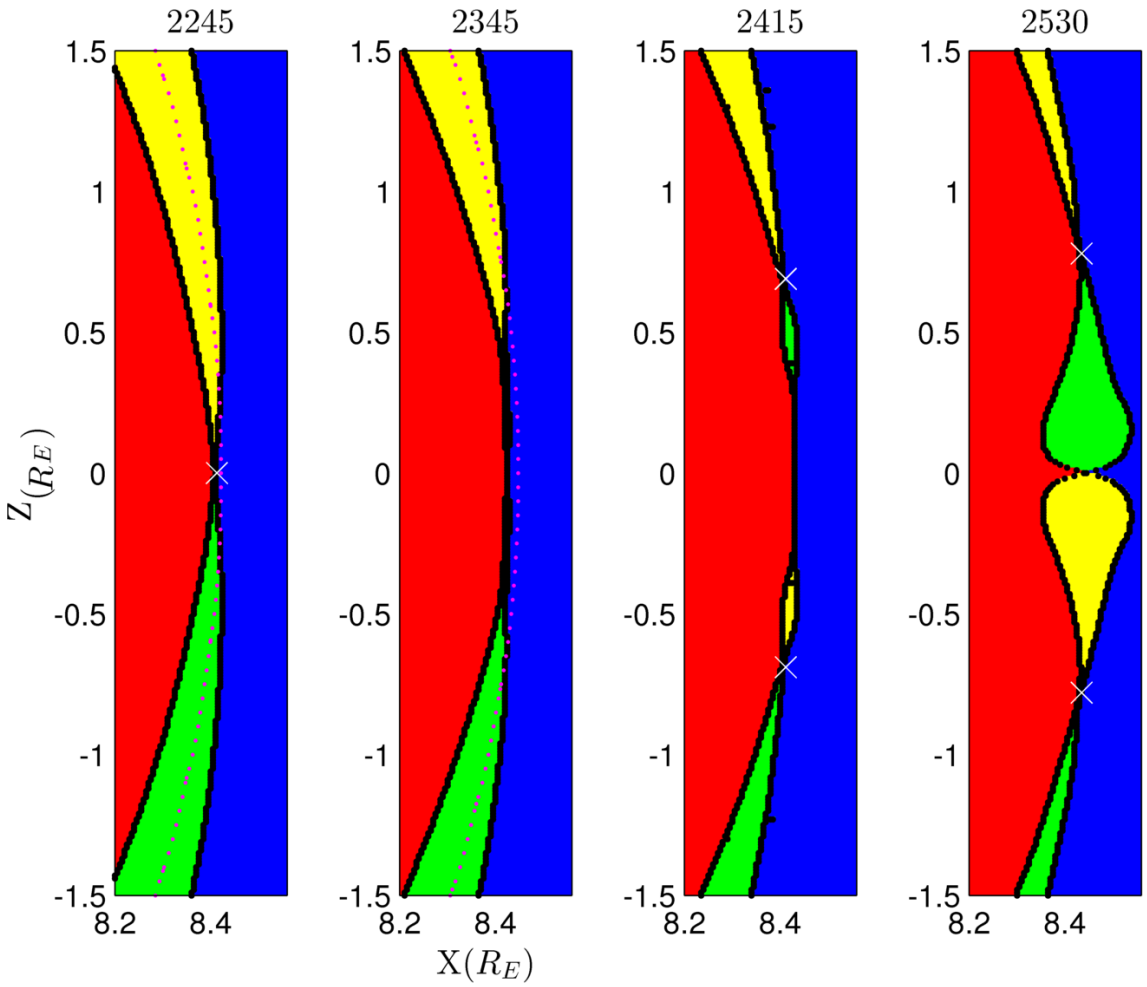

Figure 4.11 - Change of the magnetic topology for the noon-midnight plane ($Y = 0R_E$ plane) for different times. The colors represent the magnetic topology as: red, closed; green, one end connected to the south and the other open; yellow, one end connected to the north and the other open; and blue, IMF lines. The white cross markers show likely reconnection points. The dotted magenta line indicates the intersection of the isosurface of $B_Z = 0$ with the noon-midnight plane.

We identified the following sequence of events during the generation of the FTE1:

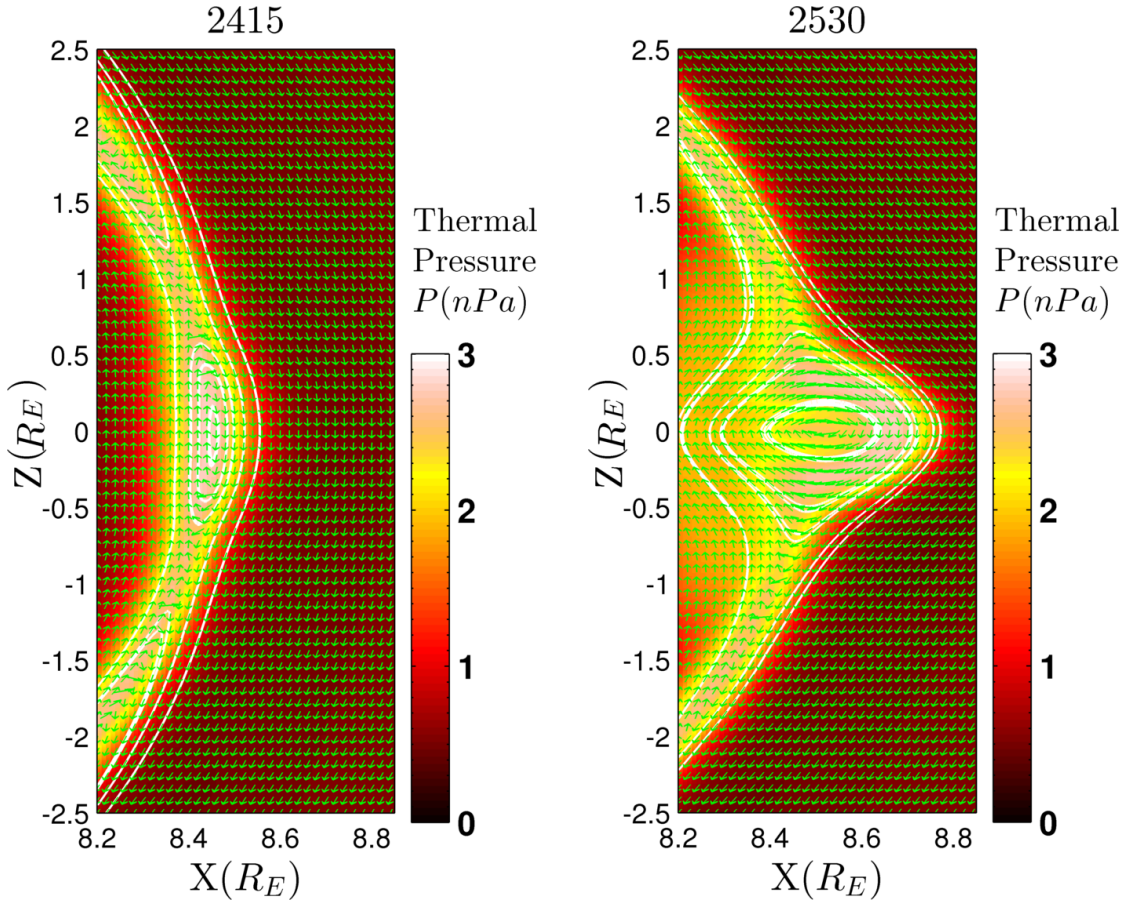

(a) (b)

Figure 4.12 - Formation of the FTE1 for the noon-midnight plane. The plasma thermal pressure is shown in color code. The green arrows indicate the projection of the magnetic field on the $X - Z$ plane. The white lines are projected magnetic field lines. **a)** Beginning of the formation of the pressure bulge at 24:15. **b)** The magnetic structure is well formed with a rotational magnetic field at 25:30.

1- Figure 4.11 (first and second panel) shows that at some time between 22:45 and 23:45 the reconnection topology starts to change. First, at 22:45 a X-point type separating the four different topology regions, as defined by Laitinen et al. (2006), is observed at the center of the first panel of Figure 4.11 (see white cross marker). At the time 23:45 the X-point has disappeared, i.e, there is not a X point where the four topology regions meet. Instead there are two Y type points at $\sim \pm 0.5 R_E$ where three topology regions meet (yellow, red and blue at $0.5 R_E$ and green, red and blue at $-0.5 R_E$). The two Y points are joined by a line that separates the closed (red) and IMF (blue) topological regions.

2- In Figure 4.10(b) it is shown how the change of topology explained above affect

the reconnection line. At the time 23:45 the reconnection site at the magnetopause is no more an extended line as the Gonzalez and Mozer (1974) model. At the subsolar region the IMF magnetic field starts to accumulate producing a deformation of the reconnection line. The vertical black line of Figure 4.10(b) indicates the intersection of the isosurface of $B_Z = 0$ with the noon-midnight plane of Figure 4.11 (second panel), similarly, the dotted color line in Figure 4.11 (second panel) represents the same intersection, but in the $Y = 0$ plane. Gathering the two images it can be seen that the change of topology is restricted to $Y \approx \pm 1.5 R_E$, $Z \approx \pm 1 R_E$, therefore outside this region the magnetic reconnection process is steady (or quasi-steady) along the same X-reconnection line.

3- Figure 4.12(a) shows the projection of the magnetic field over the noon-midnight plane, the green arrows represent the direction (not the magnitude) of the projected magnetic field, the white lines are streamlines of the projected magnetic field and the color code represents the thermal pressure. The accumulation of IMF at the subsolar magnetopause, shown in Figure 4.10(b), causes a bending of the magnetic field in that region and as consequence the creation of an "O" type point. At about $\pm 0.75 R_E$ of Figure 4.12(a) the formation of two X-points at the edges of the "O" shape structure can be observed (similar to the tearing instability). To confirm that these X-points of the projected magnetic field are actually reconnection points we look at Figure 4.11 at $t = 24 : 15$. It can be observed that approximately in the same area ($\pm 0.75 R_E$) there are two points where the four topology regions meet (white cross symbols), therefore this points are places where magnetic reconnection occurs according to Laitinen et al. (2006). Thus, two reconnection places have been formed in the Northern and Southern Hemisphere. Later on in this section we will give more details that complement this idea.

4- Starting from the time $t = 24 : 15$, magnetic reconnection at the new formed X-points produces new topological structures. In the Northern Hemisphere at $\sim 0.75 R_E$ (see Figure 4.11 third and fourth panel), reconnection produces northward and southward connected field lines. Similarly, in the Southern Hemisphere magnetic reconnection at $\sim -0.75 R_E$ produces southward and northward magnetic field lines. As result of the reconnection at the two points, a structure of semi-open magnetic field lines connected to South has formed in the Northern Hemisphere (green lobe of Figure 4.11 fourth panel) and a structure of semi-open magnetic field lines connected to north has developed in the Southern Hemisphere (yellow lobe of Figure 4.11 fourth panel).

This structure was first detected in the same simulation run by Cardoso et al. (2013) and is named interlinked flux tubes. This results confirm the Cardoso et al. (2013) observations of the interlinked flux tubes and also confirm the idea that this peculiar magnetic configuration is due to magnetic reconnection northward and southward of the subsolar point, i.e, multiple X-reconnection lines.

Figure 4.12(b) shows the plasma pressure and the magnetic field projection in the noon-midnight plane for the time 25 : 30. At that time the interlinked flux tubes have already been formed according to the magnetic topology pictures (last panel in Figure 4.11). It can be observed in Figure 4.12(b) a pressure bulge of $\sim 1R_E$ extension in the Z direction. However, the most important aspect in this figure, is that the projected magnetic field has the characteristics of a magnetic flux rope: first, a clear rotation of the magnetic field in two dimension is observed, which is characterized by the formation of an "O" neutral point (see white lines and green arrows at the center of the FTE); second, a large core magnetic field characterized by a large out-of-plane magnetic field component of about $100nT$ is present (see Figure 4.13 which is the same as Figure 4.12(b) but in this case the B_Y component is shown in color code).

A clear 3D view of the interlinked flux tubes at t=25:30 is shown in Figure 4.14. To trace the magnetic field lines, points inside of the northward (green) and southward (yellow) topological lobes of Figure 4.11 (fourth panel) have been chosen as seed points. Two flux tubes with an elbow-like structure can be distinguished. One of them has one side connected to the Northern Polar Cap and the other side to the IMF (green lines). The second flux tube has one side connected to the Southern Polar Cap and the other side to the IMF (magenta lines). The peculiarity lies in that the two flux tubes are interlinked, then when these flux tubes convect to the tail, they are forced to move against each other. Also the B_Y component of the magnetic field is presented in color code for a meridional cut ($Y = 0R_E$) centered at the subsolar magnetopause. An intensification of the B_Y magnetic field component is observed in the region where the two flux tubes meet. This region is very close to the subsolar point, hence the B_Y component can be considered a good approximation of the B_M component of the boundary normal system.

It is interesting to note that the analysis of the projected magnetic field, in conjunction with the topological study gives a correct understanding of the magnetic structure. However, if we use only the projected magnetic field may get an erroneous interpretation of the FTE magnetic configuration. This aspect was pointed out in

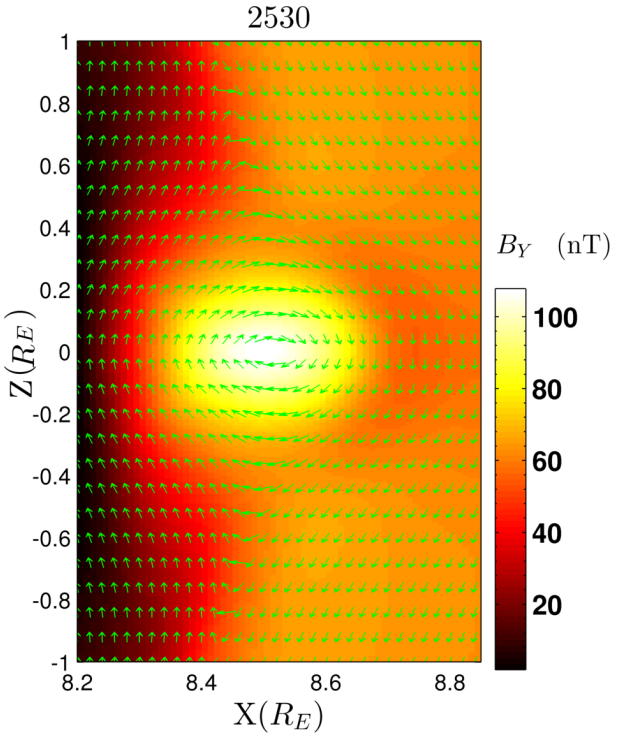

Figure 4.13 - Enhancement of the core magnetic field for the noon-midnight plane. The color code represents the GSM Y component of the magnetic field. The green arrows indicates the direction (not the magnitude) of the projected magnetic field in the noon-midnight plane.

Dorelli and Bhattacharjee (2009).

Looking at Figures 4.12(b) and 4.13, we observe a good similarity with the 2D reconstruction of a flux rope using Cluster spacecraft, (Figure 2 of Sonnerup et al. (2004)). The flux rope reconstructed in that paper shows a strong core magnetic field in the axial (out-of-plane) direction similar to the found in Figure 4.13. Also a pressure bulge of $\sim 1R_E$ is detected in Sonnerup et al. (2004). In that case the thermal pressure is higher at the edges of the FTE than at the center, in order to keep the total pressure (thermal + magnetic pressure) almost constant. In Figure 4.12(b) this pressure bulge is identified, also the thermal pressure is higher at the edges than at the center, indicating the existence of a force balance between the magnetic and thermal pressure. The last clue that tented us to identify this structure as a flux rope is the rotational projected magnetic field, which is found typically in a cross-section view of the flux rope. This rotation of the magnetic field is responsible for the bipolar B_N signature shown in Figure 4.5. A spacecraft that transverse the FTE from north (south) sees first a magnetic field outward (inward) normal to the

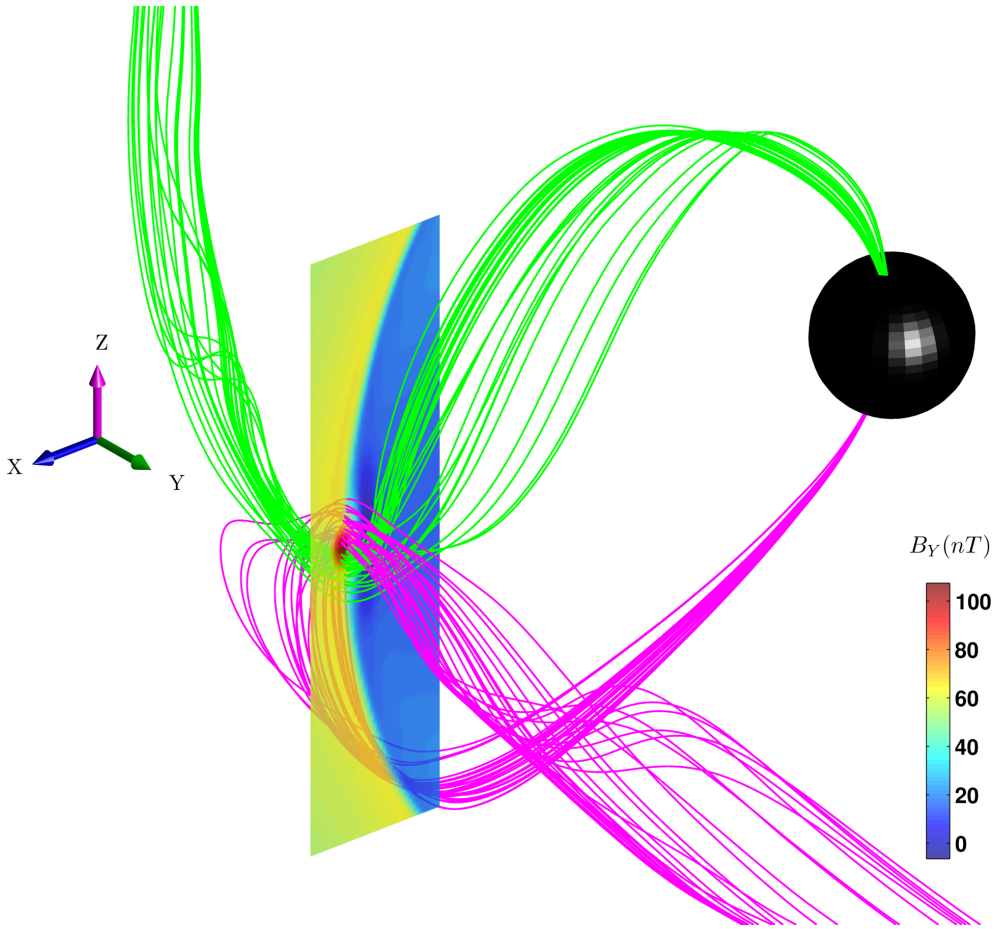

Figure 4.14 - 3D perspective of the interlinked flux tubes. The view is from the north-duskward direction. The black sphere is the Earth. The color coded plane shows the intensity of the Y component of the magnetic field for the noon-midnight cut.

magnetopause and later an inward (outward) B_N component.

If we combine now the topological information in 2D (Figure 4.11) and 3D (Figure 4.14) we are able to identify correctly the magnetic structure. From Figure 4.14 we deduce that the rotational magnetic field is not due to a flux rope, instead it is because of the linkage of two independent flux tubes. In the region where the two tubes approaches, they exert magnetic tension against each other, which produces a bending of the magnetic field and an enhancement of the core magnetic field in the region where the tubes meet.

If we follow the two flux tubes starting from the polar caps, it can be seen that the magnetic lines of both tubes cross the magnetopause from the magnetosphere side to the magnetosheath side. The magnetopause can be approximately identified in the

noon-midnight cut of Figure 4.14, as the separation line between blue ($B_Y \approx 0nT$) and yellow ($B_Y > 0nT$) color regions. The direction of the magnetic field of the southern connected (magenta) flux tube is tangent to the magnetic field lines and outward from the polar cap, then it points from the magnetospheric side to the magnetosheath side, i.e outward (+) from the magnetosphere. On the contrary, the magnetic field direction of the northern connected (green) flux tube is tangent to the magnetic field lines, but inward to the Northern Polar Cap, then it experiences a rotation at the magnetopause inward (-) to the magnetosphere. When the two flux tubes are projected in the noon-midnight plane, the rotational magnetic field of Figure 4.13 is reproduced. Therefore, the signatures of the FTE1 are caused by the interlinked flux tubes and not by a flux rope. Also, it is observed from the projected magnetic field and the line plot of Figure 4.5 that each tube independently do not produce the bipolar signature of B_N, this means that the magnetic field in each tube is not twisted. Cardoso et al. (2013) came up to this last conclusion using measurements from virtual satellites.

Figure 4.15 shows snapshots of the pressure bulges associated with every FTE detected after the time 24:00. The thermal pressure is presented in color code and the the greens arrows indicate the direction (not the magnitude) of the plasma velocity projected to the noon-midnight plane.

The evolution of the interlinked flux tubes (FTE1) is shown in Figure 4.15 in terms of plasma pressure. In the first snapshot the interlinked flux tubes are well formed (t = 26:30). Two possible reconnection points can be identified at this time at $\sim z = \pm 1.4 R_E$, due to bidirectional flow speeds observed around this points. The observation of the reconnection points north and south the subsolar magnetopause is consistent with the results of the topological study, which also reveals the existence of X points in the same region where the four topology zones meet. Therefore, combining this two methods we can certify that these are reconnection points. If we observe carefully Figure 4.11 (fourth panel), the subsolar point is also a meeting point of the four topology regions. However, from Figure 4.15 (t=26:30) it is shown that plasma is accumulated in this region due to it is being ejected from the reconnection points to the center of the FTE. Hence, as the flow is converging at the subsolar magnetopause instead of diverging, probably the reconnection has been suppressed in this region as pointed out by Cardoso et al. (2013). It is precisely the accumulation of the plasma coming from the reconnection points to the center, the cause of the big pressure bulge shown in Figure 4.15 at 26:30. The more probable reconnection places are in the junction of the four topological regions. However as this is a necessary

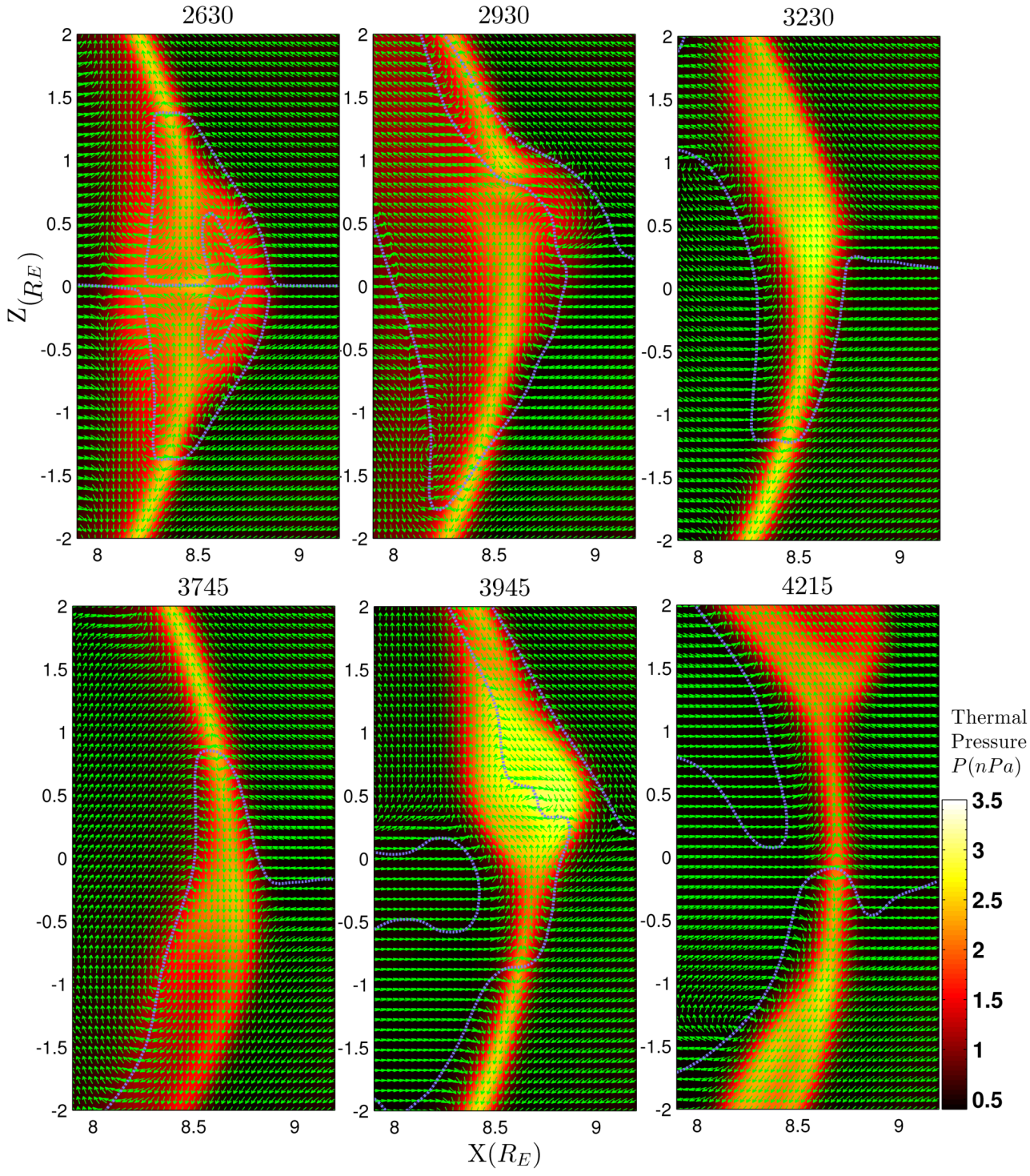

Figure 4.15 - The six panels show cuts of the noon-midnight meridional plane at different times (for each FTE). In each panel the color coding indicates the thermal pressure. The green arrows indicates the direction (not the magnitude) of the projected bulk plasma velocity vector, in order to emphasize the flow vortices. The thin dotted blue line is the zero contour of the plasma velocity Z component, i.e, it separates regions of $V_Z > 0$ from regions of $V_Z < 0$.

but not a sufficient condition there is not contradiction if the subsolar point after t = 24:00, despite to be a four-field topological junction, is not a reconnection point.

Figure 4.15 shows at the time 29:30, a snapshot of the FTE1 when the pressure bulge has moved northward from the subsolar point. According to the results of Table 4.1, the signatures of this FTE are observed up to the time $\sim 30:00$, hence at 29:30 is almost in its last stage. It is shown above (Figure 4.10) that about $24:00$ the topology at the magnetopause around $\pm 1.5 R_E$ changes and becomes unsteady. However, after and during the decay of the FTE1 (interlinked flux tubes) the magnetic topology at the magnetopause becomes even more complex and the complexity reaches a more wide area of the subsolar magnetopause (about $\pm 6 R_E$ in Y and $\pm 4 R_E$ in Z directions). We observe the creation and destruction of regions of different magnetic topology until the end of the run. This process is more dynamic during each FTE formation after the first one (FTE1). Therefore, the magnetic reconnection process is far from being a quasi-steady process along a reconnection line. Due to this unstable behavior, the reconnection places are difficult to identify by topology methods. Then we use the $V_Z = 0$ contour lines and the flow speed to get an idea of where the reconnection is happening. The $V_Z = 0$ contour line is represented as a blue dotted line in Figure 4.15. We can define this line as a "stagnation" line in the sense that it separate regions of northward flow from regions of southward flow, hence the interception of the contour line with the magnetopause is an stagnation point (Raeder, 2006).

One important result from Figure 4.15 is the shift of the stagnation points from the subsolar point. At the time $26:30$ two stagnation points are detected at $Z \approx \pm 1.4 R_E$ (see interception of the $V_Z = 0$ line with the magnetopause), in this case these stagnation points are directly associated with magnetic reconnection near that region. Plasma ejected from the stagnation points increase the thermal pressure inside the FTE. The flow pattern is almost symmetric with respect to the X axis at that time and there is a balance of force between the gradient pressure and the magnetic force that keep the symmetry. The pressure bulge grows until the balance of forces and the symmetry is broken. After that moment the FTE begins to move northward as showed in Section 4.1.1. Figure 4.15 (second top panel) shows a snapshot of the FTE1 when is moving northward. The northern stagnation point has moved northward (out of the Figure) and the southward point remained almost in the same place. As result, after the FTE1 propagation only one stagnation point (and possible reconnection point) remains southward to the equator.

The subsequent FTEs move alternately northward and southward, and the stagnation points associated with these FTEs are formed alternately southward and northward to the subsolar point. This alternation is a signature that the reconnection process is very transient and unsteady at the dayside magnetopause. However, the alternating pattern guarantee an average balance of the magnetic flux that is convected through the Northern and Southern Polar Cap toward the nightside magnetotail.

Another interesting result is the formation of flow vortices in all the FTEs starting from the time 24:00. Inspection of all snapshots of Figure 4.15, except the first one, shows that the center of the flow vortices is intercepted by the contour line of $V_Z = 0$. As the $V_Z = 0$ contour line is a boundary between regions of opposite orientation in the Z component of the plasma velocity, there is a flow shear in the proximity of this line which can generate the observed flow vortices. It is the shift of the stagnation points from the subsolar point the cause of the shear flow at the magnetopause, since if the stagnation point coincides with the subsolar point the magnetosheath and the magnetosphere flows would have the same direction close to the magnetopause and no shear flow would be present. Dorelli and Bhattacharjee (2009) also detected flow vortices in their simulations and showed that the flow vortices bring together regions of different magnetic topology which drive more processes of magnetic reconnection. We believe that the increase of the complexity of the magnetic topology at the end and after the FTE1 (interlinked flux tubes), could be due to magnetic reconnection driven by the flow vortices after the FTE1 has been formed.

4.1.3 Movement of the X-reconnection line

We get back to the question about the causes of the instability in the subsolar magnetopause starting at the time 24:00. In Section 4.1.2 we have mentioned the generation mechanism of the interlinked flux tubes (or FTE1) which is responsible for breaking the stability of the magnetopause. Here we provide further details.

Figure 4.16 shows a sequence of snapshopts of the stagnation line (black dotted line) over the magnetopause. This is the line that divides flows of $V_Z > 0$ (toward north) from flows of $V_Z < 0$ (toward south). The Z component of the plasma velocity is measured in every point of the surface and showed in color code.

At the time 23:30 the stagnation line matches very well with the reconnection line calculated using both the topology method and the Gonzalez and Mozer (1974) model. The inclination angle is the same ($\approx 13^o$). At the time 24:00 we start to

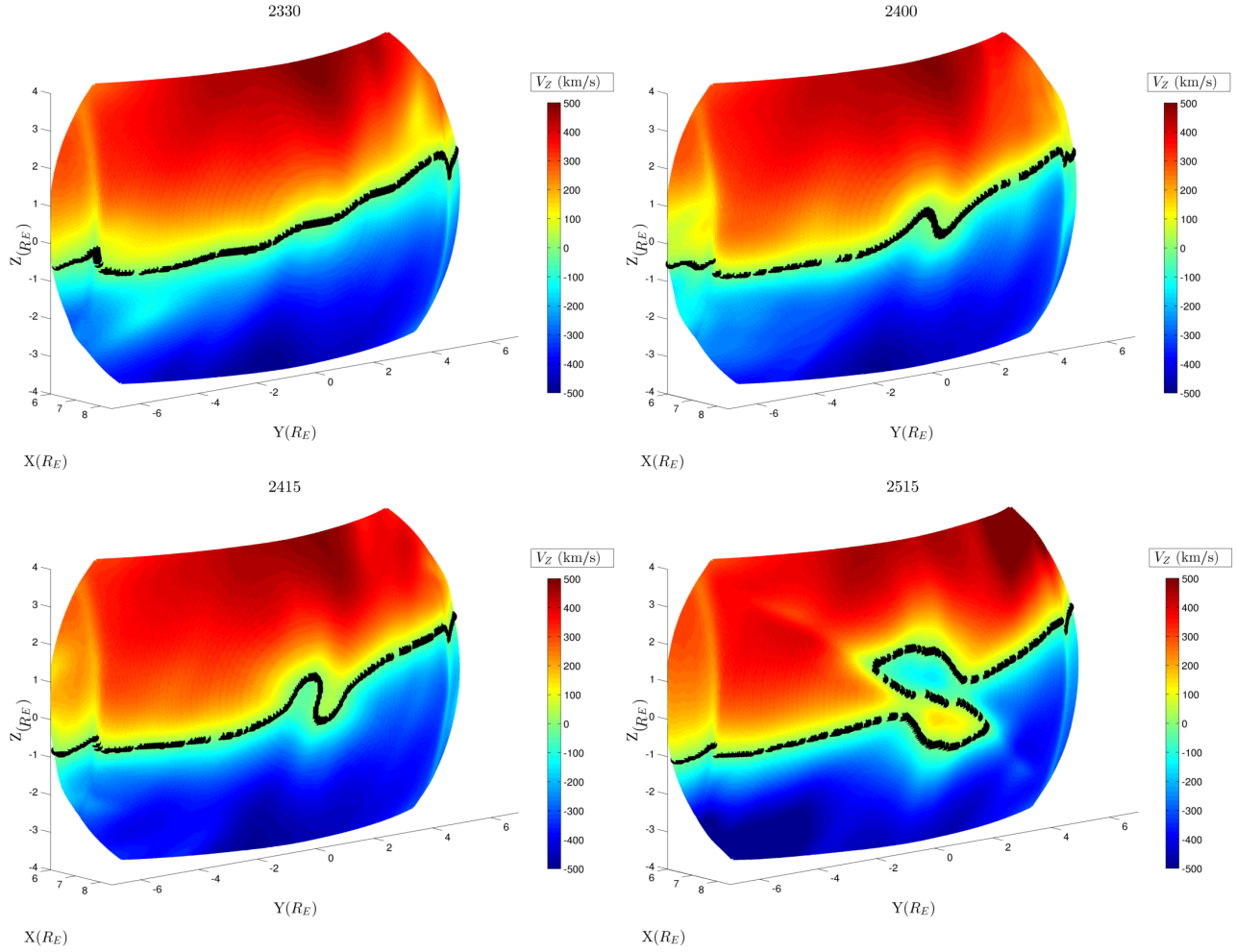

Figure 4.16 - Sequence of the subsolar magnetopause plots seen from the magnetosheath side for different times. The color coding represents the Z component of the plasma velocity over an isosurface of $B_Z = 0$ (magnetopause). The black line represents the stagnation ($V_Z = 0$) line.

observe that the stagnation line is modified from its initial extended line form. After the time 24:00 the stagnation line remains crossing the subsolar point, however at $0.3R_E$ dawnward and duskward the stagnation line has been shifted northward and southward respectively. As time goes on, the shift grows in the Z direction up to $\sim \pm 3R_E$ and remains approximately steady until the final stage of the FTE1. A more advanced snapshopt at t=25:15 shows that the stagnation line has become a kind of "S" shape near the subsolar region.

If we consider the stagnation line as an approximate location of the reconnection line, it can be observed a formation of two reconnection lines northward and southward the subsolar point. At 25:15 we observe a southward (northward) directed flow of

about $100km/s$ coming from the northern (southern) reconnection line. We believe that the subsolar point despite to be an stagnation point (in the sense of $V_Z = 0$), it is not a reconnection site because in the subsolar region these flows converge instead of diverging. Therefore, Figure 4.16 give us an interesting result: the two reconnection lines observed northward and southward the subsolar region are not two independently formed, instead it is the deformation of the quasi-steady reconnection line which produces the multiple reconnection lines.

Figure 4.17 shows the evolution of the magnetic field component normal to the magnetopause (left column) and the tangential component (right column). These quantities are calculated and shown also over the magnetopause estimated as an isosurface of $B_Z = 0$ for $\sim \pm 2R_E$ in the Y and Z directions. The magnetic reconnection process is more probable to occur in regions of low tangential magnetic field. This condition follows because the tangential components of the magnetic field perpendicular to the X-line in each side of the magnetopause are antiparallel, therefore when they meet at the X-line the overall magnitude of the tangential field to the magnetopause is reduced. On the contrary, from Figure 4.17 (right panel) we observe an increase of tangential magnetic field near the subsolar point, then this is another proof that magnetic reconnection is suppressed in that region. Simultaneously to the accumulation of the tangential magnetic field, an increase of the normal component at the peaks of the stagnation line is observed (see Figure 4.17 left column).

Using all the results of the Sections 4.1.2 and 4.1.3 we can propose a mechanism for the generation of the instability of the reconnection line. In summary, at 23:45 the IMF and geomagnetic topology regions approach each other producing an accumulation of tangential field line at the subsolar magnetopause. At some point the accumulation is faster than the reconnection rate, hence the concentration of magnetic field saturates the subsolar region and the reconnection is suppressed. The intensification of tangential magnetic field increases the magnetic pressure perpendicular to the subsolar magnetopause, which curves the magnetic field into an "O" shape. Then the reconnection line (and the stagnation line) is shifted together with the normal component of the magnetic field away from the subsolar region. The interlinked flux tubes are produced due to the reconnection lines formed northward and southward of the subsolar magnetopause. After this event the magnetopause becomes very unsteady and four FTEs are detected in sequence. We believe that the flows vortices observed after the FTE1 contribute to increase the instability and the transient magnetic reconnection on the magnetopause.

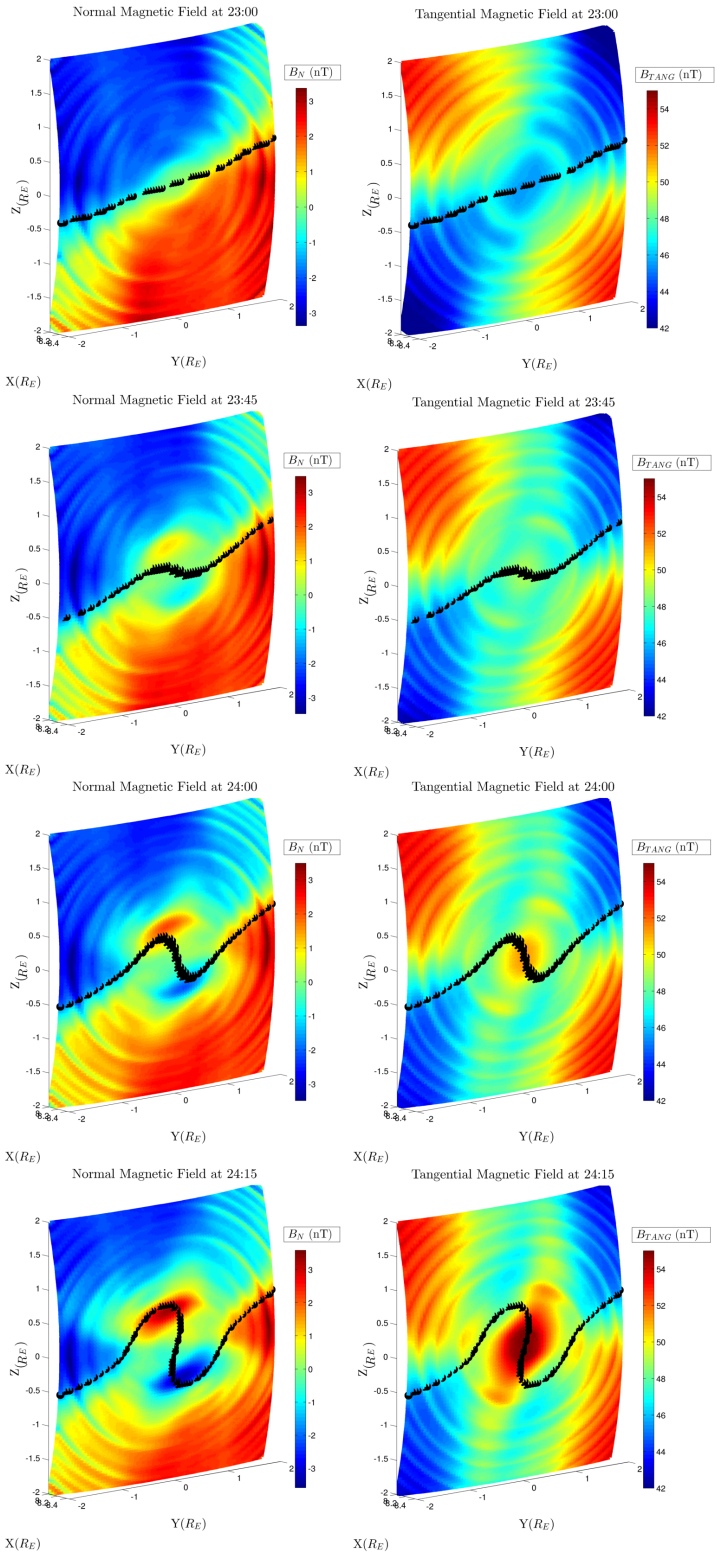

Figure 4.17 - Sequence of the subsolar magnetopause plots seen from the magnetosheath side for different times. The left column shows in color code the normal component of the magnetic field over an isosurface of $B_Z = 0$. The right column shows in color the tangential component of the magnetic field to the magnetopause. The black line represents the stagnation ($V_Z = 0$) line.

4.2 Transient magnetic reconnection in the magnetotail and variations of the polar cap potential

As it was explained in Chapter 3, an ionospheric model is coupled to the GM component, which calculates various parameters of the ionospheric polar cap, among them the polar cap potential. The PCP time series for the whole run is shown in Figure 4.18a. The increase of the PCP between 0 and 10 min is due to the initialization process before the time 00:00. The average steady convection pattern sets a PCP around $200kV$. Superposed to the average steady state there is a transient behavior that is magnified in Figure 4.18b.

We can notice in Figure 4.18b two principal oscillations of the polar cap potential. The first one starts at 20 : 30 and lasts approximately 9 min, and the second oscillation starts at 29 : 15 and lasts $\sim 13min$. The magnitude of the variation of the PCP ($\Delta\Phi_{PC}$) is $8kV$ in the first principal oscillation and $18kV$ in the second large oscillation. Superposed to the principal oscillations there are small variations of the PCP of about $\Delta\Phi_{PC} \approx 1kV$ with a time duration of ≈1-2 min. We will focus for the moment into the two principal oscillations.

As we explained in Chapter 2, if the polar cap ionosphere is perturbed by a short single burst of reconnection, the characteristic time for the resulting polar cap flows to decay is of order $10 - 15$min. This time agrees with the 9 and 13 min periods of the two principal oscillations of Figure 4.18b.

Both FTE events at the magnetopause and bursty reconnection like substorms in the tail were observed in the simulation. In this particular run, the substorm-like events seem to be more closely related with the principal oscillations of Figure 4.18b. We will present in the next Section the results concerning to the relation of these tail processes with the variations of the PCP. Also, a particular difference between the north and south polar cap potential were detected and could be related with the formation of the FTEs at the dayside magnetopause. This result is presented in Section 4.3.

4.2.1 Magnetotail magnetic reconnection processes

We detected three bursty reconnection events in the plasma sheet current. The more intense was the first one, however all the three events have a similar time evolution. The dynamics of the first event is shown in Figure 4.19 in terms of the magnetic field lines and in Figure 4.20 in terms of density N. Figure 4.19 shows the configuration

(a)

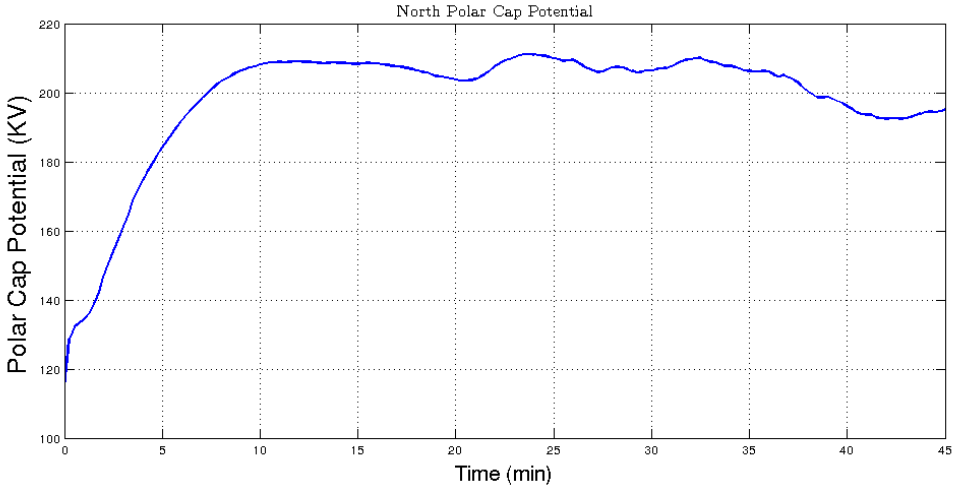

(b)

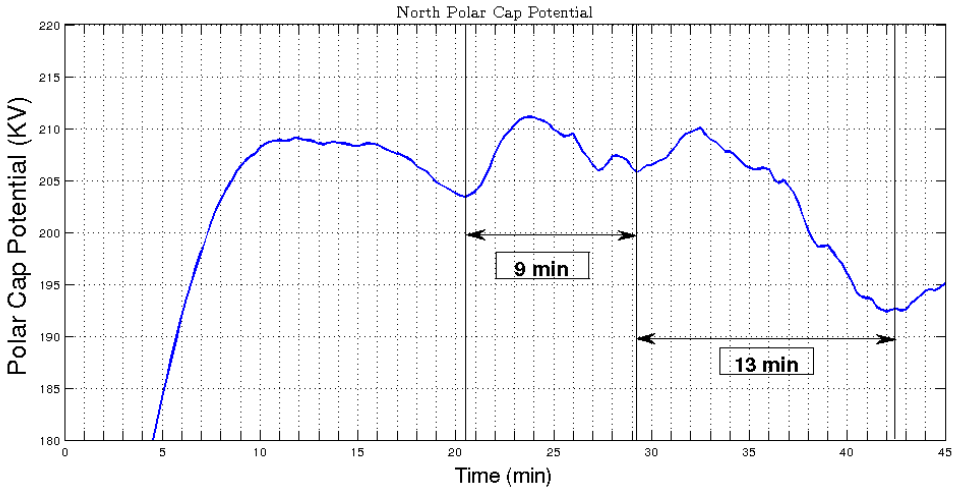

Figure 4.18 - **(a)** North Polar Cap Potential derived from our simulation. **(b)** Zoom of the graphic showed in (**a**). Two large oscillations can be observed. The double arrows and the solid lines indicate the start and the end of each oscillation.

and topology of the magnetic field lines in the magnetotail current sheet for different times. The orange lines correspond to the geomagnetic field lines. The black lines indicate magnetic field lines connected to the polar cap at one end and open to the interplanetary space at the other end, i.e., these are semi-open magnetic field lines connected to the polar cap. The blue lines indicate IMF lines, which means that the both ends are open to the interplanetary space. The Z axis has been chosen between $-3R_E$ and $3R_E$ in order to emphasize the current sheet in the magnetotail.

At the time 17 : 00 the semi-open magnetic field lines linked to the polar cap (color black) are accumulated in the plasma sheet region (Figure 4.19a). In this phase we do not identify clearly a X-line, however reconnection is taken place because of IMF lines of color blue are observed inside the magnetotail. The dipolar magnetic field (orange lines) is well established in this phase. The lack of a well defined reconnection line could be an indication that the rate of the reconnection process is low, therefore accumulation of magnetic field lines seems to dominate over the reconnection of flux tubes in this phase. No signatures of plasmoids or instabilities are observed at this time. This phase is similar to the growth phase of a substorm (Figure 2.8).

At 19 : 00 the dipolar magnetic field lines are pushed earthward (Figure 4.19b). We identify this point as the onset of the reconnection burst. A small plasmoid can be observed in Figure 4.20 (first panel) at 19 : 00. Approximately 1-2 min after the onset time the PCP starts to increase (time 20 : 30 in Figure 4.18b), this is the beginning of the first large oscillation. The delay time is due to the finite propagation velocity of the information from the reconnection site ($X \approx -15R_E$) to the ionosphere, which is of order of 2 min (Southwood, 1987).

At the time 21 : 00 (Figure 4.19c), a clear X-line around $-15R_E$ is formed. At that time the bend of the magnetic field lines resembles the typical "O" shape of the tearing instability. This is an indication that a region of high-beta and high-density plasma is wrapped by the magnetic field lines. The high kinetic pressure inside the plasmoid makes the magnetic field lines bend in the Z direction to form an "O" shape. Figure 4.20 (second and third panel) confirms the existence of a high density plasmoid. A graphic of the beta parameter is not presented here, however the results of the simulation point out that inside the plasmoid $\beta \approx 5.6$.

After its complete formation, the plasmoid is ejected tailward because of the tension force of the new reconnected field lines which pushes the plasma away from the reconnection region. As the plasmoid moves tailward (Figure 4.20), the magnetic field lines in Figure 4.19d are forced to move in the Z direction and the "O" shape is broken.

In the last phase (time 23 : 30) the plasmoid is spread at around $-50R_E$ (Figure 4.20 last panel). The geomagnetic field lines (color orange Figure 4.19e) recover to its original position, which is an indication that the plasma ejection has decreased at the X-region. Therefore, at approximately 23 min the reconnection rate in the plasma sheet at around $-20R_E$ decrease to the initial level. We believe that this moment is the end of the reconnection burst. Approximately 1 min later (minute

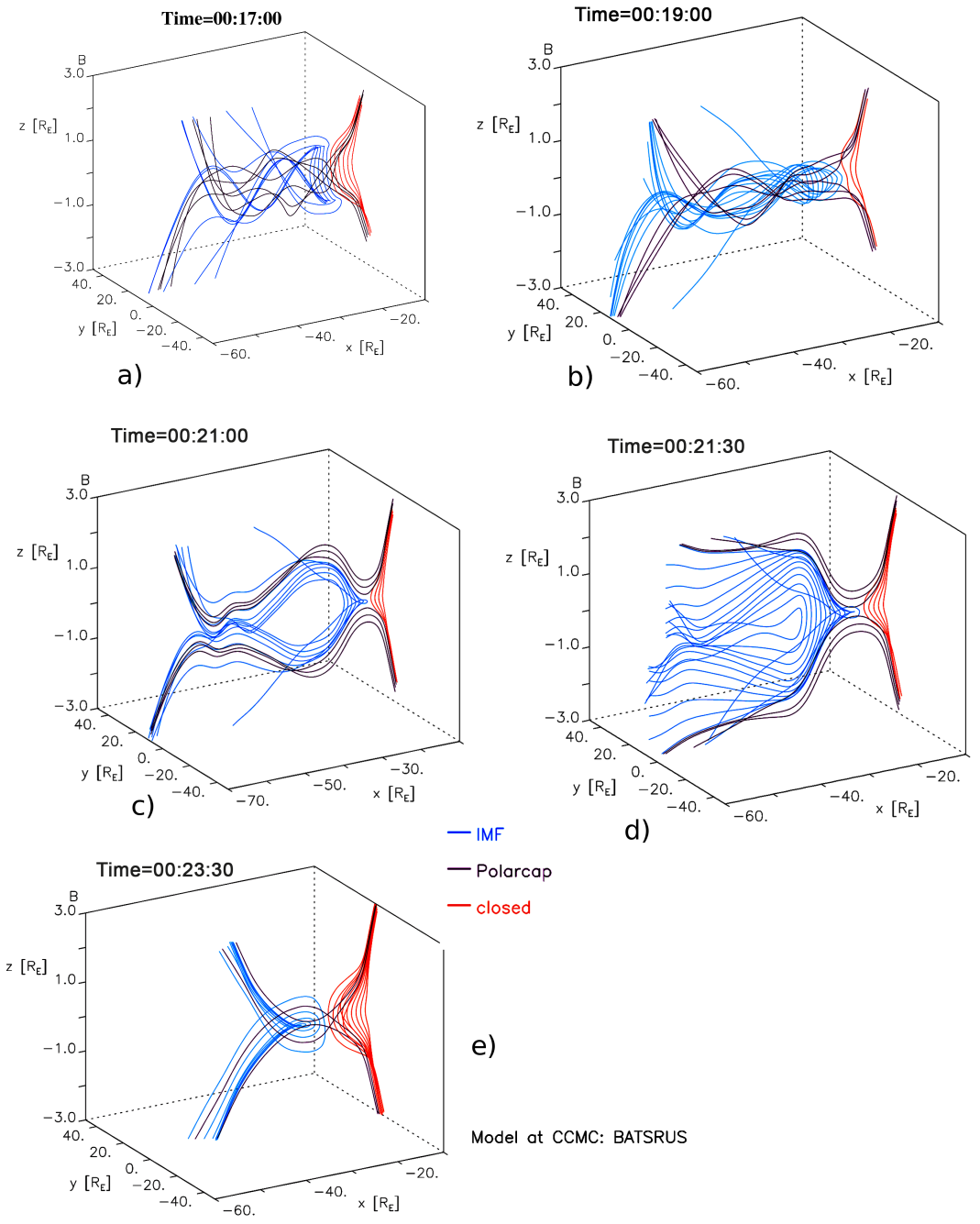

Figure 4.19 - Illustration of the magnetic field lines in 3D due to suddenly reconnection in the plasma sheet current. The color are related to the topology as orange, closed; black, conected to the polar cap; and blue, IMF. The view is from the north, dawn, and tailward side of the magnetosphere, i.e., the earth is to the right.

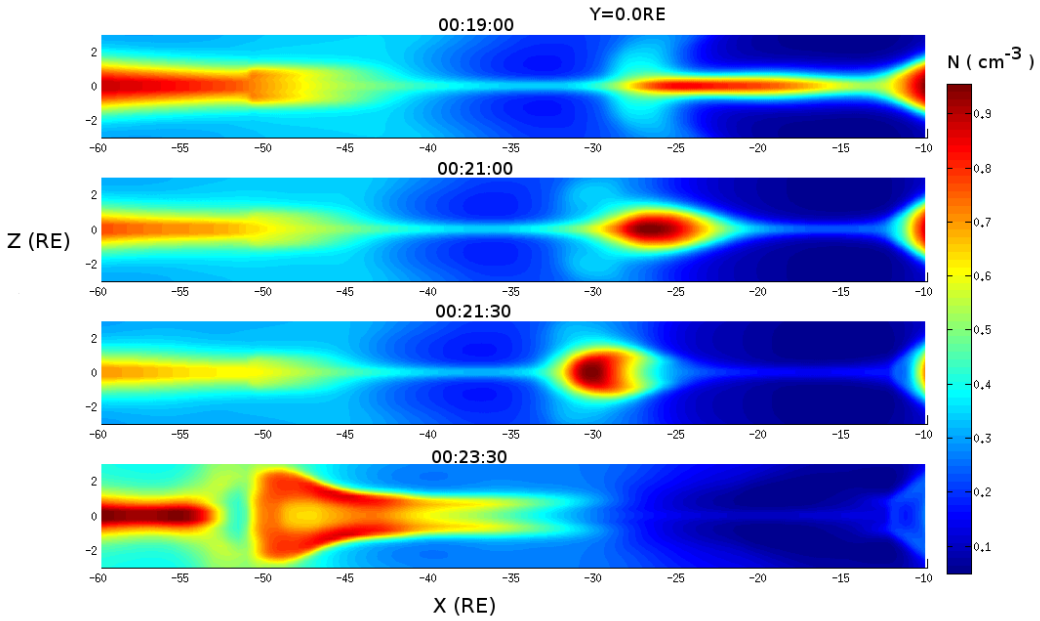

Figure 4.20 - Cuts of the magnetotail in the $X - Z$ plane at differents times, the Earth is to the right. In each panel the color coding represents the plasma density in particles per cm^3. The sequence of snapshots shows the formation, evolution and spreading of a plasmoid.

24 of Figure 4.18b), the PCP began to decrease as a consequence of the response of the ionosphere to this burst of destruction of open magnetic field.

A second burst of reconnection at the magnetotail occurs at about 28 : 00 and lasts approximately 2-3 minutes. The sequence of events is similar to the first event shown in Figures 4.19 and 4.20. The response of the polar cap potential due to this second burst of reconnection began at 29 : 15 and ended at about 13 min later. A third event occurs at that time ($\approx$ 42 : 00), however due to the simulation stops at 45 min we did not study the complete cycle of this last event.

4.2.2 Magnetic topology study of the first substorm-like event

In Section 4.2.1 we found out approximately the start time of the reconnection burst at the first event in the magnetotail. We analyzed the magnetic field line configuration and the dynamics of the plasmoid, but we observed the signatures of a plasmoid after magnetic reconnection has already started. In order to obtain a more accurate temporal study of the phases of this substorm-like event in the tail, the magnetic topology at the plasma current sheet is presented next.

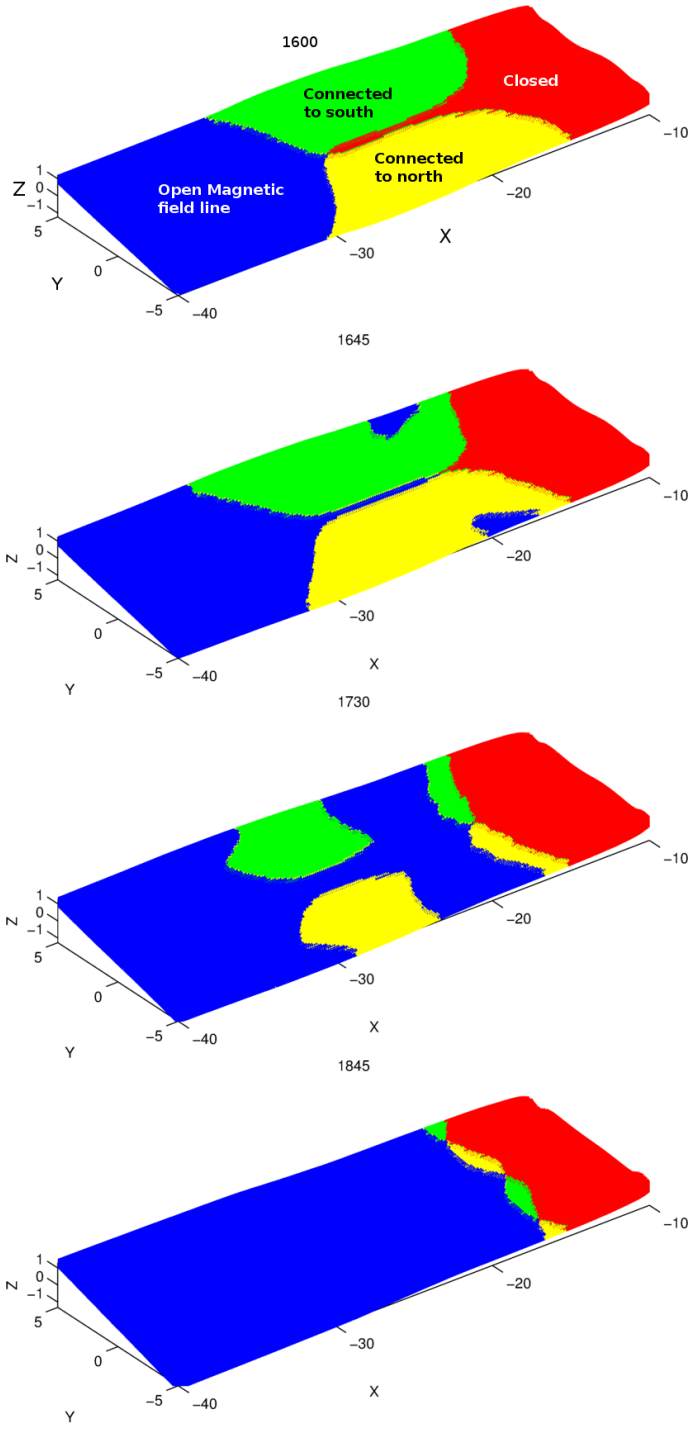

Figure 4.21 - Magnetic topology at the plasma current sheet (represented as an isosurface of $B_X = 0$ (Harris, 1962)). The surfaces are located at $Z \approx 0$ with an inclination of $\approx 11°$ respect to the ecliptic plane. The view is from above and the Earth is to the right. The colors represent areas of different magnetic field topology as red, closed; green south connected; yellow north connected; and blue open magnetic field lines.

We calculate the position of the plasma current sheet as an isosurface of $B_X = 0$. The Harris (1962) description of the magnetotail current sheet as a layer of plasma confined between two regions of oppositely directed magnetic field is followed. Figure 4.21 shows the plasma current sheet as an isosurface of $B_X = 0$. It is interesting to note the inclination of the current sheet ($\approx 11^o$) with respect to the ecliptic plane. As pointed out by Sibeck and Lin (2014) the tilt of the current sheet depends on the IMF. For example, if the IMF is south-duskward (as in our simulation) the current layer separating both hemispheres rotates counterclockwise when viewed from Earth, which is consistent with our results.

The magnetic topology is computed at the current sheet as shown in Figure 4.21. The red color means regions of closed magnetic fields; the yellow and green color means regions of semi-open magnetic field lines connected to the Northern and Southern Hemisphere respectively; and the blue area represents region of interplanetary magnetic field, i.e, not linked to the Earth.

At the time 16 : 00 of Figure 4.21 we observe a region around $X = -30R_E$ and $Y = 0R_E$, where the four topology zones meet. This region can be identified as the magnetic reconnection site, which is a point instead of a reconnection line as at the beginning of the simulation. In this phase ($t = 16 : 00$), the semi-open magnetic field lines (green and yellow zones of Figure 4.21) are accumulated in the magnetotail. During the interval between 16:00 and 16:30 the magnetic topology starts to change. The point of junction of the four topology regions has moved earthward to $X \approx -18R_E$. Reconnection at the new point between semi-open northern and southern connected field lines produces IMF lines (blue) and geomagnetic (red) field lines. At 18:45 we observe two principal regions of IMF and closed magnetic field lines, separated by a thin band of polar cap connected field lines. Starting from this moment all semi-open magnetic lines at the north and south of the plasma current sheet reconnect in the separation region extended along the Y-direction, which we believe is a new reconnection line created near Earth. The magnetic energy accumulated in the magnetotail is converted rapidly to kinetic energy due to reconnection at the new formed X-line, which in turn produces the high density and high beta plasmoid showed in Figure 4.20.

4.3 Considerations about the FTE signature in the polar ionosphere

As explained in Chapter 2 , transient magnetic reconnection at the magnetopause creates a series of FTEs which travels towards the magnetotail after its formation. The classic signature of the FTEs in the ionosphere is the perturbation of the open-

closed boundary line in the form of an equatorward bulge. Poleward plasma flow will then be excited to move the perturbed system to the new equilibrium.

Figure 4.22 shows the ionospheric potential (in color coding) computed by the IE model. The arrows represent the plasma flow and the black line indicates the boundary between closed and semi-open magnetic field lines. Observing the velocity vectors, two convection cells are observed in the polar ionosphere. For the Northern Hemisphere (Figure 4.22 top panel) the duskward cell is larger in extension than the dawnward one. In the case of the dawnward cell the convection is concentrated around the dawnward side of the open-closed boundary. The ionospheric potential is also asymmetric, with higher values in the wider convection cell. These are typical conditions of the high latitude ionospheric flow for $B_Z < 0$ and $B_Y > 0$ (Cowley; Lockwood, 1992). In the Southern Hemisphere the asymmetry is reversed in the dawn-dusk direction (see Figure 4.22 bottom panel).

The PCP is a proxy of the magnetic flux convection through the polar cap. It is calculated as the difference between the maximum and minimum values of the ionospheric potential in each polar cap. In the steady state case the flux transported through the southern and northern polar cap is the same, therefore despite the asymmetry between both hemispheres, the polar cap potential (PCP) must be the same.

Our simulation is far from being in steady state, especially after the time 24:00, when five well formed FTE were detected. Therefore, one expects some kind of signature on the open-closed polar cap boundary and in the flows. A small perturbation of the dayside open-closed boundary is observed after the first 30 min of simulation. The larger of these perturbations occurs 2-3 min after the FTE4 (formed at about $40:00$) and is shown in Figure 4.22(top) inside a blue circle. The area of the bulge is much smaller than the whole polar cap area. Hence the flows excited by this perturbation are very weak compared with the average convection pattern.

We have carefully searched for enhancement of flows associated with the FTEs. The open-closed polar cap boundary was calculated for every step of the run. We divided the open-closed boundary in sections. The mean velocity of the plasma that cross every section was calculated and plotted in function of the simulation time, but the dispersion of the data was too high to observe any correlation with the FTEs.

There are two possible explanation for the lack of FTE signatures in the polar ionosphere. The first one is that the resolution of the ionospheric model, which is 1° or

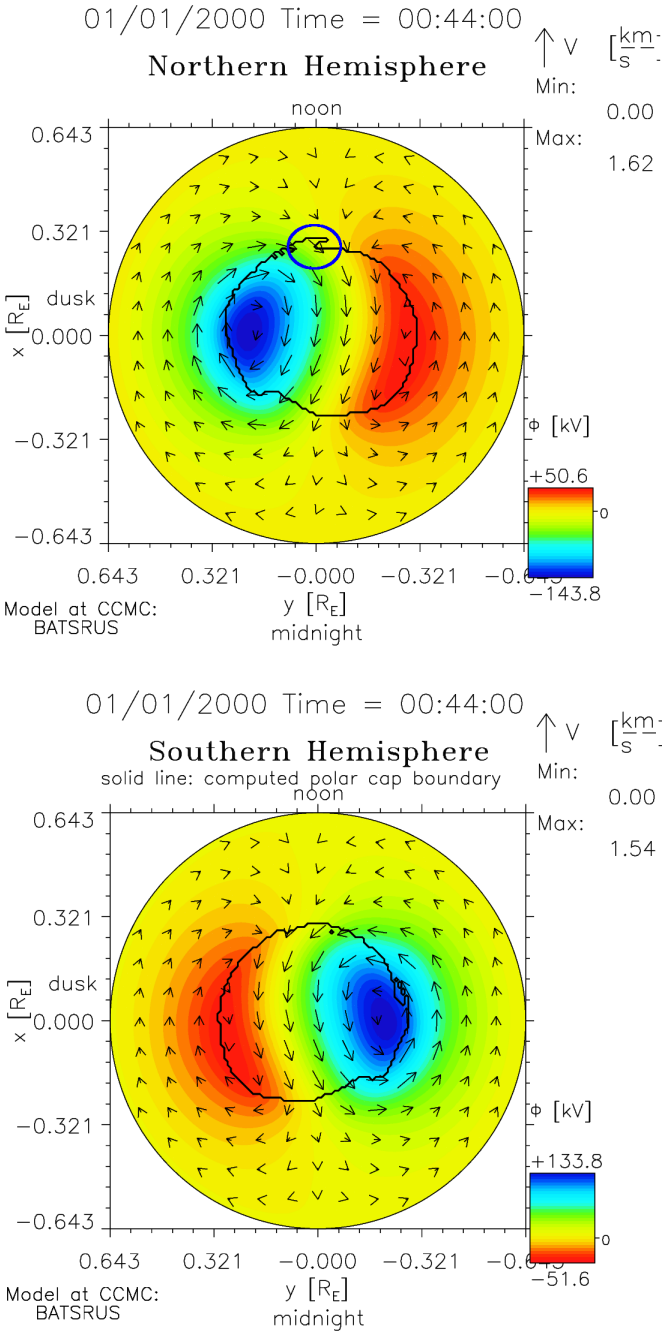

Figure 4.22 - Ionospheric potential pattern (color coded) in the polar cap. The black line and the arrows represent the open closed field line boundary and the ionospheric convection vectors respectively. **top)** Northern Hemisphere. **bottom)** Southern Hemisphere

$100km$ in the meridional direction, is comparable with the size of the perturbations of the open-closed boundary. Hence the numerical model can not resolve these small perturbations. The other cause may be that the uniform conductance pattern chosen do not allow changes of the Pedersen and Hall conductance pattern due to field aligned currents created during the reconnection process.

Despite that no direct signature of FTEs in the ionosphere were detected, an interesting result came up by comparing the northern and southern polar cap potential in Figure 4.23. The polar cap potential in the Northern and Southern Hemisphere are not equal, also the former is higher than the latter. We believe that this behavior is due to the occurrence of FTEs in the subsolar magnetopause, because the magnetic flux produced by the reconnection events in the magnetotail goes earthward and tailward, then the convection created in both polar caps are the same. This situation is different at the dayside magnetopause. In Section 4.1 it was shown that before the time 24:00 all the FTEs detected (named FTEs0) transported symmetrically magnetic flux to both hemispheres. After this time, the next observed FTEs move northward or southward in a quasi alternately way, i.e, there is an asymmetric flux transfer to the polar caps. Then, it is expected that the convection patterns created at the northern and southern polar cap would be different.

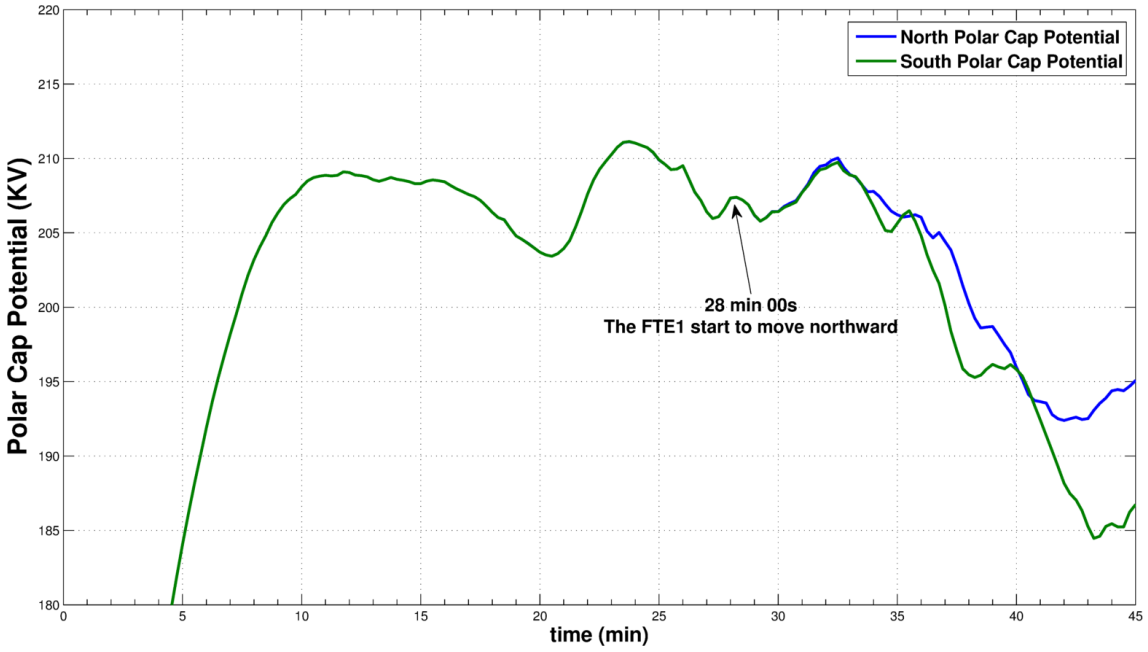

Figure 4.23 - North and South Polar Cap Potential during our simulation.

Figure 4.23 shows that around 30 min of simulation the northern and southern PCP are not more coincident, this time is approximately 2 min after the FTE1 starts to move toward north($\sim$ 28 min, see Table 4.1). We noticed also that the PCP in the Northern Hemisphere is larger than in the Southern Hemisphere during almost the rest of the simulation time. If we look at Table 4.1 (or Figure 4.24), from the five FTEs observed after the time 24 : 00, three of them (FTE1, FTE2, FTE4) move toward north and the other two (FTE3, FTE5) toward south, also the magnetic signatures are larger in the FTEs that travel northward. Therefore, more convection is created in the Northern Hemisphere. As the PCP is a proxy for the ionospheric convection, it is expected to be larger in the northern polar cap, which is consistent with the observations.

All the analyzed events in our simulations, superimposed with the PCP plots, are shown in Figure 4.24. The time onset of every FTE (except the FTEs0) are marked with a red box. The substorm-like events in the magnetotail are marked with a green rectangle, a label below the symbol specify the beginning and the end of every substorm-like event. The PCP suddenly increases between the time 00 : 00 to 10 : 00, this happens because at the beginning of the simulation the B_Z was turned southward, then reconnection begins at the dayside magnetopause increasing the convection in the polar caps. After an equilibrium is reached between dayside and nightside reconnection, the PCP is stabilized around an average value. Figure 4.24 shows the complexity of our simulation due to its diversity in magnetic reconnection events. We observe after $t \sim 17 : 00$ burst of reconnection in the magnetotail (substorm-like) followed by FTE formation at the magnetopause, which raise the question about if the FTEs on the dayside drive nightside substorms or vice versa. This question is difficult to answer. However, one aspect is clear, the magnetic reconnection processes in the dayside and nightside magnetosphere are eminently transient and unbalanced, they could be only steady in a long time scale or average sense. The variations of the PCP are an evidence of this miss-balance between dayside and nightside reconnection, since otherwise the PCP should be constant.

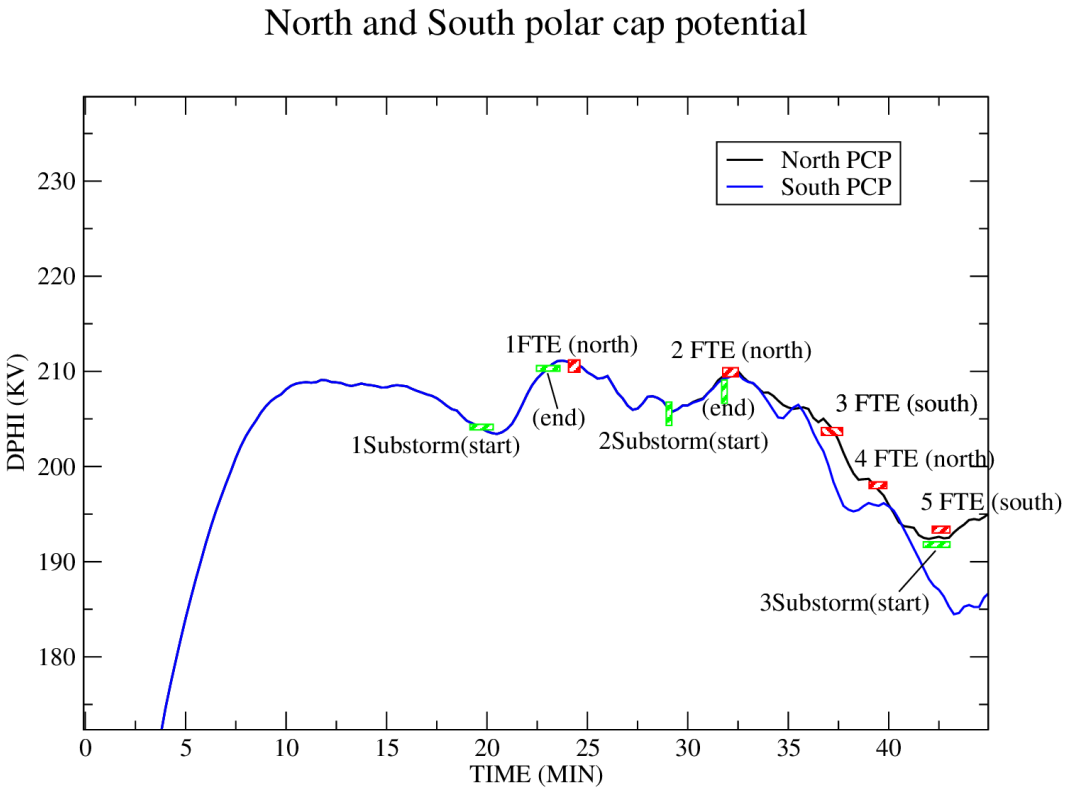

Figure 4.24 - Ionospheric polar cap potential during our simulation. The blue line represents the south PCP and the black line the north PCP. The red boxes indicate the time onset of the FTEs. The green rectangles indicate the beginning and end of every substorm as labeled bellow the symbol.

5 CONCLUSIONS

We have analyzed a global MHD simulation run of the magnetosphere. All the interplanetary conditions have been kept constant during the simulation time. The IMF has a large southward Z component and a large duskward Y component. The resolution at the subsolar magnetopause is sufficiently high to allow the formation of FTEs.

We observe the spontaneous formation of FTEs under contant solar wind conditions, in agreement with Raeder (2006) and Dorelli and Bhattacharjee (2009). To study these FTEs we measure the normal (B_N) and azimuthal (B_M) component along a path very close to the magnetopause. An isosurface of $B_Z = 0$ is used as a reference magnetopause, the normal to the isosurface is used to build the local boundary coordinate system needed to convert GSM components of the magnetic field to the LMN system.

During the first half of the simulation, before the time 24:00, a series of FTE have been detected. They occur with a periodicity of about 2 min and produce bipolar magnetic signatures in both hemispheres. These FTE are formed by symmetric flux tubes (one in each hemisphere), where one of them moves toward north and the other toward south.

Starting from 24:00 five FTEs with clear magnetic perturbation have been observed. The characteristics of these five FTEs are identified: the beginning and end of the magnetic signature, sense of propagation, speed of propagation and time of the propagation start. The FTE1, FTE3 and FTE4 travel northward, while the other two (FTE3 and FTE5) move southward. The B_N bipolar signature and the intensification of the core magnetic field (B_M) are presented in all FTE formed after the time 24:00, although these signatures are more pronounced in FTE1 and FTE4.

We calculate the magnetic topology at the magnetopause to study the reconnection processes at the subsolar region. Until the time 23:45 the reconnection takes place along an extended line with an inclination of $\approx 13^\circ$ respect to XY plane viewing from the Sun, which is in agreement with the Gonzalez and Mozer (1974) model. After this time the topology of the magnetopause changes and the reconnection processes stop being quasi-steady to become highly dynamic. We identified the source of these topology changes, as the accumulation of interplanetary magnetic field at the subsolar magnetopause due to the approach of regions of geomagnetic and IMF lines. This accumulation produces the bending of the magnetic field and the creation

of an "O" shaped type point. Then, two reconnection regions are created northward and southward the subsolar point due to the shift of the stagnation line from the subsolar point, while the reconnection at the subsolar point is suppressed. As result of the preceding sequence of events, the FTE1 (interliked flux tubes) is formed.

The cross section of the FTE1 has been analyzed in terms of the projected magnetic field, thermal pressure and core magnetic field. The typical magnetic characteristics of a flux rope are found. However, the analysis of the magnetic topology reveals that this structure is not a flux rope, instead it is formed by two interlinked flux tubes which together present the same characteristics of a flux rope. This result confirm the observations of Cardoso et al. (2013), that the interlinked flux tubes separately do not show signatures of a FTE.

During and after the interlinked flux tubes formation, flow vortices have been observed in every FTE. The shift of the stagnation line from the subsolar point create regions of oppositely directed flow, which are susceptible to the formation of vortices. As it was pointed out by Dorelli and Bhattacharjee (2009), the flow vortices bring together regions of different topology, which drive more processes of magnetic reconnection. This could be the cause of the increased complexity in the topology after the FTE1.

The magnetic reconnection processes in the magnetotail also are studied. Three bursty magnetic reconnection processes are detected in the plasma current sheet around $-20R_E$ tailward, each one lasting approximately 3 min and spaced apart from each other to about 10 min. The onset of reconnection was identified for each event. The analysis of the topology revealed that the first event evolved like a magnetospheric substorm. We identified in the first event the following phases: a growth phase where magnetic field is accumulated in the tail, the onset of reconnection characterized by a change in topology and an expansion phase where a plasmoid is released. However, we can not affirm that these events are properly substorms because the time scale of a substorm is of the order of 1-2 hours.

We have found evidences that the temporal variations of the PCP in this simulation are more related with the reconnection events in the magnetotail. The polar cap potential presents a small decrease after the beginning of the magnetotail reconnection events, but a higher increase approximately 1-2 minutes after this moment. No clear signatures of FTEs on the polar ionosphere are detected. However, due to more FTE travel toward the Northern Hemisphere than toward the Southern Hemisphere, it is expected that the ionospheric convection would be more intense in the northern

polar cap. This fact is observed in the PCP time series, where the northern PCP is largest than the southern PCP after the FTE1 moves northward.

In future works we recommend to use a nonuniform conductance model like the auroral pattern, which is more realistic than the uniform conductance pattern chosen in this work, because it allows modification of the Pedersen and Hall conductance due to the variability of the field aligned currents during the magnetic reconnection process. Maybe the signatures of the FTE could be detected using this kind of nonuniform conductance model.

REFERENCES

Axford, W. I.; Hines, C. O. A unifying theory of high-latitude geophysical phenomena and geomagnetic storms. **Canadian Journal of Physics**, v. 39, p. 1433, 1961. 1

Baumjohann, W.; Treumann, R. A. **Basic space plasma physics**. London: Imperial College Press, 1997. 93 p. 11, 17, 18

Bristow, W. A.; Greenwald, R. A.; Shepherd, S. G.; Hughes, J. M. On the observed variability of the cross-polar cap potential. **Journal of Geophysical Research (Space Physics)**, v. 109, p. 2203, feb. 2004. 4

Cardoso, F. R.; Gonzalez, W. D.; Sibeck, D. G.; Kuznetsova, M.; Koga, D. Magnetopause reconnection and interlinked flux tubes. **Annales Geophysicae**, v. 31, p. 1853–1866, oct. 2013. 22, 49, 52, 72

CCMC Kameleon. 2014. Available from: <http://ccmc.gsfc.nasa.gov/downloads/kameleon.php>. Access in: 21 July, 2014. 24, 25

Community Coordinated Modeling Center. 2014. Available from: <http://ccmc.gsfc.nasa.gov>. Access in: 21 May, 2014. 21, 22, 24

Cowley, S. W. H. The causes of convection in the earth's magnetosphere - A review of developments during the IMS. **Reviews of Geophysics and Space Physics**, v. 20, p. 531–565, aug. 1982. 1, 2, 30

Cowley, S. W. H.; Lockwood, M. Excitation and decay of solar wind-driven flows in the magnetosphere-ionosphere system. **Annales Geophysicae**, v. 10, p. 103–115, feb. 1992. 7, 8, 10, 66

_____. Time-dependent flows in the coupled solar wind-magnetosphere-ionosphere system. **Advances in Space Research**, v. 18, p. 141–150, 1996. 8, 9, 10

Dailey, R.; Cattell, C. A.; Mozer, F. S.; Berchem, J. Electric fields and convection velocities associated with flux transfer events. **Geophysical Research Letters**, v. 12, p. 843–846, dec. 1985. 37

Dorelli, J. C.; Bhattacharjee, A. On the generation and topology of flux transfer events. **Journal of Geophysical Research (Space Physics)**, v. 114, p. 6213, jun. 2009. 50, 55, 71, 72

Dungey, J. W. Interplanetary field and the auroral zones. **Physics Reviews Letters**, v. 6, n. 2, p. 47–48, 1961. 1, 13, 16

Frahm, R. A.; Winningham, J. D.; Sharber, J. R.; Link, R.; Crowley, G.; Gaines, E. E.; Chenette, D. L.; Anderson, B. J.; Potemra, T. A. The diffuse aurora: A significant source of ionization in the middle atmosphere. **Journal of Geophysical Research**, v. 102, p. 28203, dec. 1997. 23

Gonzalez, W. D.; Mozer, F. S. A quantitative model for the potential resulting from reconnection with an arbitrary interplanetary magnetic field. **Journal of Geophysical Research**, v. 79, n. Oct. 1, p. 4186–4194, 1974. 14, 45, 48, 55, 71

Haerendel, G.; Paschmann, G.; Sckopke, N.; Rosenbauer, H. The frontside boundary layer of the magnetosphere and the problem of reconnection. **Journal of Geophysical Research**, v. 83, p. 3195–3216, jul. 1978. 12

Harris, E. G. On a plasma sheath separating regions of oppositely directed magnetic field. **Il Nuovo Cimento**, 1962. xx, 64, 65

Kelly, M. C. **The earth's ionosphere : plasma physics and electrodynamics**. London: Academic Press is an imprint of Elsevier, 2009. 3

Kivelson, M. G.; Rusell, C. T. **Introduction to space physics**. New York: Cambridge University Press, 1995. 3

Laitinen, T. V.; Janhunen, P.; Pulkkinen, T. I.; Palmroth, M.; Koskinen, H. E. J. On the characterization of magnetic reconnection in global MHD simulations. **Annales Geophysicae**, v. 24, p. 3059–3069, nov. 2006. 47, 48

Lee, L. C.; Fu, Z. F. A theory of magnetic flux transfer at the earth's magnetopause. **Journal of Geophysical Research**, v. 12, p. 105–108, feb. 1985. 13, 15

Liu, Z. X.; Hu, Y. D. Local magnetic reconnection caused by vortices in the flow field. **Geophysical Research Letters**, v. 15, n. 8, p. 752?755, 1988. 16

Lockwood, M. On flow reversal boundaries and transpolar voltage in average models of high-latitude convection. **Planetary Space Sciences**, v. 39, n. 3, p. 397–409, 1991. 4

Lockwood, M.; Cowley, S. W. H.; Freeman, M. P. The excitation of plasma convection in the high-latitude ionosphere. **Journal of Geophysical Research**, v. 95, p. 7961–7972, jun. 1990. 7

Lopez, R. E.; Bhattarai, S. K.; Bruntz, R.; Pham, K.; Wiltberger, M.; Lyon, J. G.; Deng, Y.; Huang, Y. The role of dayside merging in generating the ionospheric potential during the Whole Heliospheric Interval. **Journal of Atmospheric and Solar-Terrestrial Physics**, v. 83, p. 63–69, jul. 2012. 4

Lopez, R. E.; Bruntz, R.; Mitchell, E. J.; Wiltberger, M.; Lyon, J. G.; Merkin, V. G. Role of magnetosheath force balance in regulating the dayside reconnection potential. **Journal of Geophysical Research (Space Physics)**, v. 115, p. 12216, dec. 2010. 27

Otto, A.; Schindler, K.; Birn, J. Quantitative study of the nonlinear formation and acceleration of plasmoids in the earth's magnetotail. **Journal of Geophysical Research**, v. 95, p. 15023–15037, sep. 1990. 17

Powell, K. G.; Roe, P. L.; Linde, T. J.; Gombosi, T. I.; De Zeeuw, D. L. A Solution-Adaptive Upwind Scheme for Ideal Magnetohydrodynamics. **Journal of Computational Physics**, v. 154, p. 284–309, sep. 1999. 19, 21

Raeder, J. Flux Transfer Events: 1. generation mechanism for strong southward IMF. **Annales Geophysicae**, v. 24, p. 381–392, mar. 2006. 5, 22, 27, 54, 71

Ridley, A.; Gombosi, T.; Dezeeuw, D. Ionospheric control of the magnetosphere: conductance. **Annales Geophysicae**, v. 22, p. 567–584, feb. 2004. 23

Rijnbeek, R. P.; Cowley, S. W. H.; Southwood, D. J.; Russell, C. T. Observations of reverse polarity flux transfer events at the earth's dayside magnetopause. **Nature**, v. 300, p. 23–26, nov. 1982. 31

Russell, C. T.; Elphic, R. C. Initial ISEE magnetometer results - Magnetopause observations. **Space Science Reviews**, v. 22, p. 681–715, dec. 1978. 12, 14

Schindler, K. A theory of the substorm mechanism. **Journal of Geophysical Research**, v. 79, p. 2803, 1974. 17

Scholer, M. Magnetic flux transfer at the magnetopause based on single X line bursty reconnection. **Geophysical Research Letters**, v. 15, n. 4, p. 291–294, 1988. 16, 35

Sergeev, V. A.; Tanskanen, P.; Mursula, K.; Korth, A.; Elphic, R. C. Current sheet thickness in the near-earth plasma sheet during substorm growth phase. **Journal of Geophysical Research**, v. 95, p. 3819–3828, apr. 1990. 22

Shue, J.-H.; Chao, J. K.; Fu, H. C.; Russell, C. T.; Song, P.; Khurana, K. K.; Singer, H. J. A new functional form to study the solar wind control of the magnetopause size and shape. **Journal of Geophysical Research**, v. 102, p. 9497–9512, may 1997. xvii, xviii, 32, 33, 35, 37, 39, 40

Sibeck, D. G.; Lin, R.-Q. Size and shape of the distant magnetotail. **Journal of Geophysical Research (Space Physics)**, v. 119, p. 1028–1043, feb. 2014. 65

Sonnerup, B. U. Ö.; Hasegawa, H.; Paschmann, G. Anatomy of a flux transfer event seen by Cluster. **Geophysical Research Letters**, v. 31, p. 11803, jun. 2004. 50

Southwood, D. J. The ionospheric signature of flux transfer events. **Journal of Geophysical Research**, v. 92, n. April 1, p. 3207–3213, 1987. 13, 61

Southwood, D. J.; Farrugia, C. J.; Saunders, M. A. What are flux transfer events? **Planetary and Space Science**, v. 36, p. 503–508, may 1988. 16

Torr, D. G.; Torr, M. R.; Brinton, H. C.; Brace, L. H.; Spencer, N. W.; Hedin, A. E.; Hanson, W. B.; Hoffman, J. H.; Nier, A. O.; Walker, J. C. G. An experimental and theoretical study of the mean diurnal variation of O^+, NO^+, O_2^+, and N_2^+ ions in the mid-latitude F_1 layer of the ionosphere. **Journal of Geophysical Research**, v. 84, p. 3360–3372, jul. 1979. 23

Tóth, G.; van der Holst, B.; Sokolov, I. V.; De Zeeuw, D. L.; Gombosi, T. I.; Fang, F.; Manchester, W. B.; Meng, X.; Najib, D.; Powell, K. G.; Stout, Q. F.; Glocer, A.; Ma, Y.-J.; Opher, M. Adaptive numerical algorithms in space weather modeling. **Journal of Computational Physics**, v. 231, p. 870–903, feb. 2012. 19, 21, 23

APPENDIX A - MATLAB INTERFACE TO KAMELEON SOFTWARE

The MATLAB functions we develop are listed below.

1) ***m2c_open_cdf.c*** : This function is a MATLAB wrapper to the C Kameleon function ***open_cdf.c*** (Original C Kameleon library of CCMC). The original C function performs all of the background low-level cdf functions required to open a CDF file including acquiring all the necessary variable numbers. Variable name validation is performed and any variables that are specified as arguments to ***m2c_open_cdf.c*** are loaded into main memory.

2) ***m2c_interpolate_batsrus_cdf.c*** : This function is a MATLAB wrapper to the C kameleon function ***interpolate_batsrus_cdf***. It returns an interpolated variable value for any given position in the simulation box. Requires a file to have already been opened with a ***m2c_open_cdf.c*** call.

3) ***m2c_close_cdf.c*** : This function is a MATLAB wrapper to the C Kameleon function ***close_cdf***.

4) ***plot3Bfield_lines.m*** : This function plot magnetic field lines with different color for each kind of magnetic field line, i.e closed, north polar cap connected, south polar cap connected and IMF field lines.

5) ***topology.m*** and ***topology_parallel.m*** : These functions calculate the magnetic topology of the point given by x,y,z coordinates. The difference between the two functions is that ***topology_parallel.m*** execute the calculation in parallel, which is more efficiently and take less time.

6) ***kam_streamline.m*** : This function computes the streamlines of an output variable resulting from the BATSRUS simulation code. ***kam_streamline.m*** uses the Kameleon interface function ***m2c_interpolate_batsrus_cdf.c*** to read the variable from the CDF file previously open with ***m2c_open_cdf.c*** function.

7) ***cdf_import_data.m*** : This function is used to import large block of data from a CDF file.

PUBLICAÇÕES TÉCNICO-CIENTÍFICAS EDITADAS PELO INPE

Teses e Dissertações (TDI)

Teses e Dissertações apresentadas nos Cursos de Pós-Graduação do INPE.

Notas Técnico-Científicas (NTC)

Incluem resultados preliminares de pesquisa, descrição de equipamentos, descrição e ou documentação de programas de computador, descrição de sistemas e experimentos, apresentação de testes, dados, atlas, e documentação de projetos de engenharia.

Propostas e Relatórios de Projetos (PRP)

São propostas de projetos técnico-científicos e relatórios de acompanhamento de projetos, atividades e convênios.

Publicações Seriadas

São os seriados técnico-científicos: boletins, periódicos, anuários e anais de eventos (simpósios e congressos). Constam destas publicações o Internacional Standard Serial Number (ISSN), que é um código único e definitivo para identificação de títulos de seriados.

Pré-publicações (PRE)

Todos os artigos publicados em periódicos, anais e como capítulos de livros.

Manuais Técnicos (MAN)

São publicações de caráter técnico que incluem normas, procedimentos, instruções e orientações.

Relatórios de Pesquisa (RPQ)

Reportam resultados ou progressos de pesquisas tanto de natureza técnica quanto científica, cujo nível seja compatível com o de uma publicação em periódico nacional ou internacional.

Publicações Didáticas (PUD)

Incluem apostilas, notas de aula e manuais didáticos.

Programas de Computador (PDC)

São a seqüência de instruções ou códigos, expressos em uma linguagem de programação compilada ou interpretada, a ser executada por um computador para alcançar um determinado objetivo. Aceitam-se tanto programas fonte quanto os executáveis.